5-4-2018 9:45 AM

Design of an All-dielectric Sublayer for Enhanced Transmittance In Stacked Antenna Array Applications

Matthew Bester
The University of Western Ontario

Supervisor
Wang, Xianbin
The University of Western Ontario Co-Supervisor
Bordatchev, Evgueni
The University of Western Ontario

Graduate Program in Electrical and Computer Engineering
A thesis submitted in partial fulfillment of the requirements for the degree in Master of Engineering Science

ABSTRACT

The dissipation in the energy of a forward propagating wave arising from interaction with an obstruction in the direct line-of-sight (LOS) is well-understood as the product of the reflection and absorption experienced at the peripheries and interior of the object. In stacked antenna arrays, this dissipation is imparted to a transmitted signal through the subsequent antennas whereby a significant proportion of the signal energy can be redirected towards the source or results in non-radiative electron collisions in the conductive layers. Although this exists as a practical limitation on their performance, interest in the subject remains as a result of the potential application to radome antenna design where the ability to encapsulate multiple arrays operating in distinct frequency bands under the same housing can enable the requirements for a size constrained system to be satisfied. Previous implementations considered the impedance introduced by the ground plane and feed network as the predominant mechanism of transmittance degradation and utilized a frequency selective surface (FSS) based rectification. In this investigation, emphasis is placed on the capacitive effect produced through the conductive ground plane, substrate dielectric, and patch regions as it pertains to the Schneider model for effective permittivity. The arrays are regarded as operating in the X and Ku frequency regions with center frequencies of 9 GHz and 14 GHz. In this system, the transmittance is determined with respect to the higher frequency antenna which is separated from the base antenna by a small air gap. Utilizing the transfer matrix method and effective medium approximation with the substrate permittivity varied from 4 to 30, the transmittance is observed to decline with increasing permittivity. A basic residual method is used to determine the necessary thickness and refractive index of an inserted interstitial layer across the range of tested substrate permittivites to achieve transmittance on the order of that for a high transmittance analog. This layer was

given to represent an all-dielectric material as a means of preventing further conductive losses from being introduced to the system. Concomitant with the plausible Fabry-Perot type resonance shifting and negative refractive index based spatial cancelling, both pure dielectric and all-dielectric metamaterial based implementations are considered for the layer. It is indicated that complementary values of the refractive index for the unknown medium are capable of producing the desired transmittance. These refractive indices are therefore investigated together and analyzed on their practicability. As a result of the underdetermined nonlinear nature of the objective function for the metamaterial constituents, the positive and negative refractive index values are applied in a sequential quadratic programming (SQP) technique from which the radii of the inclusions, lattice constant, and permittivity are resolved. Both negative and positive solutions are determined to have collision in their larger radii inclusions as a result of a poorly stated inequality condition. Revision of the inequality leads to only positive index implementations being viable. The tolerance of the achieved transparency to a ten percent variation in these properties is accessed in a confidence interval to illustrate the manufacturing feasibility and potential for a pure dielectric implementation. It is indicated that the limitations emplaced on the metamaterial features are beyond manufacturing capability and that the pure dielectric case is consequently more desirable. This case was used as an example of the expected bandwidth of the device when the permittivity is held at a constant value. It is believed that the attainable bandwidth is reasonable for a majority of radar applications.

ACKNOWLEDGEMENTS

I would like to thank my supervisor, Dr. Xianbin Wang, and co-supervisor, Dr. Bordatchev, for their encouragement and help in the preparation of my thesis. I would also like to acknowledge the contribution of the advisory committee and dissertation committee. I am grateful for the advice and support of the ombudsperson, Jennifer Meister, and student of graduate and post-doctoral studies representative, Jina Kum, that helped make my graduate studies experience more positive. I would like to mention Dr. Goncharova, whom provided me with an exciting research position in the Tandetron Lab and had the patience to train me in the use of the equipment and proper procedure.

Finally, I would like to thank my family and friends for their kindness and understanding throughout the course of my Master's program.

TABLE OF CONTENTS

LIST OF TABLES

LIST OF FIGURES

LIST OF ABBREVIATIONS

DNG Double Negative Gradient

EMT Effective Medium Theory

FPR Fabry-Perot Resonance

FSS Frequency Selective Surface

SQP Sequential Quadratic Programming

TMM Transverse Magnetic Mode

TEM Transverse Electric Mode

SSPP Spoof Surface Plasmon Polariton

LIST OF SYMBOLS

x_k	Coordinates of the pre-vertices for the original geometry
w_k	Coordinates of the desired vertices for a polygon in the new plane
α_k	Interior angles of the polygon
A, G	Complex constants of integration in section 2.1, not to be confused with the vector potential
θ_1	Theta function with parameters k and z
θ	Angle of incidence
K	Complete elliptic integral of the first kind
w	Width of the patch
h	Thickness of the substrate
C_0	Free-space capacitance
C	Capacitance of the medium
f_r	Resonant frequency of the patch antenna
λ	Wavelength
ε_s	Permittivity of the substrate
ε_0	Permittivity of free-space
ε	Permittivity of the medium
ε_r	Relative permittivity
ε_i	Inclusion Permittivity
ε_b	Permittivity of the background medium
ε_{eff}	Effective permittivity
μ_0	Permeability of free-space
μ	Permeability of the medium
μ_r	Relative permeability
μ_i	Inclusion permeability
μ_b	Permeability of the background medium
μ_{eff}	Effective permeability
c	Light constant
v	Phase velocity in medium
E	Electric field

E_+	Forward propagating electric field
E_-	Backward propagating electric field
E_i	Incident electric field
H	Magnetic field
D	Electric flux density
B	Magnetic flux density
n	Refractive index
J	Volumetric current density
J_s	Surface current density
ρ_s	Surface charge density
$\Gamma_{n-1,n}$	Reflection coefficient
$\Gamma_{n-1,neff}$	Effective reflection coefficient
$T_{n-1,n}$	Transmission coefficient
$T_{n-1,neff}$	Effective Transmission coefficient
A_n	Forward propagating waves
B_n	Backward propagating waves
$T_b^{n-1,n}$	Boundary transfer matrix at boundary m-1
T_φ^n	Inlayer transfer matrix for layer m
s_{ny}	Direction vector
T	Total transfer matrix
$\mathfrak{T}$	Transmittance
$\Re$	Reflectance
k, β	Wave number in medium
k_0	Free-space wave number
$\vec{k}$	Wave vector
d_m	Thickness of medium, m
ω	Angular frequency of the wave in radians
ω_0	Resonant frequency in radians
ω_p	Plasma frequency in radians
n_e	Number density of electrons

e	Electric charge
m_{eff}	Effective mass of the electron
γ	Damping of electron oscillation
r_i	Inner ring radius
w_r	Width of ring
a	Lattice constant for split-ring resonator
d	Separation between inner and outer ring
b	Separation between consecutive rings in a stack
σ_1	Unit length resistance in a sheet of the conductive material
r	Radius of sphere
r_e	Radius of electric mode coupling inclusions
r_m	Radius of magnetic mode coupling inclusions
Φ	Scalar solution to the Helmholtz equation
R	Decomposed radial portion of the scalar solution
θ	Decomposed angular portion of the scalar solution, polar
φ	Decomposed angular portion of the scalar solution, azimuth
Y_l^m	Spherical harmonic
P_l^m	Legendre polynomial
j_l	Spherical Bessel function of the first kind
h_l	Spherical Hankel function of the first kind
ℵ	Contrast parameter
χ	Size parameter
A	Vector potential used in section 2.5
s	Lattice constant for cubic lattice of resonant spheres
f_e	Volume fraction of electric mode coupling inclusions
f_m	Volume fraction of magnetic mode coupling inclusions
p	Dipole moment
p_{mol}	Molecular polarizability
P	Polarizability
N	Number of molecules per unit volume

CHAPTER

I. INTRODUCTION

1.1 General Details

Radar antenna arrays have become increasingly prevalent in modern autonomous systems as a means of assessing the conditions of the surrounding environment and providing feedback for object detection, surveillance, and reconnaissance. With this rise in automated features, the requirement for spatial awareness has become more prominent and its execution is often instituted by multiple active radar elements located on the same device. For vehicular applications, an aerodynamic and weatherproof housing, called a radome, imposes a spatial constraint on the antenna separation that can result in mutual coupling effects and array overlap [17,21]. Mutual coupling has been heavily investigated as a loss mechanism in planar array structures wherein each active element introduces a minute undesired current on the surrounding elements. The energy dissipated through this interaction can be partially negated through well-established antenna isolation techniques. A familiar example can be seen in the use of orthogonal signal polarizations for a polarization division multiplexing scheme to prevent interaction between signals of the same frequency. Unlike mutual coupling, the dissipation of wave energy through loss in the direct line-of-sight introduced by the stacking of antenna arrays has garnered little attention and solutions to this issue are accordingly scarce. The loss in this system arises as a combined effect of the feed network, ground plane, substrate, and patch regions which act as an impedance on forward wave propagation. Although previous investigations were concerned with the mitigation of feed network and ground plane based contributions, the capacitive effect generated by the remaining loss mechanisms can substantially impact the transmittance of the

base signal. It is therefore important to consider techniques that can prevent this degradation to ensure that a majority of the signal power reaches the intended target. For this purpose, all-dielectric solutions are instituted as a consequence of their prospective low conductive losses when compared with metamaterials involving metallic constituents. The practicability of these structures is supported by both plausible Fabry-Perot type resonance shifting phenomena in the case of a positive index dielectric sublayer and negative refraction induced spatial cancellation instated by an all-dielectric metamaterial (See Appendix for details on FPR). The refractive index is therefore not presumed to align with positive values exclusively but is given a range encompassing positive and negative subspaces.

This document details the design and efficacy of the dielectric sublayer for a two array stack comprised of rectangular patch elements. The basic planar rectangular patch array and general system model used in the analysis are presented in figures 1 and 2, respectively. The center frequencies of these arrays are selected to coincide with the parallel X and Ku frequency bands and reference the distinct radar applications existing under the same radome. Although the base antenna is assumed to be transmitting, the model is indifferent to the function of the uppermost antenna provided that frequency division duplexing is employed in the receiving mode. In this regime, the guard band prevents signal collision as a result of the limited bandwidth of the respective antennas. The model is simplified by considering the system from the perspective of an isolated unit cell circumscribing a single element of each array such that the impedance introduced by the uppermost antenna can be represented by an effective medium approximation of the patch antenna, as shown in figure 3. The ability to isolate the pattern produced by a single antenna element in an array configuration and subsequently, view elements in the system independently, derives from basic antenna array principles; wherein the total field pattern for the

array is governed by the product of the pattern for each element with a factor describing the relation between elements. In accordance with this principle and under the element-wise description of the configuration, the transfer matrix method is sufficient to determine the transmittance of the system and parameters of the required sublayer.

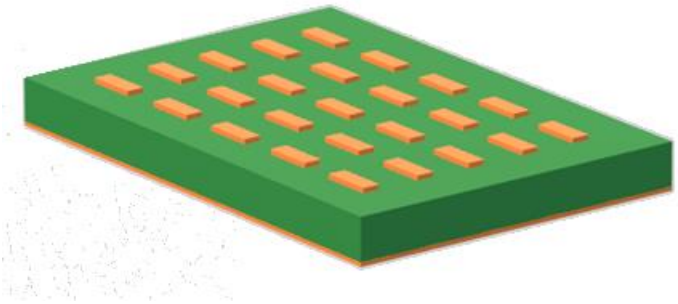

Figure 1: The simple planar antenna array comprised of rectangular elements

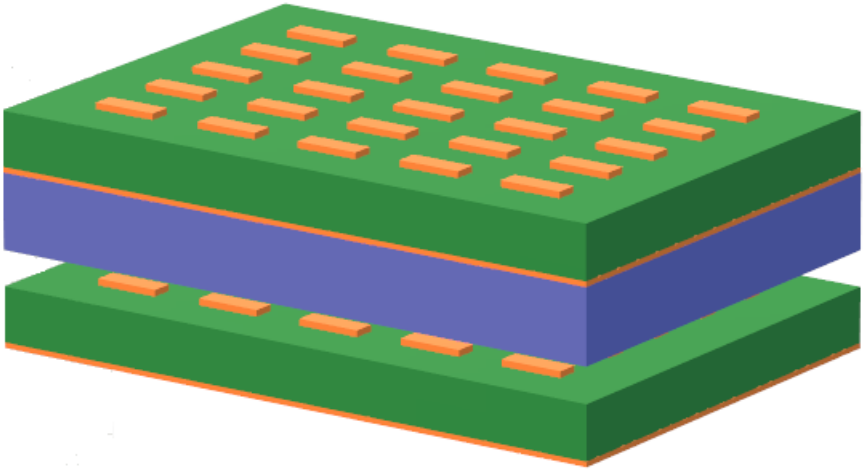

Figure 2: The layered array configuration with sublayer shown in blue

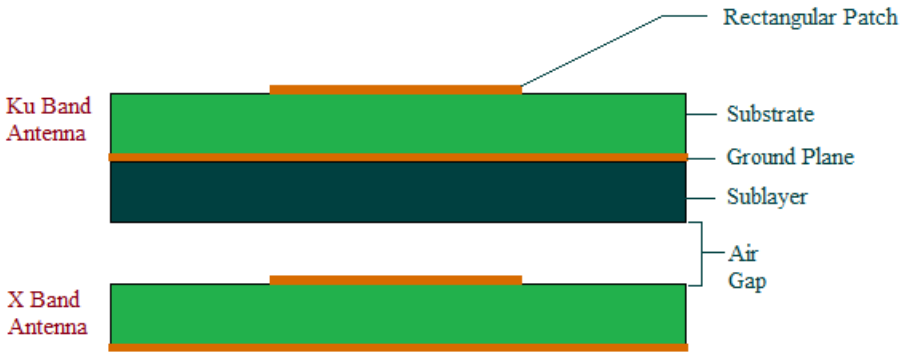

Figure 3: The single element system model used in the design procedure

1.2 Relate Work

The alignment of Fabry-Perot resonance modes arising within coated dielectric slabs to incident radiation of a given frequency has a well-known association with reflected wave suppression. The documented shifting of these modes in accordance with variations in the conductivity of the metal coating has been detailed in regard to glass substrates operating in the microwave frequency range [1,3,4]. In [1,3] the transmittance and reflectance were assessed from the field equations with the boundary condition imposed on the tangential magnetic field in proportion to the surface current density of the conductive region. This process is homologous to that of [4] where the properties of the system were determined by transmission matrix evaluation with the conductive region enforced as a shunt resistance. The theoretical observation of FPR shifting was experimentally verified with incident radiation provided by a Horn antenna in [1,4].

Expanding upon the postulate surrounding hypothetical negative index materials originally proposed by Veselago [5] prior to their realization, J. B. Pendry et al [2] suggested that an equal thickness material slab with properties that are the additive inverse of the proceeding space could effectively eliminate the contribution of that region on an incident wave regardless

of the material therein. These materials were termed complimentary media due to their antithetical properties. In conjunction with transformation optics, this method was employed in reference [6] to develop a cloak consisting of a complementary medium anti-object and shell that rectified the optical path of the radiation without obscuring the hidden object. Similar procedures have been employed in the design and development of superlenses.

In consonance with the predominant methodology detailed in the following sections, the transmission properties for stacked systems involving inhomogeneous features were evaluated in [7,8,9] through a combined effective medium/transfer matrix approach. The efficacy of an effective medium approximation for a metal-dielectric multilayer structure was analyzed in [8] through comparison of the reflectance and transmittance values to those obtained from the finite difference time domain simulation. A similar procedure was utilized in [9] for composites with arbitrary shaped dielectric inclusions where the validity of the technique was assessed from the finite element method solution. For both structures, the evaluation method was determined to provide adequate agreement to the more rigorous methods within reasonable limitation.

The negative effective material parameters arising from illumination of dielectric composites embedded with lattices of higher permittivity dielectric spherical inclusions was initially considered for constant values of the inclusion radii (see for example [10 ,11]). These lattices were later adapted to permit excitation of the magnetic and electric resonance modes by incorporation of spheres with two distinct radii [12]. An emendation of the effective medium model for the system of [12] through an improved mixing relation was presented in [13] and is the form ubiquitously utilized in application. A body centered cubic lattice formation was detailed in [14] to improve coupling between the spherical inclusions because of the enhanced packing factor with the compromise of decreased isotopy.

A similar however independent concept for achieving transparency in the field of laser optics involves stimulation by secondary sources whose frequency separation is proportional to a Raman transition for the medium [15].

1.3 Research Motivation and Objectives

There has been limited research into the prevention of signal transmission degradation when the line of sight from the transmitting antenna is impeded by subsequent overlying antenna arrays. In applications where space is tightly constrained and multiple-antennas are required, this condition is often unavoidable and it becomes essential to maintain the transparency of the antecedent arrays to the signals transmitted by the lower lying antennas. The following research articles exemplify the most recent attempts at mitigation of the blockage condition for radome applications through the design and optimization of the frequency selective surfaces and concurrent examination of the array feed network.

A frequency selective surface is a two-dimensional periodic structure of equivalently sized elements that predominantly operates as a filter for electromagnetic radiation as a result of inter-element resonance modes. In its simplest form, the array elements are comprised of finite length wires that approximate an LC circuit through the serial inductances of the parallel wires and the capacitance defined by their separation. At the resonant frequency of the effective circuit for the serial configuration, the oscillating charge density mimics that of a conductive ground plane region and the current is consequently unimpeded. The shape and arrangement of the elements vary their capacitive and inductive characteristics and can therefore enable band-pass or

band-stop functions over a desired frequency region. As a single structure, the resonance mode corresponds with ideally perfect transmission or reflection that are governed by the effective circuit properties. The FSS accordingly exhibits a narrow bandwidth about the resonant frequency where the impedance fluctuates between peripheral values. In order to improve the bandwidth, the surfaces can be cascaded such that the resonance properties exist as a composite of the distinct element configurations present in the arrays and dielectric separation layers that comprise the structure. The ability to permit the transversal of signals in a designated frequency region and concurrent ground plane behaviour make the FSS suitable for use in multilayer antenna arrays; where it is necessary to preserve the line of sight for underlying antenna arrays as well as provide the function of a ground plane for the subsequent array. This approach has been previously documented in [16] for arrays operating in the L and C bands wherein it was surmised that the blockage generated by the lower frequency array was predominantly a manifestation of the ground plane reflection at any frequency of the incident radiation and therefore ignored the scattering effects of the array itself. The focus was consequently limited to the design of an FSS to use as the ground plane in order to provide transparency across the C band. To increase the density of elements and improve the bandwidth, two 3 x 6 hexagonal element FSS were layered with a separation of a half wavelength, or half of the waveform's spatial period, and were positioned beneath the radiating array comprised of 4 series dual rhombic loop elements spaced at a quarter of their operating wavelength. It was noted that the periodicity of the structure can influence the development of surface waves, which reduces the efficacy of the FSS through grating lobe excitation and inhibition of the reflectivity property when the element spacing is less than a half wavelength. These effects, nevertheless, were indicated to be insubstantial when resistive loading was emplaced at the corners elements to dissipate the surface wave energy. It

was further assumed that the FSS functioned as a lossless filter and edge diffraction effects were minimal. Subsequent simulation exemplified the expected regions of reflectivity and transmissivity for the system, however, the prototype evaluation lead the data to be inconclusive.

Although the previous investigation detailed the ground plane behaviour of the FSS and transparency achieved therein, the feed network contribution to obstruction in the wave propagation was disregarded. It has been demonstrated in [17] that an unmodified corporate feed network behaves as a reflector of incident radiation at frequencies below the resonance condition of the array and exhibits transmission properties that are dependent upon the polarization of the wave. To improve the transmission properties of the feed network, these structures were investigated in both optimized and non-optimized configurations. The non-optimized approach examined the FSS and feed network as separate structures utilizing classical design techniques wherein the FSS operated as a ground plane for the array. This configuration exemplified preserved polarization states for the right hand circular polarized signal which would otherwise be attenuated. A prototype was constructed for a three array system comprised of overlapping L, S, and X band antennas wherein each antenna was determined to provide minimal attenuation to the other antennas. By incorporating dipole elements, it was determined that the function of the feed network and polarization independent FSS layer could be consolidated to improve the transparency and reduce the intolerance to variability in the wave polarization. Furthermore, the natural transmission features of the feed network could be preserved such that ground plane behaviour exists in the region necessary for the overlying antenna. This process was utilized in the optimized approach, which determined structural constituents of the corporate feed FSS through a quasi-Newtonian method. These structures were found to improve the gain and axial ratio over the array and corporate feed alone. Despite the applicability of the technique and

overall design problem, the impedance of the array itself was not presented as a significant contributor to the transmission degeneracy and the effects of close proximity of the periodic structures on the generation of surface waves was neglected.

In the microwave frequency region, surface waves, also colloquially known as spoof surface plasmon polaritons, can arise on metal-dielectric interfaces only in the presence of a corrugation; which acts to increase the incident momentum to match that of the SSPP mode [18]. This demonstrates a distinct advantage of utilizing dielectric implementations over those with embedded periodic metallic features such as the commonly applied FSS [19]. It is also worth mentioning that in collateral arrays, the reflectance and transmittance are not solely dependent upon the ground plane frequency rejection and feed network, but the subsequent reflection and transmission through the substrate and secondary reflection by the patch region. Although the feed network and ground plane have been investigated previously with solutions based on FSS, the antenna array itself was largely deemphasized and all-dielectric solutions have not been considered in the available documentation.

1.4 Thesis Contribution

The purpose of this thesis is to address the area of radar antenna stacking arising from spatially constrained multi-band systems operating within a mobile radome housing; wherein the typical planar configuration is impractical to implement. The main reason for their consideration is that these housings are especially restrictive in size, shape, and weight. It is foremost essential to clarify that the thesis is not intended to validate the structure or procedure but to detail a plausible technique for the resolution of a material that enacts a pseudo-transparency of the overlying array based on the hypotheses that:

1) Positive index materials, when placed below a conductive sheet, can introduce a cavity from which Fabry-Perot Resonance Shifting phenomena are possible and consequently yield improved transmission.

2) Negative index materials whose thickness and refractive index complement a subsequent spatial region can effectively cancel the contribution of that region to wave propagation.

The potential occurrence of these conditions is not surmised in the formulation but exists as the fundamental inspiration for the methodology examined in this work and distinguishes it from previous solutions. To this end, the following features can also be understood as novel to this area:

1) Investigation of a sublayer based system that maintains the ground plane and main features of the antenna array without introducing a secondary array.

2) Presentation of a simplified design procedure for both metamaterial and regular dielectric structures based on effective medium theory and the transfer matrix method.

3) Provision of a stochastic analysis for multiple iterations of the algorithm to establish confidence on the location of the population mean and approximate spread of the resultant solutions

4) Confirmation of the invalidity of all-dielectric metamaterials for this application with respect to manufacturing as a result of strong size and contrast biases.

5) Determination of the relative suitability of regular dielectric materials to enact the desired condition with adequate bandwidth as determined through the simplified methodology.

In the development of the simplified method for the resolution of the sublayer structure, some base assumptions were made that require to be detailed prior to the introduction of the theory and methodology. These assumptions are predominantly resultant from limitations in available software and the desire for improved runtime efficiency and take the form:

1) A single element is sufficient to approximate the behaviour of an array comprised of these elements.
2) The effective medium theory can appropriately handle conductivity effects while simplifying the system.
3) The media involved are non-dissipative and consequently do not exhibit an imaginary component in their permittivity values.
4) The media involved are non-magnetic and therefore have permeability on the order of free-space.
5) The media involved are non-dispersive and therefore do not exhibit frequency dependent effects.
6) The wave from the lower array is normally incident upon the surface of the overlying array.

It is believed that the under these conditions, the methodology provides an estimation of the system properties that can be revised and confirmed in subsequent work. The next section provides an overview of the topics covered in the remaining chapters

1.5 Thesis Outline

The remaining chapters detail the underlying principles, procedure, and results for the all-dielectric based transfer correction. Chapter two provides a brief introduction to the patch antenna and a corresponding derivation of the EMT formulation through the Shwarz-Christoffel mapping technique. A derivation of the transfer matrix from the time-dependent Maxwell's equations and the continuity conditions on the fields at the boundary between media is also provided in this section. The chapter concludes with an introduction to negative refraction and two common microwave frequency implementations that exemplify the basic features of metal and dielectric structures.

In chapter three, the parameters of the prospective metamaterial composite or pure dielectric are determined from evaluation of the transfer matrices in comparison to the desired optical glass transfer behaviour utilizing a rudimentary residual method. The dimensions and permittivity of the metamaterial variant are found through Mie theory with a sequential quadratic programming approach to the minimization problem. An additional evaluation of the tolerance to variability in these metrics is performed within a ten percent window about the resultant optimal value of each constituent. Herein, it is also indicated that pure dielectrics may provide a reliable substitute for the metamaterial structure. These dielectrics are subsequently utilized to establish an approximation of the expected bandwidth over which the performance of the system is acceptable.

Chapter four concludes the document with an overview of the key features detailed in the system evaluation and suggestions for potential supplementary investigations.

II. THEORETICAL FRAMEWORK

2.1 Rectangular Patch Antenna

A microstrip transmission line comprises a class of low profile antenna that exhibit radiation through the presence of fringing fields arising at the peripheries of a conductive strip when coupled to a subjacent ground plane [22]. The ground plane layer satisfies the conditions necessary for improving the antennas front-to-back ratio by introducing an opposing field in the region below the patch that partially negates reverse wave propagation and promotes the oscillation of the field. Due to the fringing effect, the conductive region must protrude beyond the exterior of the patch by two to three times the width of the separation distance to maintain a suitable ratio. Further increase in the ground plane dimensions yields diminishing returns with regards to gain enhancement as diffraction at the boundaries becomes less prominent. The interstice layer primarily determines the bandwidth of the antenna and is characteristically filled with an appropriate dielectric whose properties are concomitant with the desired performance and dimensions of the patch. A dielectric with higher permittivity can reduce the required patch size with the associated disadvantage of narrowed bandwidth, decreased gain, and increased return loss. Similarly, an increment in the dielectric thickness can yield improved gain but can cause extemporaneous effects conjoint with surface wave excitation. These constituents further influence the extent of the fringing field and consequently determine the electrical size of the patch; however, do not significantly contribute to the resonant frequency characteristics.

Excitation of the patch and signal retrieval are separately effectuated by the antenna feed contingent with the mode of operation. The feed position on the patch determines the magnitude of the impedance experienced by the wave as associated with the loci of extremes in the current and electric field along its surface. The maximum impedance coincides with the periphery of the

patch which explicates the limitation of the edge feeding technique in the absence of parallel loading. The efficacy of this feed type resides in the practicality of in-layer integration with corroborative circuitry; where viability in array application is evident from the voltage division arising between elements. Variation regarding feed location for probe and inset techniques are made pursuant to the impedance minima of the patch at approximate equidistance from the peripheries. Delineation of the conductive line along the ground plane orthonormal that is circumscribed by the substrate and congruent with the probe feeding technique, indicates a substantial reduction in bandwidth and ancillary constraint on substrate thickness. These deficiencies can be partially precluded by consolidation of the advantages of edge and probe type feed techniques by means of inset feeding at the impedance minimum through a line coplanar with the patch; however, the displacement of the conductive strip about the feed line introduces distortions in the radiation pattern. In practice, the choice of feedline is dependent on the application and permissible concession in performance characteristics.

The perturbation in static field components arising from interaction with an arbitrary planar patch geometry can be resolved in a discretized representation of the system through the finite element method about the antenna subspace. In situations where knowledge of the field components existing internal to the patch are unnecessary, the system can be alternatively regarded through its bulk properties. The conformal mapping technique can be applied to rectify an uncertain open polygonal profile to one for which the solution is known within the constraint of static or quasi-static field [23]. In complex analysis, a conformal map represents a method of conversion between two differentiable arcs through an analytic function that conserves local angles. This technique is commonly applied to boundary value problems involving the Laplace equation in an intricate planar region whose solution is the potential arising from a given charge

density. A notable example application of the Laplace equation is in the determination of the potential in a parallel plate capacitor; which can be seen to resemble, the profile of a planar patch antenna. In consonance with the transmission line model, the patch can be viewed as forming an asymmetric parallel plate about the horizontal axis of the cross section that can be adapted to an equivalent capacitor configuration in a secondary complex plane. The direct Schwarz-Christoffel method maps the upper half-plane in complex space to the region contained within an arbitrary polygon through the transform (2.1.1) [24].

$$w(z) = A + G\int_{z_0}^{z}\prod_{k=1}^{n-1}(\xi - x_k)^{\alpha_k - 1}d\xi \tag{2.1.1}$$

where the x_k are pre-vertices existing in the original complex z space, w_k are the desired counter clockwise complex vertices of the polygon in the w plane, $\alpha_k$are the counter clockwise interior angles of the polygon, and A and G are complex constants determined through boundary condition equivalence. More precisely, the pre-vertices or preimage of the vertices are the proportion of elements in the original domain that are mapped to the vertices in a codomain or target domain that form the polygon through a given transform. Using this method, the Schwarz-Christoffel equation for mapping of the upper half plane to a contained rectangular region can then be expressed as (2.1.2) [25].

$$w(z) = \int_{z_0}^{z}\frac{d\xi}{(\xi - x_1)^{\frac{1}{2}}(\xi - x_2)^{\frac{1}{2}}(\xi - x_3)^{\frac{1}{2}}(\xi - x_4)^{\frac{1}{2}}} \tag{2.1.2}$$

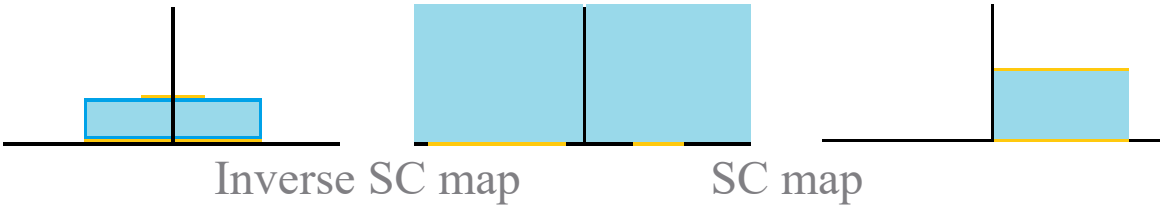

Figure 4: Visualization of the forward and inverse Shwarz-Christoffel methods

The complex constants can be neglected for axisymmetric geometries, where they are nullified in evaluation at the boundaries. The patch antenna is approximated as a rectangular cross section in the complex plane by assuming negligible patch thickness. To configure this profile as an equivalent capacitor in u space, the cross-section must first be converted to the upper-half plane as the inverse of the previous expression. The substitution of the pre-vertices at selected values x=-a,-1, 1, a into (II) with restitution of z_0 to zero yields the elliptic integral of the first kind (2.1.3).

$$w(z) = \int_0^z \frac{d\xi}{\sqrt{(1-\xi^2)\left(1-\frac{1}{a^2}\xi^2\right)}} \tag{2.1.3}$$

The inversion of this equation involves the Jacobi elliptic functions which can be expressed in terms of their corresponding theta functions, θ_1. For a patch defined by the vertices at w = $\frac{-\omega}{2}, \frac{-\omega}{2}+ih, \frac{\omega}{2}+ih, \frac{\omega}{2}$ where ω is the patch width and h is the substrate thickness, the vertices in the z plane can be determined through the map (2.1.4) [23].

$$w(z) = \frac{-2hK}{\pi}\frac{\delta \ln \theta_1(z,k)}{\delta z} \tag{2.1.4}$$

Where k is the theta function parameter and K is the complete elliptic integral of the first kind. The upper half plane describing the patch geometry is translated to a distinctive region in u space circumscribed by collateral sides of a rectangle wherein the established capacitance equations are valid. The effective permittivity can then be formalised as the ratio of the system capacitance to free space in accordance with Schneider's model (2.1.5).

$$\varepsilon_{eff} = \frac{C}{C_0} = \frac{\varepsilon_s + 1}{2} + \frac{\varepsilon_s - 1}{2} \frac{1}{\sqrt{1 + \frac{12h}{w}}} \tag{2.1.5}$$

This equation is suitable in the description of interactions with any rectangular patch geometry and can be alternatively applied to circular patch configurations; being cognisant of the Wolff model equivalence between their profiles [26]. Due to the reciprocity of the configurations, focus in this report is restricted to a rectangular patch wherein the required patch width can be determined from the desired resonant frequency and substrate permittivity through equation (2.1.6) [27].

$$w = \frac{c}{2f_r} \sqrt{\frac{2}{\varepsilon_s + 1}} \tag{2.1.6}$$

where the light constant represented by the lower-case c should not be confused with the capacitances of equation (2.1.5). A direct consequence of the previous equation is that as the permittivity of the substrate is increased, the patch width can be reduced; enabling further miniaturization of antenna systems and supporting the consideration of higher permittivity values in the design process.

Figure 5: Rectangular patch antenna dimensions showing the width, w, the substrate thickness, h, and the amount by which the ground plane exceeds the patch region. It should be mentioned that only w and h are necessary for the Schneider model

2.2 Refractive Index

The refractive index describes the concomitant effect on the transmission of an electromagnetic wave produced by discontinuity in the wave velocity at the interface between media. The rate at which a wave traverses a homogeneous volume is related to the permittivity, ε, and permeability, μ, that arise as a consequence of its susceptibility to engage internal electric and magnetic stimuli. The permittivity and permeability are somewhat opposite features of a material in that the former indicates the propensity to resist the electric field induction in the material, whereas the latter indicates the propensity of the material to sustain a magnetic field. The aforementioned relationship with the material is substantiated by the solution to (2.2.1) the curl of the Maxwell-Faraday equation in concurrence with (2.2.2) Ampere's law [28].

$$\nabla \times (\nabla \times E) = \nabla^2 \mathrm{E} - \nabla \cdot \mathrm{E} = \nabla \times \left(\frac{-\delta B}{\delta t}\right) \tag{2.2.1}$$

$$\nabla \times \mathrm{B} = \mu\varepsilon \frac{\delta E}{\delta t} \tag{2.2.2}$$

In the absence of charged particles in the environment, the divergence operator takes on a null value with the resultant system being described by the vector wave equation (2.2.3).

$$\nabla^2 E = \mu_0 \varepsilon_0 \frac{\delta^2 E}{\delta t^2} \tag{2.2.3}$$

This equation has a solution of the form $E = Asin\left(\frac{2\pi}{\lambda}(x + ct)\right)$, which upon substitution into (2.2.3) yields the familiar correlation for the light constant (2.2.4).

$$c = \frac{1}{\sqrt{\mu_0 \varepsilon_0}} \tag{2.2.4}$$

This constant dictates the rate at which a wave propagates under vacuum conditions. It can be demonstrated that the phase velocity, v, of a wave in any medium is similarly procured with an emendation of the free-space parameters to their material specific values. The significance of this velocity can be observed in the refractive index whereby it is normalized with respect to free-space to operate as a comparative measure of the mediums effect (2.2.5).

$$n = \frac{c}{v} = \frac{\sqrt{\mu\varepsilon}}{\sqrt{\mu_0 \varepsilon_0}} = \sqrt{\mu_r \varepsilon_r} \tag{2.2.5}$$

The Huygens-Fresnel principle offers a more qualitatively intuitive description for the resultant refractive index equation. In this interpretation, planes of equal phase- termed wavefronts- are represented as the sum of spherical waves that propagate at the appropriate phase velocity for the medium [29]. The material parameters thus constitute a macroscopic aggregation of the internal delays in state transitions under the incident field that dampen this velocity without effecting the frequency. Upon contact with a surface, an additional delay is introduced

to the wavefront in accordance with the surfaces azimuth; where the spherical waves are shifted relative to one another at the intersection.

2.3 Snell's Law

The difference in phase velocity of a wave between collocated media when inclined relative to the surface normal, introduces a deflection in the wavefront that is mathematically formalised by Snell's law (2.3.1) and indicated in the Huygen-Fresnel principle.

$$n_1 sin\theta_1 = n_2 sin\theta_2 \tag{2.3.1}$$

The equation is invariant to substitution of the phase velocity with their respective refractive index; resultant from the angle being governed by the ratio of parameters.

2.4 The Transfer Matrix Method

The transfer matrix quantifies the exchange between forward and backward propagating waves at antithetical boundaries of concatenated semi-infinite media as the aggregate of the contributions imparted through spatial domain segmentation at medial boundaries and phase change introduced through layer traversal in a product of the matrices representing the total volume [30]. The Fresnel equations which are fundamental in the transfer matrix formulation, extend the continuity condition on the tangential electric and magnetic fields to determine the value associated with this reflection with respect to the incident field and the corresponding fraction transmitted beyond the boundary. The coefficients determined thereby are dependent upon the constituent material refractive indices and polarization of the wave transmitted through the medium with respect to the plane enclosing the surface normal and the line of incidence. In the case of normal incidence and under the non-magnetic material assumption, the equations are indifferent to the polarization of the wave and depend only on the refractive indices of the

interfacing media. For magnetic media, the refractive indices are simply substituted for the wave impedance values. It is implicit in the following formulation that the coefficients are reliant upon material parameter uniformity as designated by the homogeneous refractive index.

The resolution of the integral form of Maxwell's equations illustrates the continuity conditions arising at media boundaries (2.4.1)-(2.4.4) [31].

$$\oint_s D \cdot ds = \int_v \rho \cdot dv \tag{2.4.1}$$

$$\oint_c E \cdot dl = -\int_s \frac{dB}{dt} \cdot ds \tag{2.4.2}$$

$$\oint_s B \cdot ds = 0 \tag{2.4.3}$$

$$\oint_c H \cdot dl = \int_s \left(J + \frac{dD}{dt}\right) \cdot ds \tag{2.4.4}$$

where D is the electric flux density, E is the electric field intensity, H is the magnetic field intensity, and B is the magnetic flux density. The flux densities describe the corresponding field flowing through a given area and differ from the field intensities in their independence from material properties. The fields themselves represent the force exerted on a point charge by an electric or magnetic stimulus. For simplicity, the surface considered in the equations has the form of a Gaussian pillbox whose thickness approaches infinitesimal values. The pillbox face denoted by S represents the boundary contact with the surface of the medium and is defined in this form to be circular with an area, ΔS. In a material with perfect electric conductivity at the boundary,

the electric charge density, ρ, and volumetric current density, J, are semi-infinite and must be accounted for in the continuity conditions analogous to energy conservation. From Gauss' law (2.4.1), the following equation is obtained (2.4.5).

$$\hat{n} \cdot (D_1 - D_2)\Delta S + \int_{height} (\hat{t} \cdot D)\, ds = \Delta S \int_{-\frac{h}{2}}^{\frac{h}{2}} \rho\, d\gamma \tag{2.4.5}$$

The terms on the left-hand side of equation (2.4.5) delineate the proportion of the electric flux density collateral with the surface normal of the pillbox base and side. In dielectric media where finite electric charge density is displayed, the right-hand integration over the side region is inconsequential and the resultant equation is entirely determined by the term independent of pillbox thickness (2.4.6). The $\hat{t}$ and γ terms denote the unit normal of the pillbox side and coordinate perpendicular to the surface, respectively. Conversely, conductive materials exhibit a reliance of the continuity on the surface electric charge density, ρ_s, arising on the material boundary (2.4.7).

$$\hat{n} \cdot (D_1 - D_2) = 0 \tag{2.4.6}$$

$$\hat{n} \cdot (D_1 - D_2) = \rho_s \tag{2.4.7}$$

The conditions indicate that the proportion of electric flux density tangential to the surface is continuous across the boundary of the medium with respect to the occurrence of surface based charges. The continuity of the electric and magnetic field intensity at the interface can be analogously derived from (2.4.2) and (2.4.4). Noting that the integral about the closed contour is equivalent to the surface integral of the normal cross product with the respective field, we have

(2.4.8)-(2.4.10). The dependence of the magnetic field intensity on the current density requires the contribution to be included in the continuity conditions for materials which are capable of supporting surface current; establishing a similar condition to the electric flux density.

$$\hat{n} \times (E_1 - E_2) = 0 \tag{2.4.8}$$

$$\hat{n} \times (H_1 - H_2) = 0 \tag{2.4.9}$$

$$\hat{n} \times (H_1 - H_2) = J_s \tag{2.4.10}$$

$$\hat{n} \cdot (B_1 - B_2) = 0 \tag{2.4.11}$$

From (2.4.8) and (2.4.9) it is evident that the component of the fields aligned with the plane of the interface are continuous across its boundary. Equation (2.4.11) clarifies the coherence of the tangential magnetic flux density and consequently, bears semblance to that described in (2.4.6) for the corresponding electric coequal.

For an S-polarized wave incident on dielectric, the electric field intensity parallels the surface of the interface and therefore suggests the plausibility of the full system description through equations (2.4.8) and (2.4.9). This is resultant from the proportionality of the electric flux density to the electric field whose dot product with the surface normal in (2.4.6) yields a nullity. The associated magnetic field can contain both collinear and tangential contributions depending on the azimuth of the line of incidence with the surface normal. Considering equations (2.4.8) and (2.4.9) contingent with plane wave propagation through a boundary separating non-magnetic dielectric media, the continuity conditions can be written as (2.4.12) and (2.4.13).

$$E_i + E_r = E_t \tag{2.4.12}$$

$$H_i \cos\theta_i + H_r \cos\theta_r = H_t \cos\theta_t \tag{2.4.13}$$

Utilizing the correlation between the electric and magnetic field derived from the time harmonic interpretation of Faraday's law conjoint with the constitutive relation for magnetic flux density, equation (2.4.13) can be rewritten in terms of the electric field (2.4.14).

$$E_i\, n_1 \cos\theta_i + E_r n_1 \cos\theta_r = E_t n_2 \cos\theta_t \qquad (2.4.14)$$

where the subscripts 1 and 2 delineate the refractive indices of the interfacing media. From (2.4.12) and (2.4.14) the reflection and transmission coefficients can be determined as the ratio of the respective reflected and transmitted amplitudes to the incident. The coefficients for a P-polarized wave are similarly obtained with rectification of field intensities to positions opposing that of S-polarization. Under normal incidence, the values of the coefficients are irrespective of the polarization type. These results are summarised in table 1.

Polarization	S/TE	P/TM	Normal incidence
Reflection, $\Gamma_{1,2}$	$\frac{n_1 cos\theta_1 - n_2 cos\theta_2}{n_1 cos\theta_1 + n_2 cos\theta_2}$	$\frac{n_2 cos\theta_1 - n_1 cos\theta_2}{n_2 cos\theta_1 + n_1 cos\theta_2}$	$\frac{n_1 - n_2}{n_1 + n_2}$
Transmission, $T_{1,2}$	$\frac{2n_1 cos\theta_1}{n_1 cos\theta_1 + n_2 cos\theta_2}$	$\frac{2n_1 cos\theta_1}{n_1 cos\theta_2 + n_2 cos\theta_2}$	$\frac{2n_1}{n_1 + n_2}$

Table 1: Fresnel coefficients based on angle of incidence and polarization

The transfer matrix method involves the concatenation of matrices describing the physical effects related to wave interaction at planar dielectric boundaries and concomitant through layer propagation. The derivation for the boundary transmission matrix can be understood from the Huygen-Fresnel principle as discussed in section 2.2, where a wavefront incident on a medial boundary produces divergent hemispherical waves along the surface that propagate as plane

waves within both half-spaces. The interference of the transmitted and reflected waves result in intensity peaks that are concurrent with the aggregation of infinite decaying wavefronts. The incorporated fronts therefore behave as opposing amalgamated plane waves whose bisected amplitudes are associated with the matrix (2.4.22) and whose phase is determined by (2.4.23) with variable distance from the interface.

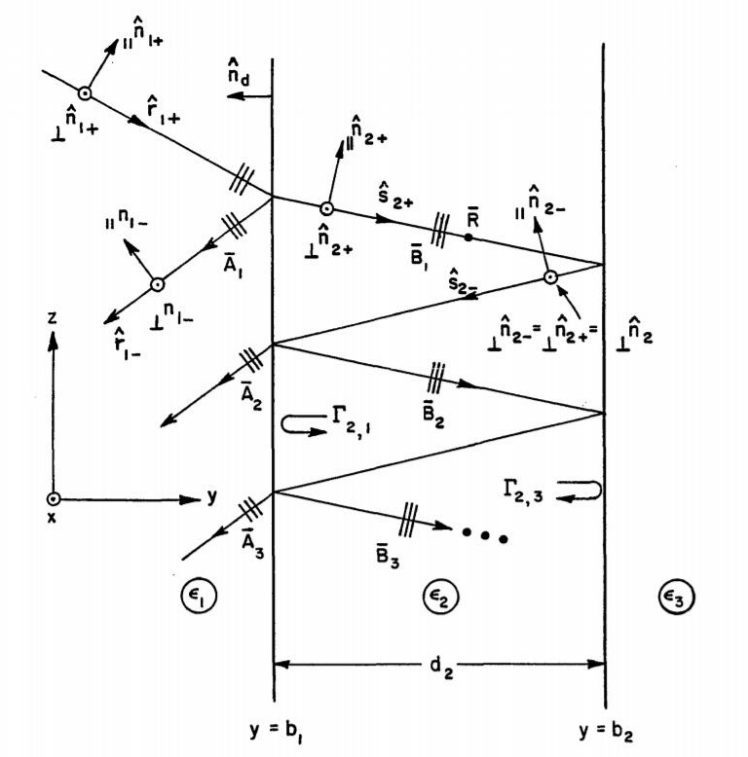

Figure 6: Image of plane wave transmission and reflection in a dielectric slab taken from page 7 of L. W. Henderson's dissertation: "The Scattering of Planar Arrays of Arbitrarily Shaped Slots and/or Wire Elements in a Stratified Dielectric Medium." [32]

The constituent matrix equations for the transfer matrix method are comprised of elements derived from the time-harmonic representation of Faraday's induction law in a Fourier series expansion. Although elegant in its final form, the cumbersome derivation process can be more compendiously described through the intuitive propagation mechanism of a plane wave incident

on a homogeneous semi-infinite dielectric layer. The waves internal to the slab are distinguished in accordance with their direction relative to the interface as either forward or backward propagating. These waves represent components of an infinite series as a sum of their phase-shifted wave amplitudes which result from the perpetuation of reflection and transmission at the boundaries and transmission through the medium. The aggregate of these values determines the total transmitted, E_+, and reflected, E_-, proportions. Based on [32] the waves are given the form:

$$E_- = \sum_{n=0}^{\infty} A_n$$

$$E_+ = \sum_{n=0}^{\infty} B_n$$

Where the A_n and B_n represent segments of the total reflected and transmitted fields, respectively. It is a well-established property of semi-infinite media that their reflection and transmission coefficients are interdependent and can be described through the relation, 1+Γ=T. Defining the transmission coefficient in this form, the first few forward directed waves for a single slab of dielectric, have the form:

$$B_1 = (1 + \Gamma_{1,2})E_i$$

$$B_2 = B_1\Gamma_{2,3}e^{-j\beta_2 d_2 s_{2y}}\Gamma_{2,1}e^{-j\beta_2 d_2 s_{2y}} = B_1\Gamma_{2,1}\Gamma_{2,3}e^{-j2\beta_2 d_2 s_{2y}}$$

$$B_3 = B_2\Gamma_{2,3}e^{-j\beta_2 d_2 s_{2y}}\Gamma_{2,1}e^{-j\beta_2 d_2 s_{2y}} = B_1{\Gamma_{2,1}}^2{\Gamma_{2,3}}^2e^{-j4\beta_2 d_2 s_{2y}}$$

Where the phase change in the media, constituting the exponential term, is comprised of the mediums wavenumber, β, thickness, d, and direction vector, s. Denoting the recurrent

multiplicative factor as a variable, c, the infinite summation can be recognized as a geometric series wherein the condition on the magnitude of the reflection coefficient product leads the system to converge as $n \to \infty$, in the following manner:

$$c = \Gamma_{2,1}\Gamma_{2,3}e^{-j2\beta_2 d_2 s_{2y}}$$

$$E_+ = \left(1 + \Gamma_{1,2}\right)E_i \sum_{n=0}^{\infty} c^n = \frac{\left(1 + \Gamma_{1,2}\right)E_i}{1 - \Gamma_{2,1}\Gamma_{2,3}e^{-j2\beta_2 d_2 s_{2y}}}$$

This can be reconstituted as an effective transmission by designating the left hand side as the ratio of the total forward propagating wave in the second medium to that of the incident:

$$T_{1,2eff} = \frac{E_+}{E_i} = \frac{1 + \Gamma_{1,2}}{1 - \Gamma_{2,1}\Gamma_{2,3}e^{-j2\beta_2 d_2 s_{2y}}}$$

The backward propagating waves can be similarly addressed. Making use of the variable, c, described previously, the first few terms are given by:

$$A_1 = \Gamma_{1,2}E_i$$

$$A_2 = \frac{E_i\left(1 + \Gamma_{1,2}\right)}{\Gamma_{2,1}}c\left(1 + \Gamma_{2,1}\right)$$

$$A_3 = \frac{E_i\left(1 + \Gamma_{1,2}\right)}{\Gamma_{2,1}}c^2\left(1 + \Gamma_{2,1}\right)$$

Which can likewise be defined as a geometric series with respect to the c term. Utilizing the same convergence condition exhibited for the previous case and provided that the reflection coefficients share the relation, $\Gamma_{2,1} = -\Gamma_{1,2}$, the backward propagating wave can be given as:

$$E_- = \frac{\left(\Gamma_{1,2} + \Gamma_{2,3}e^{-j2\beta_2 d_2 s_{2y}}\right)E_i}{1 - \Gamma_{2,1}\Gamma_{2,3}e^{-j2\beta_2 d_2 s_{2y}}}$$

The effective reflection coefficient can then be derived as the ratio of the backward propagating wave to the incident as follows:

$$\Gamma_{1,2eff} = \frac{E_-}{E_i} = \frac{\Gamma_{1,2} + \Gamma_{2,3} e^{-j2\beta_2 d_2 s_{2y}}}{1 - \Gamma_{2,1}\Gamma_{2,3} e^{-j2\beta_2 d_2 s_{2y}}}$$

In conjunction with the effective transmission coefficient, these terms conveniently describe the recursion of transmitted and reflected waves for a single slab of lossless dielectric material. For the case of a multilayered dielectric structure, the coefficients can be extended to account for subsequent reflection and transmission at each boundary layer that contribute to the total forward and backward propagating wave amplitudes. Considering the previous equation, a generalized expression can be derived by substitution of the reflection at the succeeding right interface with its effective value. For slab n-1, this recursion is then given by:

$$\Gamma_{n-1,n\,eff} = \frac{E_{n-1}^-}{E_{n-1}^+} = \frac{\Gamma_{n-1,n} + \Gamma_{n,n+1\,eff} e^{-j2\beta_n d_n s_{ny}}}{1 - \Gamma_{n,n-1}\Gamma_{n,n+1\,eff} e^{-j2\beta_n d_n s_{ny}}}$$

The effective value at interface n, n+1 can be understood as the ratio of the reflected field in slab n to the corresponding field incident upon slab n+1

$$\Gamma_{n,n+1\,eff} = \frac{E_n^-}{E_n^+}$$

In this regard, the formula can be composed to prescribe the interdependency of the waves in each medium:

$$\frac{E_{n-1}^-}{E_{n-1}^+} = \frac{\Gamma_{n-1,n} + \frac{E_n^-}{E_n^+}\, e^{-j2\beta_n d_n s_{ny}}}{1 - \Gamma_{n,n-1}\, \frac{E_n^-}{E_n^+}\, e^{-j2\beta_n d_n s_{ny}}}$$

Taking the product of the numerator and denominator on the right hand side with $e^{j\beta_n d_n s_{ny}}$ and E_n^+, the equation becomes:

$$\frac{E_{n-1}^-}{E_{n-1}^+} = \frac{E_n^+ \Gamma_{n-1,n} e^{j\beta_n d_n s_{ny}} + E_n^- e^{-j\beta_n d_n s_{ny}}}{E_n^+ e^{j\beta_n d_n s_{ny}} - \Gamma_{n,n-1} E_n^- e^{-j\beta_n d_n s_{ny}}}$$

In order to decouple the equations representing the forward propagating wave from that describing the backward in medium for medium n-1, the equations are multiplied by a common factor, $1/T_{n-1,n}$, determined from boundary relations, whereby we have:

$$E_{n-1}^- = \frac{1}{T_{n-1,n}} \left(E_n^+ \Gamma_{n-1,n} e^{j\beta_n d_n s_{ny}} + E_n^- e^{-j\beta_n d_n s_{ny}} \right)$$

$$E_{n-1}^+ = \frac{1}{T_{n-1,n}} \left(E_n^+ e^{j\beta_n d_n s_{ny}} - \Gamma_{n,n-1} E_n^- e^{-j\beta_n d_n s_{ny}} \right)$$

It is clear from the description that the system of equations can be represented as a matrix:

$$\begin{bmatrix} E_{n-1}^+ \\ E_{n-1}^- \end{bmatrix} = \frac{1}{T_{n-1,n}} \begin{bmatrix} e^{j\beta_n d_n s_{ny}} & \Gamma_{n,n-1} e^{-j\beta_n d_n s_{ny}} \\ \Gamma_{n-1,n} e^{j\beta_n d_n s_{ny}} & e^{-j\beta_n d_n s_{ny}} \end{bmatrix} \begin{bmatrix} E_n^+ \\ E_n^- \end{bmatrix}$$

Which can be delineated in accordance with the boundary and phase contributions in a more elegant format:

$$\begin{bmatrix} E_{n-1}^+ \\ E_{n-1}^- \end{bmatrix} = \frac{1}{T_{n-1,n}} \begin{bmatrix} 1 & \Gamma_{n,n-1} \\ \Gamma_{n-1,n} & 1 \end{bmatrix} \begin{bmatrix} e^{j\beta_n d_n s_{ny}} & 0 \\ 0 & e^{-j\beta_n d_n s_{ny}} \end{bmatrix} \begin{bmatrix} E_n^+ \\ E_n^- \end{bmatrix}$$

The coefficient matrix can be understood as relating the forward and backward waves in both media and is consequently known as the transfer matrix for the slab. Separating the individual components into those encompassing the interface, $T_b^{n-1,n}$, and interstitial transmission, T_φ^n, the transfer matrices can be seen to have the typical form presented in literature:

$$T_b^{n-1,n} = \frac{1}{T_{n-1,n}} \begin{bmatrix} 1 & \Gamma_{n,n-1} \\ \Gamma_{n-1,n} & 1 \end{bmatrix} \tag{2.4.15}$$

$$T_\varphi^n = \begin{bmatrix} e^{j\beta_n d_n s_{ny}} & 0 \\ 0 & e^{-j\beta_n d_n s_{ny}} \end{bmatrix} \tag{2.4.16}$$

The comprehensive transfer matrix for a system of *N* layers can then be written as:

$$T = T_b^{1,2} T_\varphi^2 T_b^{2,3} \dots T_b^{n-1,n} \tag{2.4.17}$$

The matrix elements are not in themselves indicative of the strength of the transmitted signal and can therefore be misinterpreted to display promising attributes which are invalidated by subsequent calculation. It is advantageous to use the transmittance, $\mathfrak{T}$, and reflectance, $\mathfrak{R}$, which designate the proportion of power permitted or precluded from transfer across the object. These values can be calculated directly as the modulus squared ratio of transfer matrix elements:

$$\mathfrak{T} = \left| \frac{1}{A_{11}} \right|^2 \tag{2.4.18}$$

$$\mathfrak{R} = \left| \frac{A_{21}}{A_{11}} \right|^2 \tag{2.4.19}$$

The summation of these quantities can invariably be assumed to have a value of unity because of the energy conservation in the absence of further perturbation by secondary sources and material related dissipative effects. Therefore, it is sufficient to consider only the transmittance coefficient in design formulation.

2.5 Negative Refraction

The designation of a system as possessing negative refractive index properties encompasses any whose effective material parameters are incongruously or concurrently negative. The former system denotes a single negative material wherein the purely imaginary index prohibits the sustenance of the wave beyond evanescent [33]. The industrial practicability of such a material is therefore limited by their inability to promote propagation. Conversely, the adopted sign convention for double negative media follows from the exhibited unconventional left-handed relationship between the wave vector and electric and magnetic fields, irrespective of the demonstrable positive real-valued index [5]. The propagation in such media is defined by the anti-parallel phase velocity with respect to the direction of energy flow and field quantities. Maxwell's field equations explain this relationship when contrasted with plane wave propagation in standard dielectric media (2.5.1) and (2.5.2); where opposition in the sign of the material parameters negates the right-hand side of the wave vector cross product.

$$\vec{k} \times E = \frac{\omega}{c} \mu H \tag{2.5.1}$$

$$\vec{k} \times H = -\frac{\omega}{c} \varepsilon E \tag{2.5.2}$$

The wave vector, $\vec{k}$, expresses both the spatial phase velocity in the medium and the direction of energy progression of the wave; and can be thought of as the angular frequency's spatial derivative. Further analysis of the equation for refractive index yields the conclusion that the phase velocity of a wave in DNG materials must also be directed toward the source. Therefore, a wavefront incident on the media surface would deflect into the half-space containing the source on the opposing side of the boundary. The associated effect of this refraction and index

permutation on the transfer matrix formulation is evident from the Fresnel coefficients and concurrent phase shift.

In the microwave frequency region, natural materials are fundamentally incapable of effectuating negative refraction and therefore implementation requires a composite whose size, shape, and constituents determine the effective properties exhibited. Subsections 2.5.1 and 2.5.2 detail some common metamaterial configurations for the achievement of negative refraction within this region.

2.5.1 Split Ring Resonators and Wire Composites

The displaced electron density in conductive media generated through interaction with an electromagnetic field experiences a harmonic restorative force whose oscillations are determined by the associated plasma frequency (2.5.1.1) [34]. At the systems natural resonance, the excitation and plasma frequency are equivalent and the wave experiences little attenuation as it negotiates the medium; exemplifying a theoretically zero permittivity when dissipation is negligible. External to this region of congruence, the mediums capacity to perpetuate propagation diminishes as a function of their proportion. These characteristics constitute the susceptibility of the conductive media to incident waves and accordingly classify the macroscopic dielectric function (2.5.1.2); with the implication that the system will exhibit negative permittivity when bisected by radiation of frequency less than the plasma frequency for the medium.

$$\omega_p = \sqrt{\frac{n_e e^2}{\varepsilon_0 m_{eff}}} \qquad (2.5.1.1)$$

$$\varepsilon(\omega) = 1 - \frac{{\omega_p}^2}{\omega(\omega + i\gamma)} \qquad (2.5.1.2)$$

The variables constituting the equations are as follows: n_e is the number density of electrons; e is the electron charge; ω_p is the electron plasma frequency that describes the frequency with which the electrons would naturally oscillate given a small charge displacement; γ is the electron damping caused by internal collisions and radiation; and m_{eff} is the effective mass that the system exhibits and accounts for internal interactions and band structure characteristics. The dissipation term in the dielectric function becomes dominant when the discrepancy in frequency is significant; with the function necessarily assuming complex values. In conductive media, the plasma frequency generally resides within the ultraviolet spectrum and consequently requires adjustments to the arrangement of the structure to enable real valued negative permittivity below optical frequencies. For applications in the microwave frequency region, these adjustments come in the form of arrays of thin conductive wires that confine the electrons therein to amend their effective mass and density. The disparity in the magnitude to which these parameters are afflicted constitutes a collective decrease in the plasma frequency and subsequent decrease in the frequency required to achieve negative permittivity.

Conductive media similarly represent the practicable diversification of attainable magnetic properties in the absence of ferromagnetic materials through selectivity in feature topography [35]. The magnetic susceptibility (2.5.1.5) for the common circular split-ring element is derived from that observed in conductive cylinders with the addition of enhanced capacitive characteristics; where the capacitance is aided mutually by the separation between rings and internal discontinuities. The effective behavior of the system emulates an LC resonator and correspondingly induces a magnetic dipole moment when intercepting waves at its resonant

frequency. The bandwidth for negative permeability is determined by the separation between this resonant (2.5.1.3) and magnetic plasma (2.5.1.4) frequency where the induced dipole moment is out of phase with the incident wave. The interstice between frequencies is entirely resultant from the proportion of the area external to the conductive rings. Although variations on the split ring resonator exist, their fundamental operation remains similar to the original circular design.

$$\omega_0 = \sqrt{\frac{3dc^2}{\pi^2 r^3}} \tag{2.5.1.3}$$

$$\omega_p = \sqrt{\frac{3dc^2}{\pi^2 {r_i}^3 \left(1 - \frac{\pi {r_i}^2}{a^2}\right)}} \tag{2.5.1.4}$$

$$\mu_{eff} = 1 - \frac{\frac{\pi {r_i}^2}{a^2}}{1 + \frac{2b\sigma_1}{\omega r_i \mu_0} - \frac{3bc^2}{\pi\omega^2 \ln\frac{2w_r}{d} {r_i}^3}} \tag{2.5.1.5}$$

In the previous equations, the variables d and b denote the separation between the inner and outer rings in the unit cell and separation between consecutive rings in a stack; a is the lattice constant; σ_1 is the sheet resistance of the metal; w_r is the width of the rings; and r_i is the inner ring radius. The composite formed by the amalgamation of split ring and wire elements with aligned negative effective material parameters can operate as either a DNG or zero index medium over the frequency band limited by their regions of congruence. External to this region, the system may be classified as both single negative and double positive contingent on the strength of the alignment. Although variations on this configuration exist, the fundamental principles underlying their operation are predominantly homologous.

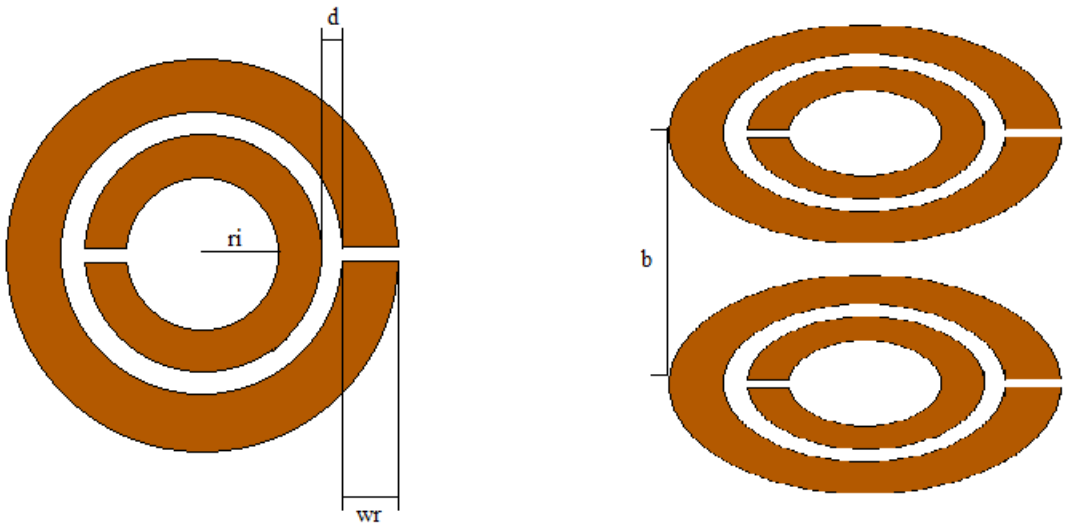

Figure 7: Split-ring resonator

2.5.2 Mie Theory and All Dielectric Metamaterial

The resonant conditions arising within externally illuminated particulate is asseverated by consequence of Mie theory; where the arguments of the vector potential comprising the internal and external fields are expansions of the spherical harmonics in the scalar domain [36,37]. The formulation necessitates the particle to exhibit approximate spherical symmetry and therefore implies a preference to the utilization of a spherical coordinate system. In this regard, the Fourier method enables the determination of the antecedent harmonic components through the solution to the scalar Helmholtz equation (2.5.2.2).

$$\Phi(r,\omega) = R(r)\theta(\vartheta)\varphi(\psi) \tag{2.5.2.1}$$

$$\left[\frac{1}{r^2}\frac{\delta}{\delta r}\left(r^2\frac{\delta}{\delta r}\right) + \frac{1}{r^2 sin\theta}\frac{\delta}{\delta\vartheta}\left(sin\vartheta\frac{\delta}{\delta\vartheta}\right) + \frac{1}{r^2 sin^2\vartheta}\frac{\delta}{\delta\psi} + k^2\right]\Phi = 0 \tag{2.5.2.2}$$

Substitution of the decomposition described by (2.5.2.1) which delineates radial, $R(r)$, polar, $\theta(\vartheta)$, and azimuthal $\varphi(\psi)$ contributions into (2.5.2.2) and subsequent multiplication by $\frac{r^2}{R\theta\varphi}$ leads to the resolution of the scalar field into three distinctive differential equations that are analogous to the separation functions. The associated constants m and $l(l+1)$ are introduced to effectuate this transition to divisible quantities. These differential equations have the solutions (2.5.2.3), (2.5.2.4), and (2.5.2.5), which determine the angular and radial dependence of the superimposed scalar function (2.5.2.6).

$$\varphi = e^{\pm im\psi} \tag{2.5.2.3}$$

$$\theta = P_l^m(cos\vartheta) = \frac{(1-cos\vartheta^2)^{m/2}}{2^l l!}\frac{d^{l+m}(cos\vartheta^2-1)^l}{d(cos\vartheta)^{l+m}} \tag{2.5.2.4}$$

$$R = \begin{Bmatrix} r^l \\ r^{-l-1} \end{Bmatrix} \tag{2.5.2.5}$$

$$\boldsymbol{\phi} = \begin{Bmatrix} r^l \\ r^{-l-1} \end{Bmatrix} P_l^m(cos\vartheta)e^{\pm im\phi} \tag{2.5.2.6}$$

Under the assumption of spherically symmetric potential, the radial components to the solution of Euler's equation, r^l and r^{-l-1} , can be inferred as indicative of the respective incident and transmitted or scattered field. In circumstances where this assumption is invalidated, the terms are replaced by the spherical Bessel's and Neumann functions of the first kind. The function that denotes the azimuthal dependence, $P_l^m(cos\vartheta)$, is the well-known associated Legendre polynomial whose derivation requires the separation constant, l, in the form described heretofore; a result that permits the convergence of the power series delineating θ. In literature, the scalar potential is customarily rewritten as a multipole expansion through the Laplace series

of spherical harmonics, $Y_l^m(\vartheta, \phi)$, which enables the isolation of radial and angular contributions (2.5.2.7). The harmonics represent the amalgamation of angular terms in the previous function.

$$\boldsymbol{\phi} = \sum_{l=0}^{\infty} \sum_{m=-l}^{l} (a_{lm} r^l + b_{lm} r^{-l-1}) \, Y_l^m(\vartheta, \phi) \tag{2.5.2.7}$$

where

$$Y_l^m(\vartheta, \phi) = (-1)^m \sqrt{\frac{(2l+1)(l-m)!}{4\pi(l+m)!}} P_l^m(cos\vartheta) e^{im\phi}$$

The coefficients, a_{lm} and b_{lm}, in (2.5.2.7) ensure that the potential is bounded with respect to the radial distance; remaining non-singular at the origin and finite as the interstice converges on infinity. This solution can be restated as a component of the independent vector equation equivalent. Neglecting the element corresponding to longitudinal waves, the constituents of the vector solution have the form:

$$M_{l,m} = \nabla \times \hat{r}(r\phi)$$

$$N_{l,m} = \frac{\nabla \times M_{l,m}}{k}$$

Wherein the harmonics of (2.5.2.7) describe the modes arising on the spherical particle; with $M_{l,m}$ and $N_{l,m}$ existing as solenoidal functions attributed to the relationship between electric and magnetic field quantities. The vector potential, A, can then be written as an amalgamation of these functions through (2.5.2.8).

$$A = \frac{i}{\omega} \sum_{l=0}^{\infty} \sum_{m=-l}^{l} \left(A_{l,m} M_{\,l,m} + B_{l,m} N_{l,m} \right) \tag{2.5.2.8}$$

The interdependence of the electric and magnetic fields accompanied by its established correspondence to the vector potential facilitates the formulation of these fields in terms of the vector spherical harmonics (2.5.2.9) and (2.5.2.10):

$$H = \frac{1}{\mu}\nabla \times A = \frac{-ik_m}{\omega\mu}\sum_{l=0}^{\infty}\sum_{m=-l}^{l}\left(A_{l,m}N_{l,m} + B_{l,m}M_{\,l,m}\right) \tag{2.5.2.9}$$

$$E = \frac{1}{i\omega\varepsilon}\nabla \times H = \frac{k_m}{\omega^2\varepsilon_m\mu}\sum_{l=0}^{\infty}\sum_{m=-l}^{l}\left(A_{l,m}M_{\,l,m} + B_{l,m}N_{l,m}\right) \tag{2.5.2.10}$$

The scattered and internal fields can then be derived as aggregated components of the comprehensive field through the insertion of appropriate coefficients - α_l, γ_l, β_l, and δ_l –which lead to (2.5.2.11) and (2.5.2.12).

$$H_{\begin{Bmatrix}s\\i\end{Bmatrix}} = \frac{-ik_m}{\omega\mu}\sum_{l=0}^{\infty}\sum_{m=-l}^{l}\left(A_{l,m}\begin{Bmatrix}\alpha_l\\\gamma_l\end{Bmatrix}N_{l,m} + B_{l,m}\begin{Bmatrix}\beta_l\\\delta_l\end{Bmatrix}M_{\,l,m}\right) \tag{2.5.2.11}$$

$$E_{\begin{Bmatrix}s\\i\end{Bmatrix}} = \frac{k_m}{\omega^2\varepsilon_m\mu}\sum_{l=0}^{\infty}\sum_{m=-l}^{l}\left(A_{l,m}\begin{Bmatrix}\alpha_l\\\gamma_l\end{Bmatrix}M_{\,l,m} + B_{l,m}\begin{Bmatrix}\beta_l\\\delta_l\end{Bmatrix}N_{l,m}\right) \tag{2.5.2.12}$$

These coefficients determine the amplitude of the field quantities as ascertained from their relationship with the relative size or size parameter, χ, and ratio of the refractive index between inclusion and base material or contrast parameter, א, of the scatterer. The resolution of their magnitudes is conducted by means of the continuity conditions on the tangential field components at the particles surface. The interest herein resides with the potential to develop functions for the electric and magnetic polarizabilities of the system as they relate to the scattering parameters. Therefore, the focus is restricted to the development of the scattering Mie coefficients α and β, which have the form:

$$\alpha_l = \frac{\aleph^2 j_l(\aleph\chi)[\chi j_l(\chi)]' - j_l(\chi)[\aleph\chi j_l(\aleph\chi)]'}{\aleph^2 j_l(\aleph\chi)[\chi j_l(\chi)]' - h_l(\chi)[\aleph\chi j_l(\aleph\chi)]'}$$

$$\beta_l = \frac{j_l(\aleph\chi)[\chi j_l(\chi)]' - j_l(\chi)[\aleph\chi j_l(\aleph\chi)]'}{j_l(\aleph\chi)[\chi j_l(\chi)]' - h_l(\chi)[\aleph\chi j_l(\aleph\chi)]'}$$

With

$$\aleph = n_{particle}/n_{background}$$

$$\chi = kr = \frac{2\pi r}{\lambda}$$

where j_l and h_l are the spherical Bessel and Neumann functions of the first kind. In applications where the particle radii are appreciably exceeded by the wavelength of the incident beam, the coefficients can be approximated by their first term in accordance with the Rayleigh scattering mechanism [38]. This approach assumes the behaviour of the particle as that of a solitary dipole and therefore neglects higher order terms. The coefficients can then be described by [13]:

$$\alpha_1 = j\frac{2}{3}({k_0}^2\mu_b\varepsilon_b)^{3/2}\frac{\mu_b - \mu_i F(\theta)}{2\mu_b + \mu_i F(\theta)}r^3$$

$$\beta_1 = j\frac{2}{3}({k_0}^2\mu_b\varepsilon_b)^{3/2}\frac{\varepsilon_b - \varepsilon_i F(\theta)}{2\varepsilon_b + \varepsilon_i F(\theta)}r^3$$

$$F(\theta) = \frac{2(sin\theta - \theta cos\theta)}{(\theta^2 - 1)sin\theta + \theta cos\theta}$$

$$\theta = k_0 r\sqrt{\varepsilon_i\mu_i}$$

where $F(\theta)$ is a function describing the angular dependence; ε_b and ε_i are the permittivity of the base dielectric and inclusion, respectively; μ_i and μ_b are the permeability of the background and inclusions; and *r* represents the inclusion radius. The scattering matrix elements are comprised

from the far field limit of equation (2.5.2.11 and 2.5.2.12) designated in accordance with its angular dependency; where they display solitary reliance on the first order Mie coefficients [38]. In accordance with the desire to develop effective attributes for media with spherical inclusions, it is convenient to revise the scattering parameters in terms of the electric and magnetic polarizabilities. The formulation can thereby ascribe the consolidated properties to Mie theory under the stipulated dipolar behaviour of the inclusions by association with the Rayleigh scattering mechanism [13].

$$S_1 = \frac{3}{2}[\alpha_1 + \beta_1]$$

$$S_1 = S_e + S_m$$

$$S_e = \frac{jk^3\xi}{4\pi\varepsilon_b}$$

$$S_m = \frac{jk^3\varrho}{4\pi\mu_b}$$

where S_e and S_m are the respective electric and magnetic dipole moments. The molecular propensity to initiate dipole formation as dependent upon the internal polarizabilities, ξ and ϱ, is attributed to the macroscopic permittivity and permeability through the Clausius-Mossotti relation. The atomic structure can be considered as archetypically analogous to the unified behaviour of the metamaterial; with the latter able to assume similar relations. Concomitantly, the polarizabilities determined by collation of the scattering parameter equations enable the development of effective material parameters for media with spherical inclusions as established through the Clausius-Mossotti method:

$$\frac{\varepsilon_{eff} - \varepsilon_b}{\varepsilon_{eff} + 2\varepsilon_b} = \frac{\eta_e \xi_e}{3\varepsilon_b} + \frac{\eta_m \xi_m}{3\varepsilon_b}$$

$$\frac{\mu_{eff} - 1}{\mu_{eff} + 2} = \frac{\eta_m \varrho_m}{3\mu_b}$$

with the terms η_e and η_m expressing the number densities of the electric and magnetic components. The internal polarizabilities are determined by comparison of the scattering parameter equations where the rectified spherical volume is replaced with the equivalent ratio of the comprised volume fraction:

$$\xi = \frac{3f\varepsilon_b}{n} \frac{\varepsilon_b - \varepsilon_i F(\theta)}{2\varepsilon_b + \varepsilon_i F(\theta)}$$

$$\varrho = \frac{3f}{n} \frac{1 - \mu_i F(\theta)}{2 + \mu_i F(\theta)}$$

It is assumed in the derivation that the background media is dielectric and accordingly has a permeability equivalent to free space. Upon substitution of the polarizabilities into the Claussius-Mossotti relation the equations delineating the effective values for permittivity and permeability become (2.5.2.13) and (2.5.2.14).

$$\frac{\varepsilon_{eff} - \varepsilon_b}{\varepsilon_{eff} + 2\varepsilon_b} = f_e \frac{2\varepsilon_b + \varepsilon_i F(\theta_e)}{\varepsilon_b - \varepsilon_i F(\theta_e)} + f_m \frac{2\varepsilon_b + \varepsilon_i F(\theta_m)}{\varepsilon_b - \varepsilon_i F(\theta_m)} \qquad (2.5.2.13)$$

$$\frac{\mu_{eff} - 1}{\mu_{eff} + 2} = f_m \frac{2 + \mu_i F(\theta_m)}{1 - \mu_i F(\theta_m)} \qquad (2.5.2.14)$$

Where,

$$f_e = \frac{4}{3}\pi \frac{{r_e}^3}{s^3}$$

$$f_m = \frac{4}{3}\pi \frac{{r_m}^3}{s^3}$$

$$\theta_e = k_0 r_e \sqrt{\varepsilon_i \mu_i}$$

$$\theta_m = k_0 r_m \sqrt{\varepsilon_i \mu_i}$$

where f_e and f_m are the relative volume fraction of the inclusions; r_e and r_m are the electric and magnetic coupling particle radii; and s is the lattice constant. It is assumed that the inclusions are non-magnetic such that μ_i can be given a value of 1. The equations can then be rewritten in terms of the effective material parameters (2.5.2.15 and 2.5.2.16).

$$\varepsilon_{eff} = \frac{2\left(\frac{f_e}{\varepsilon_b}\frac{2\varepsilon_b + \varepsilon_i F(\theta_e)}{\varepsilon_b - \varepsilon_i F(\theta_e)} + \frac{f_m}{\varepsilon_b}\frac{2\varepsilon_b + \varepsilon_i F(\theta_m)}{\varepsilon_b - \varepsilon_i F(\theta_m)}\right) + 1}{1 - \frac{f_e}{\varepsilon_b}\frac{2\varepsilon_b + \varepsilon_i F(\theta_e)}{\varepsilon_b - \varepsilon_i F(\theta_e)} + \frac{f_m}{\varepsilon_b}\frac{2\varepsilon_b + \varepsilon_i F(\theta_m)}{\varepsilon_b - \varepsilon_i F(\theta_m)}} \qquad (2.5.2.15)$$

$$\mu_{eff} = \frac{4f_m + 2f_m\mu_i F(\theta_m) + \mu_i F(\theta_m) - 1}{1 - \mu_i F(\theta_m) - 2f_m - f_m\mu_i F(\theta_m)} \qquad (2.5.2.16)$$

From the derivation, it follows that a material comprised of a doubly periodic array of embedded dielectric spheres, as depicted in Figure 4, display a negative refractive index where the first electric and magnetic resonance modes coincide and the effective material parameters consequently take on negative values. This type of resonance is known classically as morphologically dependent and arises as the combined result of a large contrast in the material parameters of the inclusion and surrounding media, and size distributions of the particles.

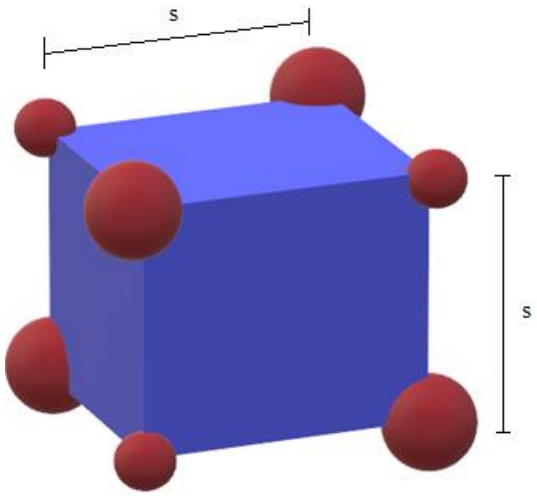

Figure 8:Cubic lattice of doubly periodic spherical inclusions

III. EXPERIMENTAL PROCEDURE AND EVALUATION

3.1 Patch Antenna Model

Consideration of the rectangular patch region as an equivalent semi-infinite homogeneous system establishes a one-dimensional problem whose resolution can be instituted by the transfer matrix method. The Schneider model discussed previously capacitates effective medium properties to be used in lieu of the heterogeneous antenna system. The contribution of patch geometry to the effective permittivity is governed by the width of the conductive rectangular element and likewise amenable to the desired resonant frequency and substrate permittivity. The form of this relationship is given by (2.1.6) and rewritten here for convenience.

$$w = \frac{c}{2f_r}\sqrt{\frac{2}{\varepsilon_s + 1}}$$

In accordance with the above formulation, an increment in the permittivity of the substrate material implies a reduction in the width of the patch necessary for resonance at a given frequency. Variability in this permittivity is therefore anticipated and dependent upon the design constraints for the system in a trade-off with performance. Regarding the permittivity indiscriminately within a region of interest allows the development of a general procedure for sublayer formation. This region is selected to be congruent with a given lower and upper extremity in substrate values from which a unity step is sufficient to provide a general trend in the transmittance attributes. Although commonly in the range of 2.2 to 12, substrate permittivities greater than 35 have been reported in literature [39,40]. It is readily verifiable that the first few lowest terms have an inconsequential effect on transmittance and can accordingly be neglected. Furthermore, it is anticipated that the magnitude of the negative refractive index required to negate attenuation of the transmitted signal scales with the permittivity of the

substrate; precluding inordinately high permittivity substrates. A suitable region is therefore selected to be confined within a median of permittivity values extending from 5 to 30.

In a frequency division duplex scheme, a guard band between the uplink and downlink channels is necessary to prevent errors and non-idealities in the system from impeding the performance characteristics of the distinctive transmit and receive antennas [41]. Regarding the development of the Schneider model approximation of the patch, the selection of channel separation utilized is somewhat arbitrary as the dielectric relaxation in the permittivity predominantly responsible for variation in the effective permittivity is insubstantial within a small spectral region outside of electron resonance as discussed further in section 3.5. Where wide frequency separations are present, the inverse proportionality that the resonant frequency shares with the patch width can be predicated to more significantly impact the effective constant value. The center frequency for transmission and reception are chosen to correspond with the X and Ku frequency bands and have values of 9 and 14 GHz, respectively. The frequencies selected herein can be viewed as overemphasizing the guard band in the transmit/receive scheme. However, the separation is such that the transmission frequency is almost entirely deterministic of the transfer behaviour; with the same procedure remaining viable irrespective of the frequencies chosen.

Within a free-space region, the transfer matrix equation for the effective patch model has a form concomitant with equation (2.4.17), as given by (3.1.1).

$$T_{tot} = T_b^{air,patch} T_\varphi^{patch} T_b^{patch,air} \tag{3.1.1}$$

Under the assumption of normal incidence, the Fresnel coefficients constituting the amplitude matrices can be formulated from column 3 of Table 1 with the refractive indices n_{air}=1.00027 and $n_{patch}=\sqrt{\varepsilon_{eff}}$ (3.1.2a,b,c,d).

$$\Gamma_{air,patch} = \frac{n_{air} - n_{patch}}{n_{air} + n_{patch}} \quad (3.1.2a)$$

$$T_{air,patch} = \frac{2n_{air}}{n_{air} + n_{patch}} \quad (3.1.2b)$$

$$\Gamma_{patch,air} = \frac{n_{patch} - n_{air}}{n_{air} + n_{patch}} \quad (3.1.2c)$$

$$T_{patch,air} = \frac{2n_{patch}}{n_{air} + n_{patch}} \quad (3.1.2d)$$

In accordance with the Schneider model, the effective permittivity and thickness are contingent upon the substrate height. Observation of the effect of permittivity independent of this variable requires its contribution to the coefficient and phase matrix to be negated by holding it at a constant value. The substrate height is therefore selected to be 1.6 mm throughout simulation.

The transfer matrices were evaluated in the MATLAB environment as functions of the input substrate permittivity and transmission carrier frequency to determine the transmittance of the patch antenna at each value of the dielectric constant. For convenience, the effective permittivity was resolved distinctly in correspondence with its efficacy throughout all stages of the simulation. With the individual permittivities, frequencies, and patch dimensions given as above, the transmittance through the homogenized layer can be plotted as in Figure 9.

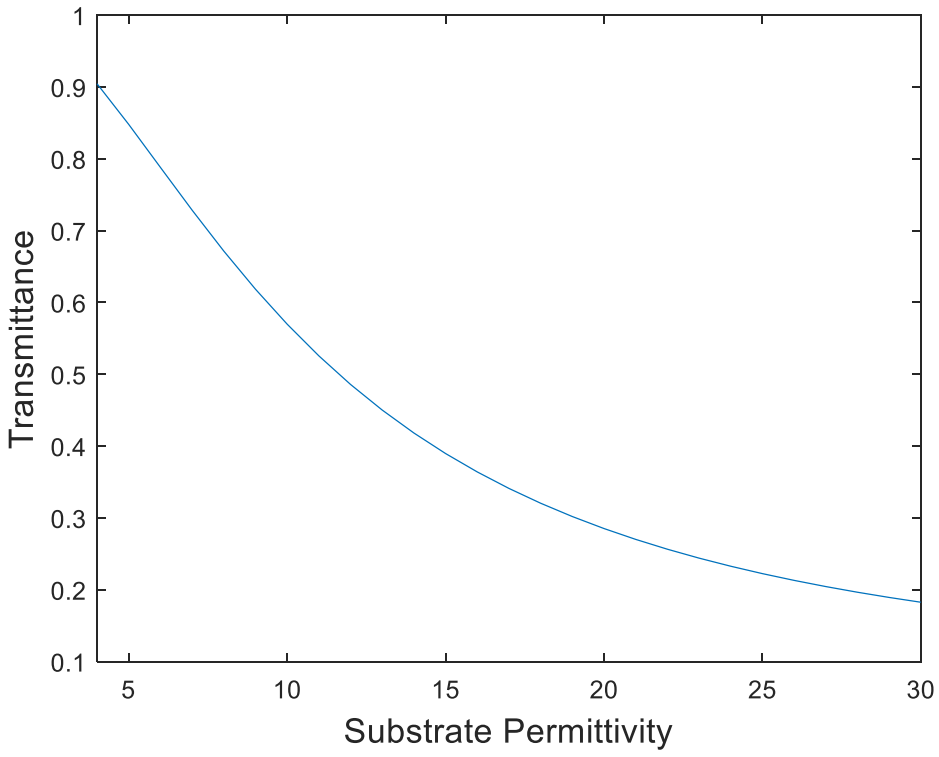

Figure 9:Transmittance versus substrate permittivity for a rectangular patch with a resonant frequency of 14 GHz being bisected by transmission at a frequency of 9 GHz

It is readily understood from the derivation in section 2.4 that the reflected wave at the initial interface increases with the difference in the refractive index between free-space and the substrate material. Their magnitudes grow or diminish as the result of subsequent reflection that add up in or out of phase. The outcome displayed above can therefore be seen as indicative of increasing reflection from the initial boundary, abated, slightly, by moderately out of phase reflections from the foremost interface. In the absence of a corrective layer, the potential destructive interference is governed only by the effective impedance and thickness of the patch antenna model.

3.2 Optical Glass Transfer

Pursuant to the inefficiencies in transmittance displayed in evaluation of the patch antenna transfer matrices, it is evident that the system requires rectification through the imposition of conditions on the transfer properties in accordance with a known high transmittance reference. Unlike the finite boundaries of a cavity region that can be tuned to facilitate destructive interference of reflected waves within the cavity itself, the specular reflection into free-space is restricted by phase misalignment with the total backward propagating waves from the upper regions. Although theoretically plausible, it is anticipated that the compensatory effect generated by the sublayer cannot be presumed to enable complete transmission through the medium but can be made to predominately negate the backward travelling wave. The high transmittance reference does not presuppose speculative full transmission of the wave through the medium but relies on an example of a real system to define its properties. For a given thickness, crown glass variants operating in the visible frequency region are attributed with favourable transparency resulting from the exhibition of refractive indices on the order of free-space [42]. The ubiquity in industrial application and corresponding abundance of documentation designate SHOTT B270 Ultra-White crown glass as preponderant to the investigation [43]. This variant is recognized as having a refractive index of 1.523 at a wavelength of 598 nm and exhibits luminous transmittance of 91.7 percent when the layer thickness is set at 2 mm. Following a similar procedure to that detailed in the previous section, an iterative examination of the transmittance for a range of layer thicknesses can be executed to determine the optimal value. In a physical system, the molecular dissipation of energy through dipole formation is mathematically accounted for by the imaginary component of the material parameter. This component is often disregarded in transfer matrix formulation and can correspondingly lead to systems exhibiting

specious unity transmittances. For such a reference system, the additional reduction in the available equation set resultant from the null reflectance establishes an underdetermined problem in the designable parameters of the sublayer; thereby precluding it from further consideration. It is however, plausible for a given system to have a transmittance exceeding 99 percent under the condition of a low loss tangent in the constituent materials. For this reason, only layer thickness yielding transmittances on the order of 99 percent are considered. In this system, the transfer matrix has the following form (3.2.1).

$$T_{tot} = T_b^{air,glass} T_\varphi^{glass} T_b^{glass,air} \tag{3.2.1}$$

Under the assumed refractive index and wavelength, the transmittance was evaluated for every glass thickness in the range 1 mm to 20 mm at an increment of 250 μm. Despite considerable sensitivity of the transmittance to variation in the layer thickness, the differences in the peak values are exiguous; permitting the desired behaviour to be selected arbitrarily. For this purpose, the 19 mm thickness was determined to be sufficient; displaying a transmittance and reflectance of 0.9925 and 0.0075, respectively.

3.3 Basic Properties of the Sublayer

By consequence of the result detailed in the previous section, a system of equations can be formulated in accordance with the prospective transmittance and reflectance to yield the necessary thickness and refractive index of an unknown antecedent layer (3.3.1a,b).

$$\mathfrak{T}(T_{glasstot}) = \mathfrak{T}(T_b^{air,unk} T_\varphi^{unk} T_b^{unk,ant} T_\varphi^{ant} T_b^{ant,air}) \tag{3.3.1a}$$

$$\mathfrak{R}(T_{glasstot}) = \mathfrak{R}(T_b^{air,unk} T_\varphi^{unk} T_b^{unk,ant} T_\varphi^{ant} T_b^{ant,air}) \tag{3.3.1b}$$

Where $\mathfrak{T}(T)$ and $\mathfrak{R}$(T) represent the transmittance and reflectance taken from the respective transfer matrices according to equations (2.4.18) and (2.4.19).

The quantities arising from the right-hand side of the previous equation pertain to a nonlinear set in the design variables concordant with the definitions in (2.4.15) and (2.4.16). For a system of functions delineated by the operation (3.3.2) which display nonlinearity with respect to x, it is possible to resolve the components utilizing a minimization of the sum of squares. The trust region method employed in the MATLAB function *fsolve*, appropriates a proportion of a quadratic model around a given search point considered to adequately approximate the behaviour of the function, as a designated trust region [44]. The model is chosen to be congruous with the first two terms of the Taylor series expansion for the function whereby a fluctuating spherical or ellipsoidal region defines the sufficiency.

$$F(x) = 0 \tag{3.3.2}$$

$$q_k(p) = f(x_k) + \nabla f(x_k)^T p + \frac{1}{2} p^t B_k p$$

To reduce the run time, the optimization solver confines the trust region to a surface whose extent is determined by a preconditioned conjugate gradient process. The dogleg method applies a polygonal approximation to the curvilinear path instated by the quasi-Newtonian simplified model of the function Hessian. Although the resolution to the thickness and refractive index from equation (3.3.1a,b) is theoretically achievable utilizing the trust region method under these simplifications, in practice, the algorithm failed to yield satisfactory results.

For a system in which the solution space is constrained to a definitive region of expected values in the unknown quantities, the method of residuals at discrete locations along a fine mesh of the space can provide reasonable agreement to the desired system behaviour. Regarding the properties of the sublayer, the residual can be defined as the absolute magnitude of the difference between the transmittance value attained from the nodal position coincident with specified values

of the index and layer thickness, and the transmittance as determined for B270. As predicated in the work in reference [5], negative refractive indices were implicated but not presupposed to demarcate the solution space. Concordant with the values assumed for antireflection coating applications, the supposition of positive indices in the sublayer can reasonably ameliorate transmittance and represent a prospective reduction in system complexity. It is therefore suitable to uniformly distribute the refractive index in a region extending both negative and positive values; with upper and lower bounds extending the region from -7 to 7, respectively. In this region, the complementary media based cancellation is possible as a result of the bounds incorporating negative refractive indices on the order of the effective refractive index for the patch antenna. The layer thickness can be similarly restricted to a region wherein the dimensions are considered reasonable with respect to fabrication limitations without impeding practicability. For this application, a region extending from 1 mm to 15 mm is utilized. Although these dimensions appear excessive, it is important to remember that the metamaterial requires at least one cubic lattice to conform to the provided space. The subspace is evenly segmented into 50 nodal points along each unknown variable axis where the minimum of the residual is found in agreement with the thicknesses and indices of Figures 2 and 3. The difference equation comprising the residual introduces non-unique solutions in the refractive index that exist as reflections about the origin. These reflected terms, hereafter referred to as complementary, can be seen in Figure 2a and are enhanced in 2b and 2c to better display the values.

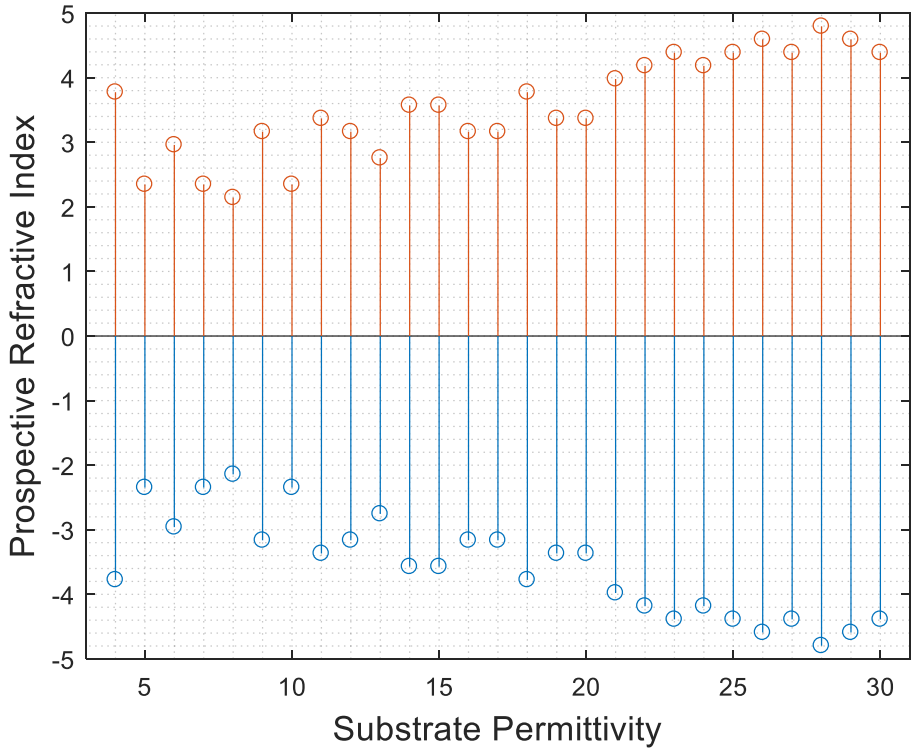

Figure 10: Prospective required refractive index to attain desired transmittance

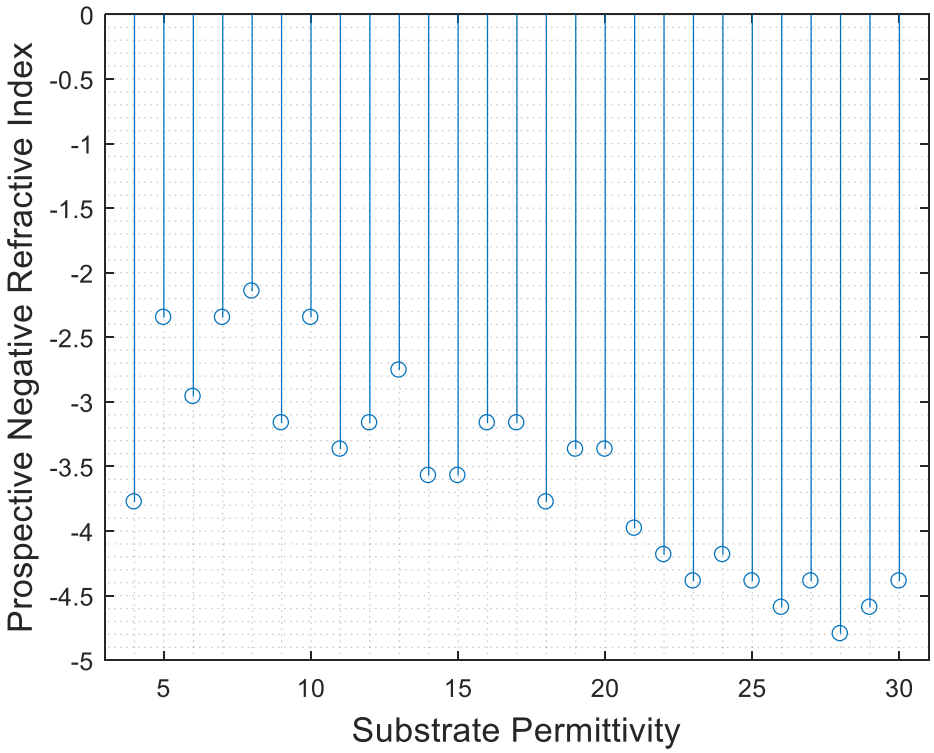

Figure 11: Enhanced view of the negative index case

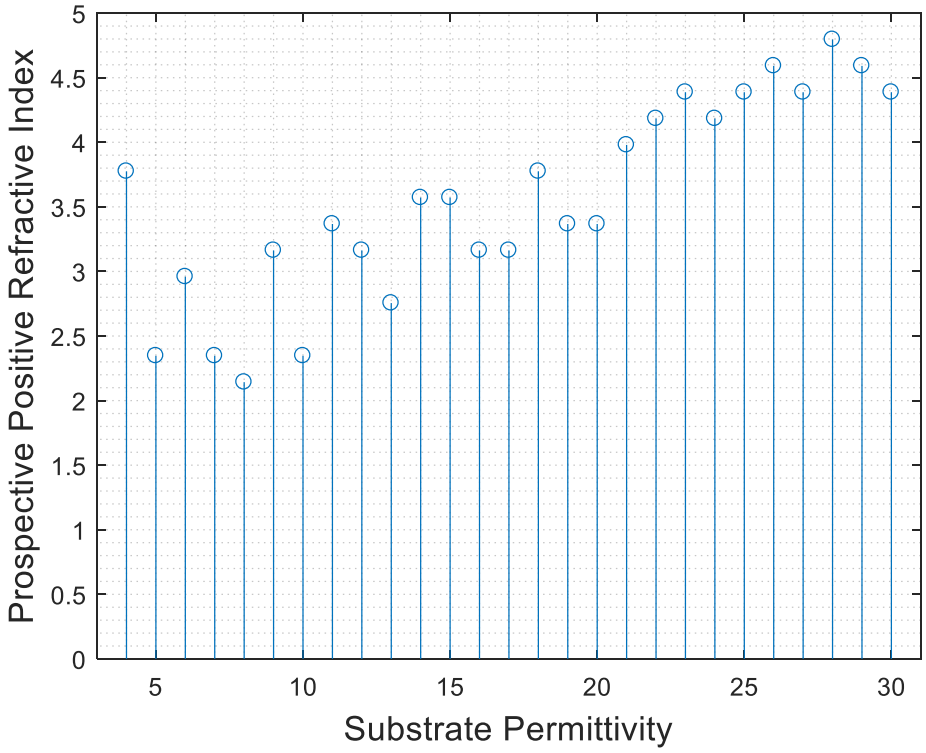

Figure 12: Enhanced view of the positive index case

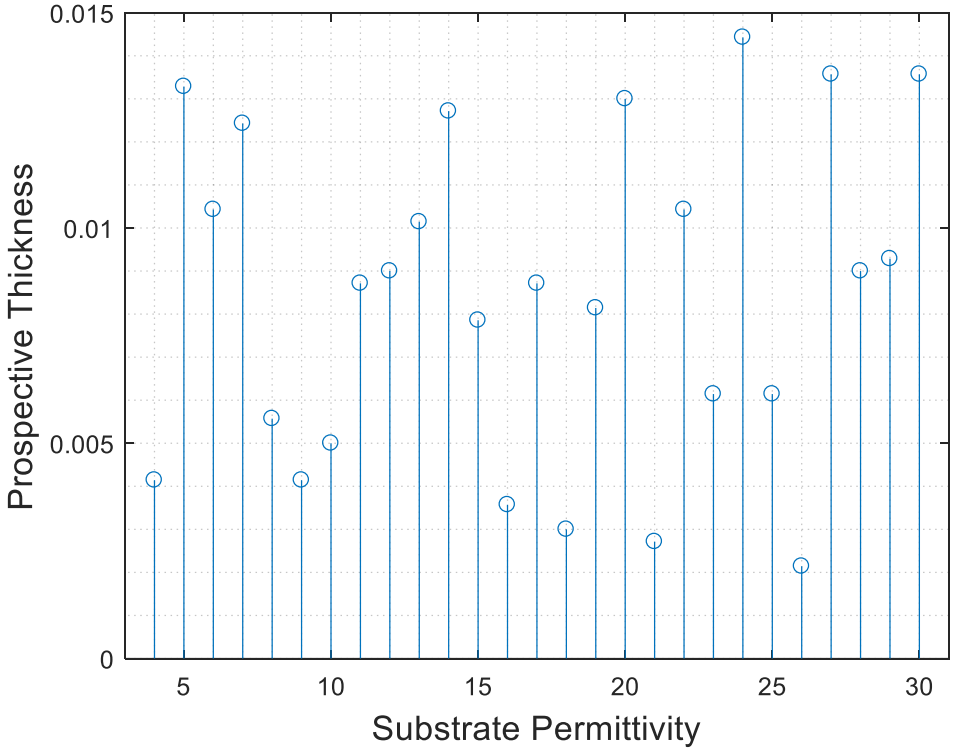

Figure 13: Prospective required thickness to attain desired transmittance

It can be understood from the negative indices of Figure 2b that the complementary media interpretation is not applicable as the subsumed material parameter values in the determined refractive indices are incongruous with the negative of the corresponding effective medium interpretation of the patch antenna [2]. Moreover, considering the thicknesses presented in Figure 3 with the index determined at the same substrate permittivity, the phase change in the medium can be resolved to indicate discrepancies with those required for Fabry-Perot resonance to occur in the cavity ($k_n d = (2n + 1)\pi/2$) [1]. This is likely a consequence of the effective medium theory which regards the system as a homogenized dielectric and therefore renders some of the conductive features nondescript. Subsequently, the resonance shifting condition in the cavity which is emplaced through an additional requirement on the surface conductivity in relation to the permittivity of the dielectric medium cannot be accurately described by the current method. It is important to acknowledge that the plane wave represents a cyclic function wherein the phase change exhibited at a given thickness in a medium is recurrent. The thickness values detailed in the figure are therefore not unique solutions to the transmittance problem but exist as a product of the utilized solution space. Reducing the lower boundary on the layer thickness enables the consideration of substantially thinner regions that are more appropriate and practical for regular dielectric composites but can prevent the formation of the metamaterial lattice. The refractive index is likewise an element in the phase shift term through its contribution to the wavenumber, however, this value is not exclusively deterministic of its value due to the presence of the Fresnel coefficients in the formulation. It can be seen that the reflected terms of the refractive index depicted in Figures 2b and 2c show a piecewise linear progression that increases in magnitude in accordance with the substrate permittivity. The discontinuity in the distribution is a consequence of the discretization process on the substrate and unknown constituent values that lead to

quantized solutions with inexact congruence to the desired transmittance. The transmittance attained through this process is presented in the figure below.

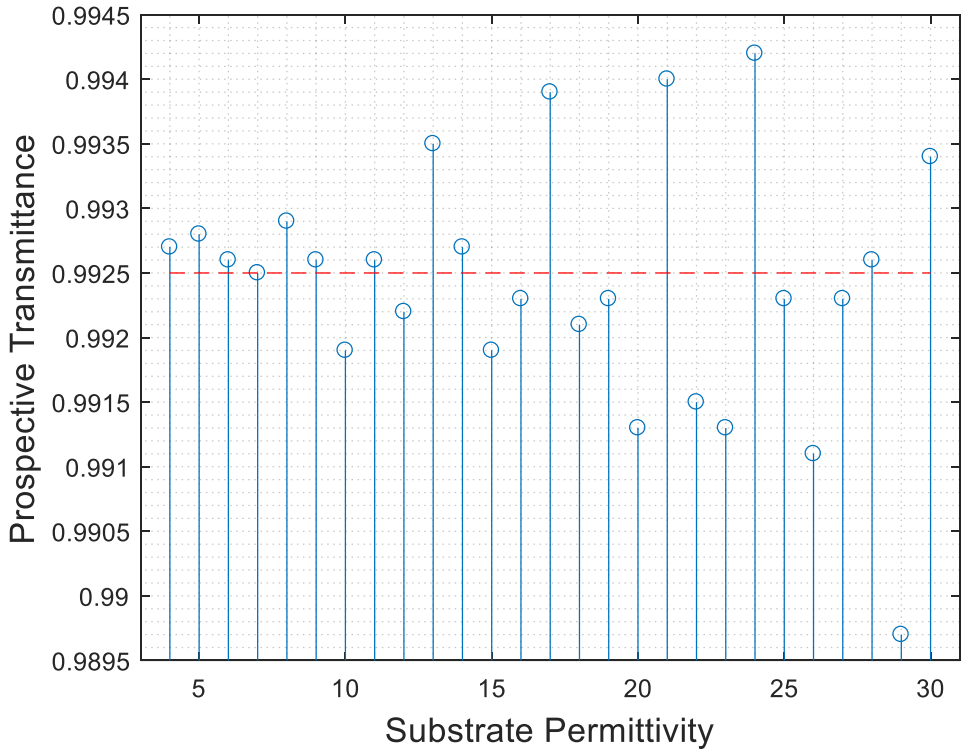

Figure 14: Achievable Transmittance with the sublayer in place

The transmittance can be perceived to fluctuate about the desired value with a mean of 0.9924 and a maximum offset from the expected value of 0.28 percent in both the negative and positive index cases. Increasing the number of sample locations along the discretized subspace can yield improved correlation for both cases at the cost of computation time. Further restriction on the parameters of the sublayer emplaced by enhancement in the precision would denote refined tolerances; with the consequence of reduced expediency in fabrication and concurrent reduction in economy. The concession to values exhibiting minor discrepancy with regard to the transmittance metric can therefore be vindicated as required to maintain practicability.

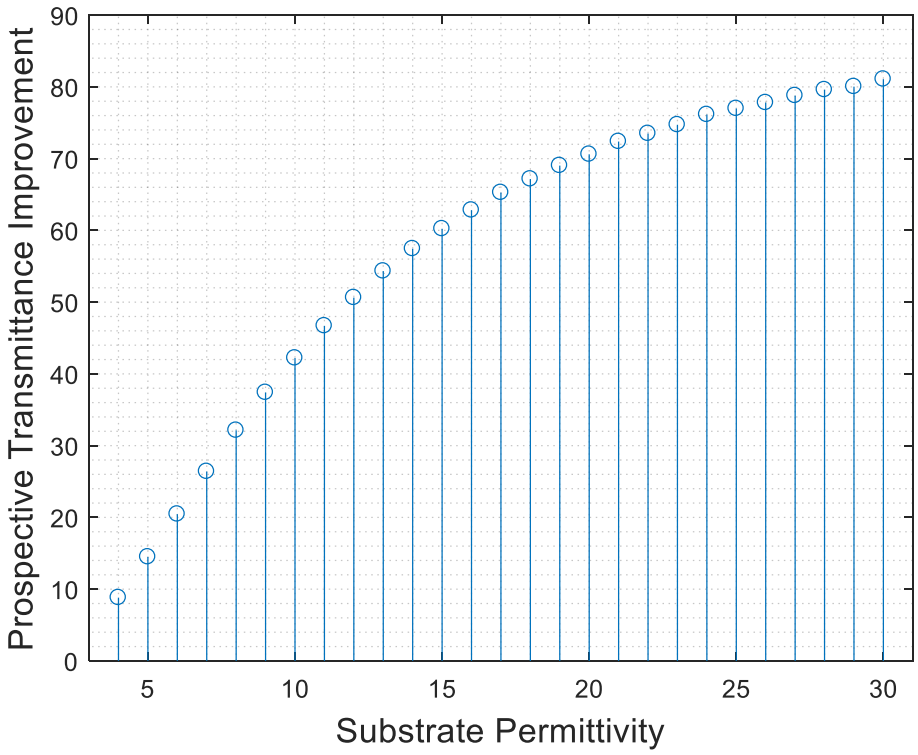

Figure 15: Achievable improvement in the transmittance over the original system

Comparison of the transmittance behaviour established for the layered system to that of the isolated patch antenna indicates a prospective gain as illustrated in Figure 5; where the sublayer can be seen to provide a compensatory effect whose magnitude compliments the original system.

3.4 Metamaterial Design

The complementary index values for the sublayer, consistent with the analysis of the preceding section, institute the use of a composite whose effective properties resemble their magnitude and sign. Pursuant to the discussion of section 2.7, the split-ring resonator/wire configuration is precluded based on introducing additional coupling elements to the system and consequently abating the designs utility. The investigation is therefore restricted to all-dielectric permutations

involving resonant spherical inclusions; wherein refinement of lattice dimensions and constituent permittivities facilitate the effective behaviour to be procured in congruence with the desired. From equations (2.5.2.15) and (2.5.2.16), the refractive index for the all-dielectric metamaterial can be written as (3.4.1).

$$n_{eff} = \sqrt{\varepsilon_{eff}\mu_{eff}} \tag{3.41}$$

Inconsistencies in the formulation arise when the effective material parameters assume concomitantly negative values whereby the function would erroneously predict equivalency to the corresponding positive system. For this reason, a variable whose value is given by the inequality operator (3.4.2) is introduced to the right-hand side to differentiate between the prospective causata.

$$i^{((\varepsilon_{eff}<0)\&\&(\mu_{eff}<0))\times((\varepsilon_{eff}<0)+(\mu_{eff}<0))} \tag{3.42}$$

In a system for which the effective material parameters are positive valued, the sign rectification operator yields a result of unity. Contrastingly, a double negative system will produce a likewise negative value concordant with the square of the imaginary number, *i*. It can be seen that the operator holds a value of one concurrently for parameters associated with imaginary indices; however, the fitness of the objective function can be made to reflect this attribute through a Boolean expression that reduces the value of the objective function to zero in instances where an imaginary index is encountered.

The effective medium parameters comprising the refractive index equation imply that ambiguity exists in the solution set for the unknown internal radii and permittivity instated by the underdetermined nature of the equality with the single known desired value. The degrees of freedom for the problem can be reduced by assuming that the constituents are non-magnetic and

that the base material exhibits permittivity on the order of free-space. In the microwave frequency region, this assumption is validated by the presence of foam composites whose permittivity can be approximated as free-space as a result of air filled inclusions within the matrix of the material. Incongruously, the values for the remaining unknown constituent properties of the metamaterial cannot be regarded as independent variables and consequently, require system solver to determine.

In a sequential quadratic programming approach, the nonlinear underdetermined objective function is regarded in terms of quadratic approximations at each step that regulate the following iterative in congruence with their resolution [45]. These subproblems are formulated from the quadratic model of the Lagrangian through a Taylor series expansion in the unknown quantities subject to a linearized variant of the real system equality and inequality conditions. For a system whose Hessian is positive semidefinite, the quadratic method becomes a convex problem and accordingly parallels the simplicity of its linear counterpart. The utility of this technique therefore lies in its ability to resolve complex nonlinear systems to a sequence of more manageable quadratic systems which resemble local properties of the original. At each iteration, the multipliers of the Lagrangian are adjusted in congruence with the optimum value for the subproblem. An ancillary term denoting the progress of the system in relation to the desired behaviour is introduced to ensure global convergence. The SQP algorithm can be implemented in MATLAB as an option in the *fmincon* function [46]. Regarding the metamaterial design for reflection mitigation proposed in congruence with the previous subsections, the objective function can be specified as having the form (3.4.3).

$$\min_{x} \left| n_{desired} - n_{eff} \right| \tag{3.4.3}$$

where *x* denotes a vector of the remaining unknown variables ε_i, s, r_e, and r_m. The constitutive effective term establishes a deficiency in the current implementation resulting from the potential to assume complex values that cannot be adequately negotiated by the algorithm. Consequently, a viable solution is attainable only through the introduction of a conditional operator that nullifies the effective terms exhibiting complex or imaginary quantities. A more computationally efficient permutation of the instated objective function supersedes the refractive indices with their corresponding transmittance value as given below (3.4.4).

$$\min_x \left| \mathfrak{T}_{desired} - \mathfrak{T}_{eff} \right| \tag{3.4.4}$$

This equation is subject to the inequality conditions (3.4.5a,b).

$$r_e + r_m < s \tag{3.4.5a}$$

$$r_e + r_m + s < d \tag{3.4.5b}$$

where the first inequality delineates the requirement for the inclusions to remain distinct which is contingent upon the value of the lattice constant exceeding the sum of inclusion radii; and the second inequality ensures that the total width of the cubic lattice is less than the metamaterial thickness. In the *fmincon* function, these inequalities are imposed by a similar condition which permits the equivalence of left and right-hand sides (3.4.6).

$$A \cdot x \leq B \tag{3.4.6}$$

It is therefore necessary to verify that the conditions have been satisfied proceeding each function evaluation. The elements of the matrix A are given as the coefficients of the unknown variables in the inequalities distinguished in accordance with the row occupied. In terms of the conditions recorded in (3.4.5a,b), the matrix equation has the form (3.4.7).

$$\begin{bmatrix} 0 & 1 & 1 & -1 \\ 0 & 1 & 1 & 1 \end{bmatrix} \begin{bmatrix} \varepsilon_i \\ r_e \\ r_m \\ s \end{bmatrix} \leq \begin{bmatrix} 0 \\ d \end{bmatrix} \tag{3.4.7}$$

This equation can be implemented directly in the *createOptimProblem* function along with specified conditions on the starting point and lower and upper bounds on the unknown variables [47]. The effective medium approximations instate a supplementary constraint on the analysis for inclusion permittivity to high value regions in contrast with the base as a means of achieving negative refractive indices; the highest value of which is selected to be consistent with variants of barium strontium titanate [48]. Concomitantly, the inclusion radii are selected such that their sum is less than the lattice constant at each boundary. Pursuant to the default step-size for the *fmincon* function, it is beneficial to set the permittivity as a predefined proportion of the real value which is subsequently rectified upon substitution into the effective refractive index equation. In this regard, the lower and upper bounds can be given as follows:

	$\frac{\varepsilon_i}{10^7}$	r_e	r_m	s
L_B	2×10^{-5}	1×10^{-6}	1×10^{-6}	4×10^{-5}
U_B	1×10^{-4}	1000×10^{-6}	1000×10^{-6}	500×10^{-5}

Table 2: Lower and upper bounds on the design variables

The upper bound on the radius of the magnetic inclusions can be observed to exceed the limit set on the corresponding electric inclusions which is consistent with the requirement for the metamaterial to engage separate modes concurrently. The initial evaluation point is chosen to be arbitrarily situated within this search region circumscribed by the upper and lower bounds.

$$x_0 = [7 \times 10^{-5}, 50 \times 10^{-6}, 100 \times 10^{-6}, 400 \times 10^{-5}]$$

To prevent convergence to a local minimum in an objective function exhibiting high variability, an algorithm that distributes sample locations throughout the solution space can be instituted. Provided an initial search location, the *MULTISTART* algorithm in the MATLAB optimization toolbox generates k-1 random additional locations which independently converge to minima in the solution space; with the contributions that led to the best fit, recorded in the output vector, *x* [49]. In accordance with the degrees of freedom introduced by the metamaterial parameter equations, the solutions achieved by this algorithm are not unique but exist as sets which independently satisfy the minimization criteria of the objective equivalently. The results obtained in this section consequently illustrate one possible configuration and provide a template for further evaluation. It is also important to consider the potential for the randomly distributed initial search locations established by the MULTISTART algorithm to exist outside of the preferred domain of the unknown parameters. The options for the algorithm can be made to reject these infeasible initial locations in accordance with the boundary and inequality conditions by setting the *StartPointsToRun* property to *'bounds-ineqs'*. Explicit delineation between positive and negative index values in the objective function is inhibited by the subsumed transmittance values wherein information about the sign of the material properties is lost. It is therefore necessary to instate this condition in the transmittance equation through a Boolean operator that provides poor fitness based on the sign of the desired quantity. To illustrate this property, consider the case of a negative valued objective for the refractive index. Following from the previous section, concurrent maxima in the fitness of the transmittance are evident at complementary values of the index. In order to classify the terms such that only constituents

yielding negative values are considered, a penalty is emplaced upon the positive index transmittance on the order of fifty percent of the maximum attainable value:

$$\mathfrak{T} = \mathfrak{T} - \frac{1}{2}(sign(n) \geq 0)$$

Similarly, the positive index equivalent can be enforced by inverting the sign of the inequality operator. Specifying the conditions as stated above within the *fmincon* function and utilizing a fifty point *MULTISTART* yields the values of the unknown variables as detailed in the following figures. To this end, a brief demonstration of the fallibility of the approach is provided.

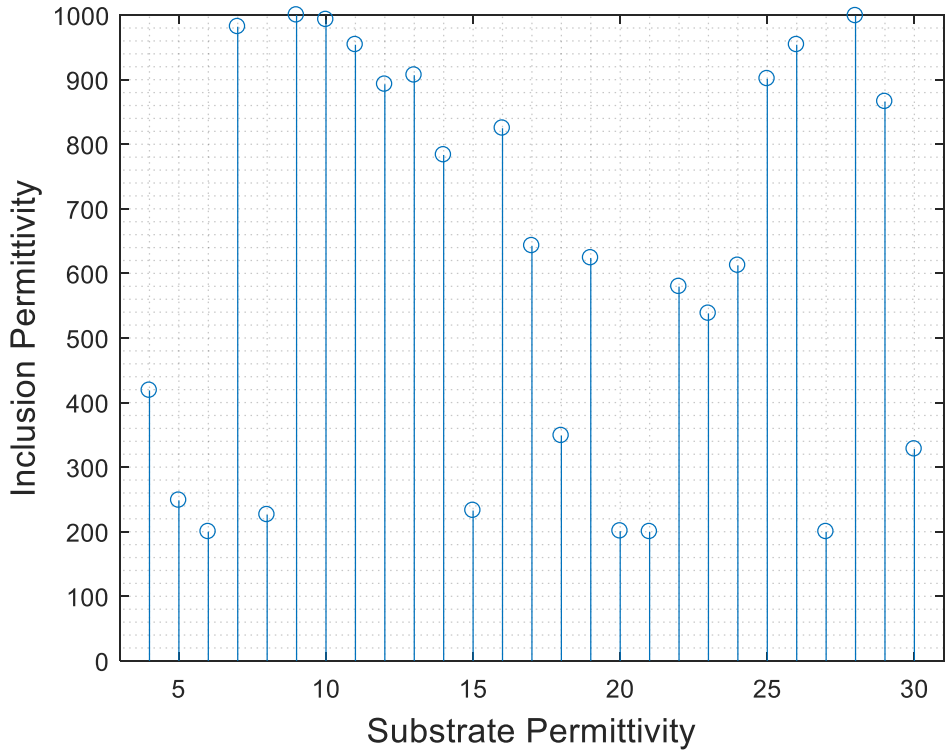

Figure 16: Required inclusion permittivity for the positive refractive index implementation

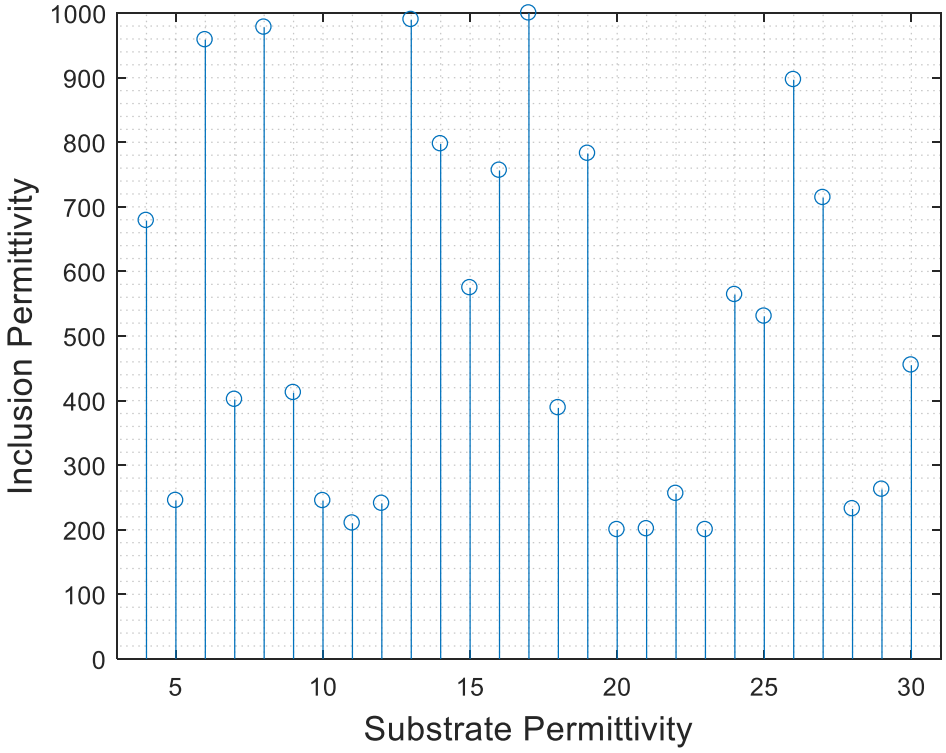

Figure 17: Required inclusion permittivity for the negative refractive index implementation

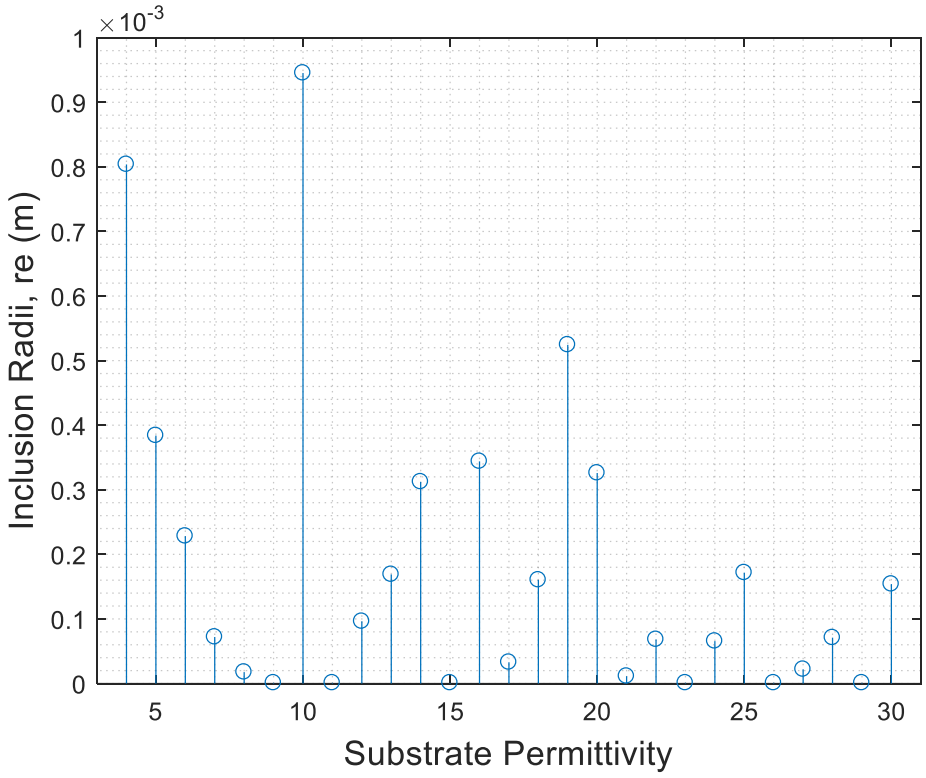

Figure 18: Required electric mode inclusion radii for the positive refractive index implementation

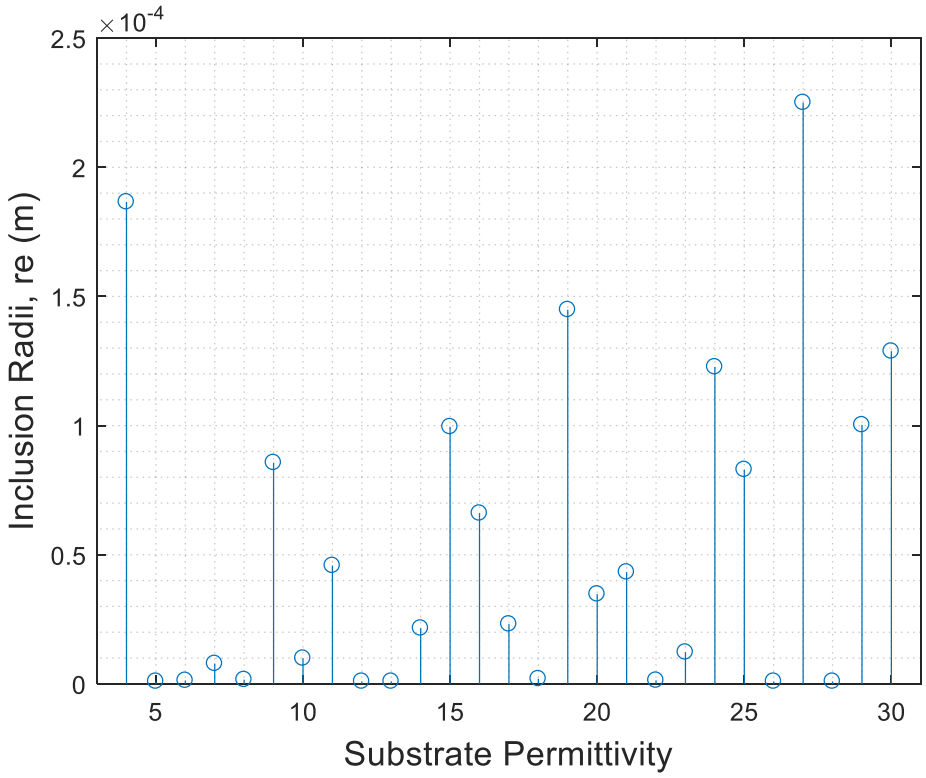

Figure 19: Required electric mode inclusion radii for the negative refractive index implementation

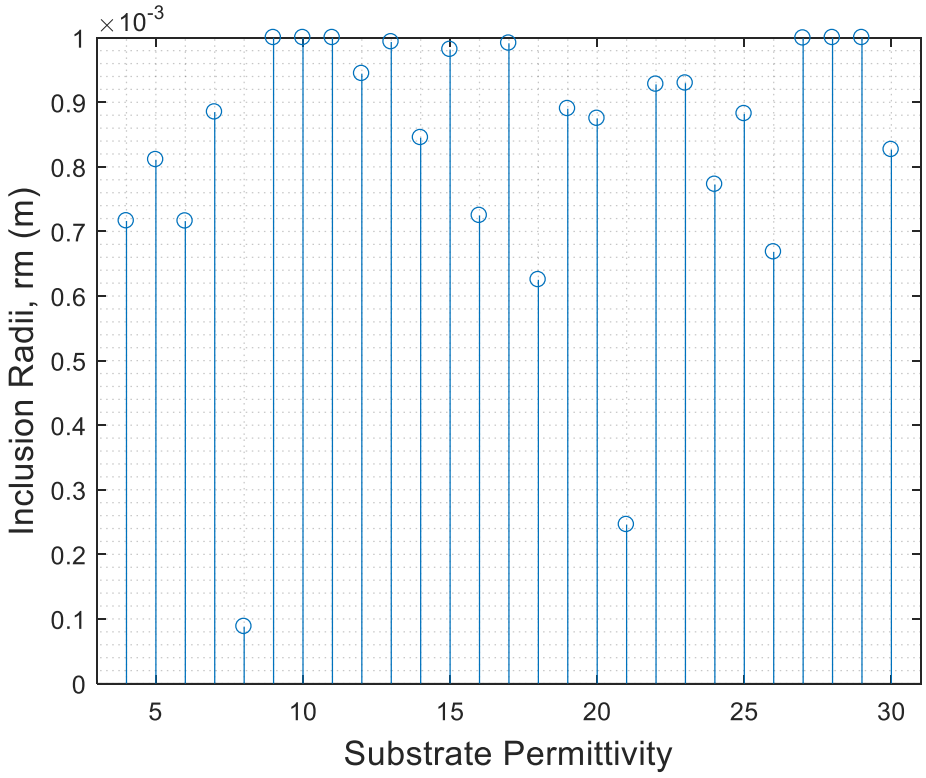

Figure 20: Required magnetic mode inclusion radii for the positive refractive index implementation

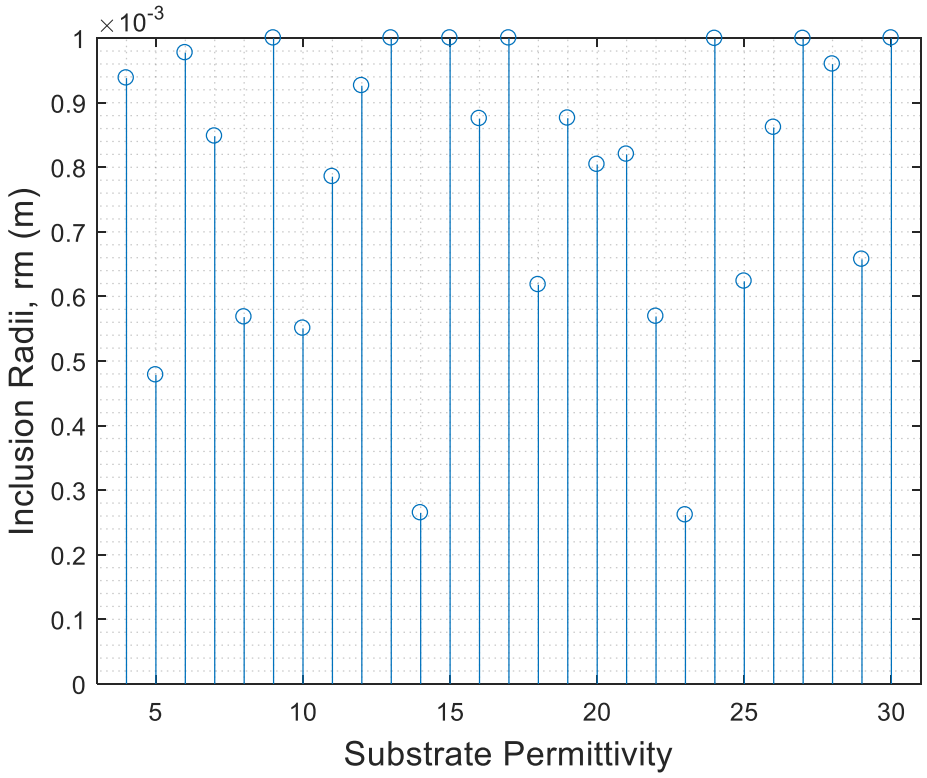

Figure 21: Required magnetic mode inclusion radii for the negative refractive index implementation

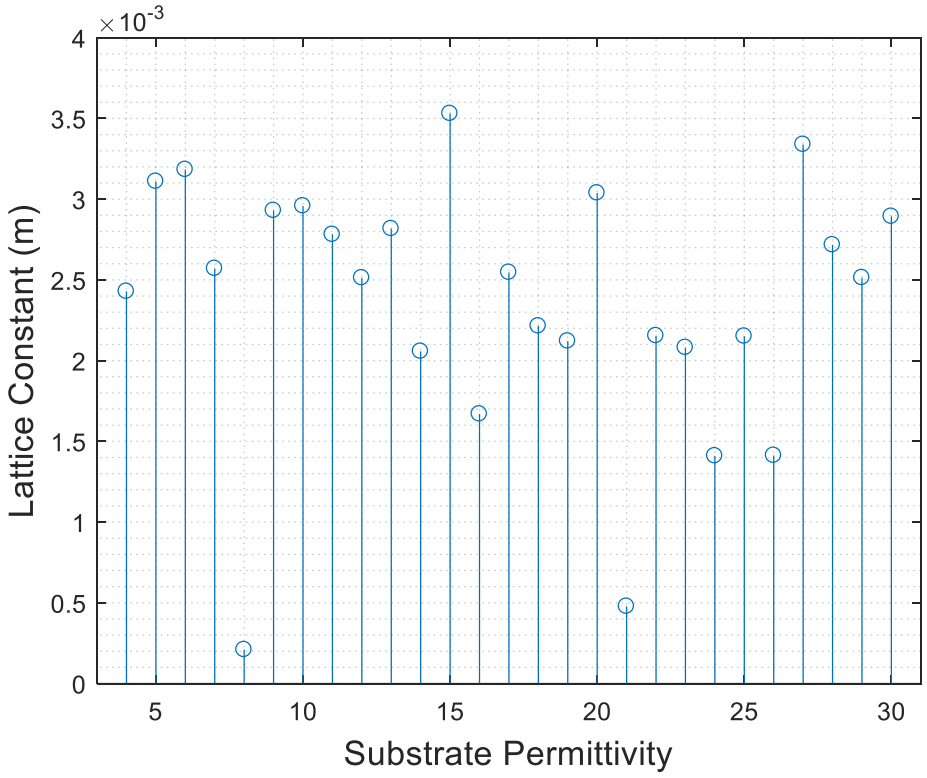

Figure 22: Required lattice constant for the positive refractive index implementation

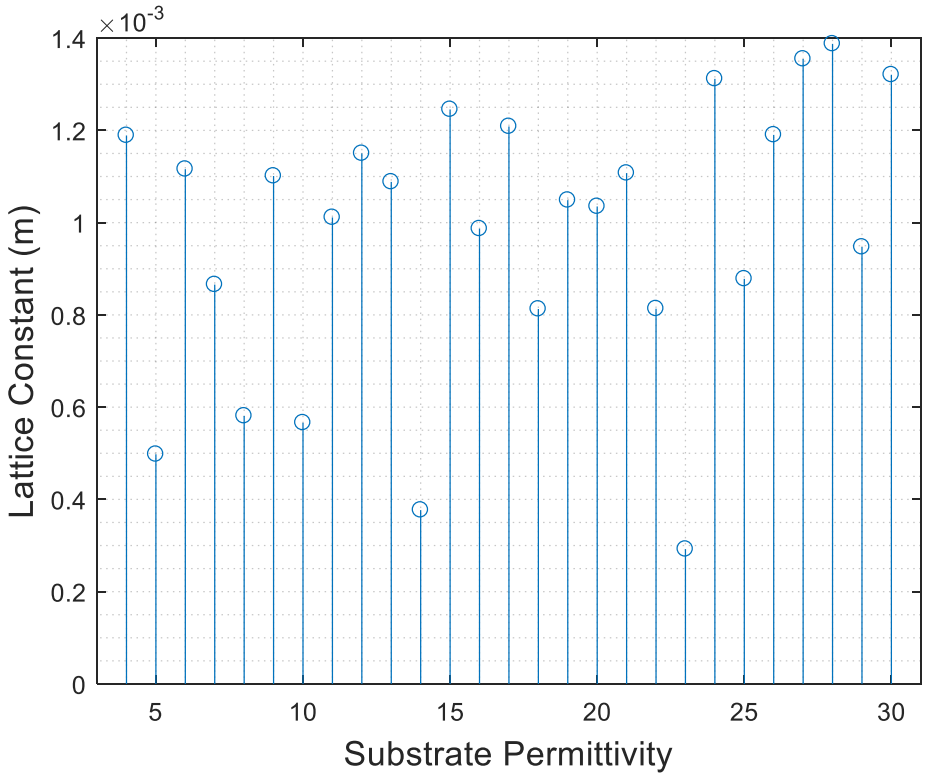

Figure 23: Required lattice constant for the negative refractive index implementation

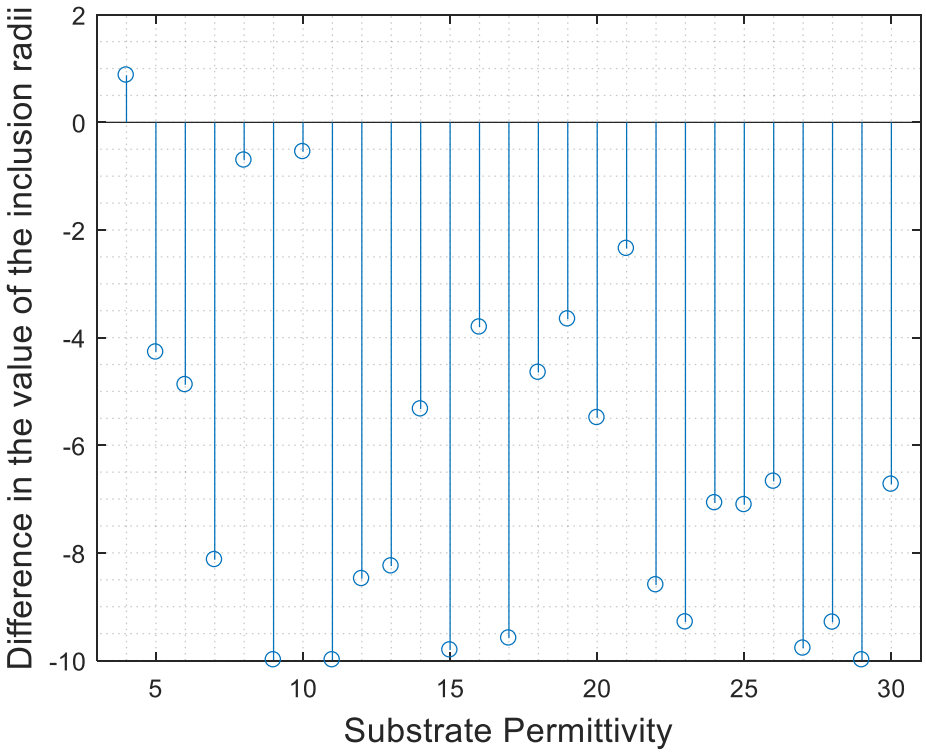

Figure 24: Difference between electric and magnetic mode radii (re-rm) for the positive index case

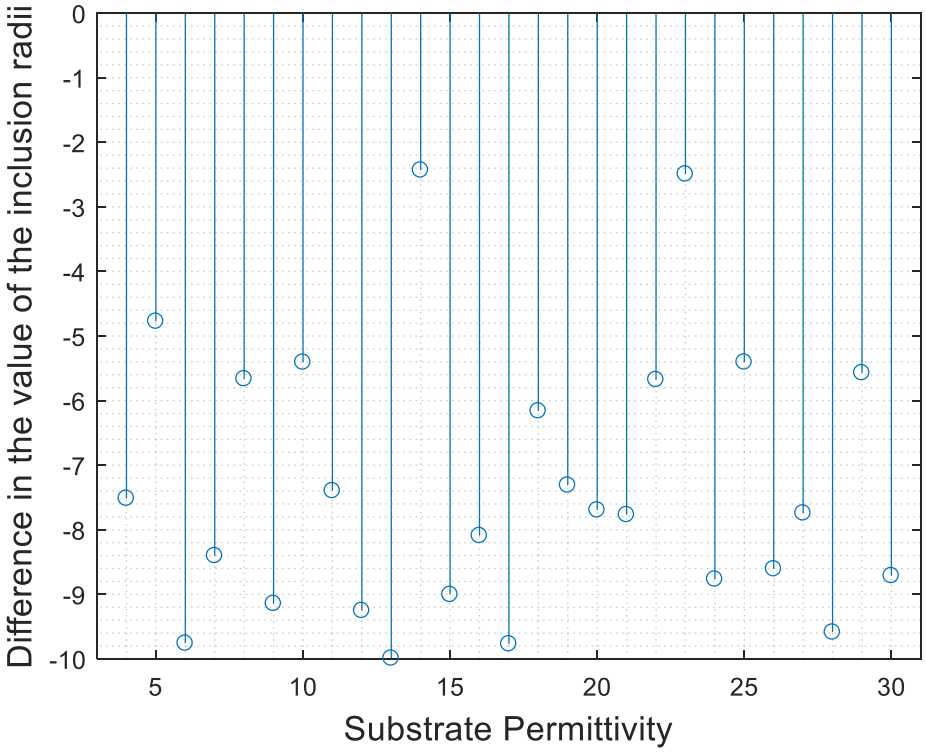

Figure 25: Difference between electric and magnetic mode radii (re-rm) for the negative index case

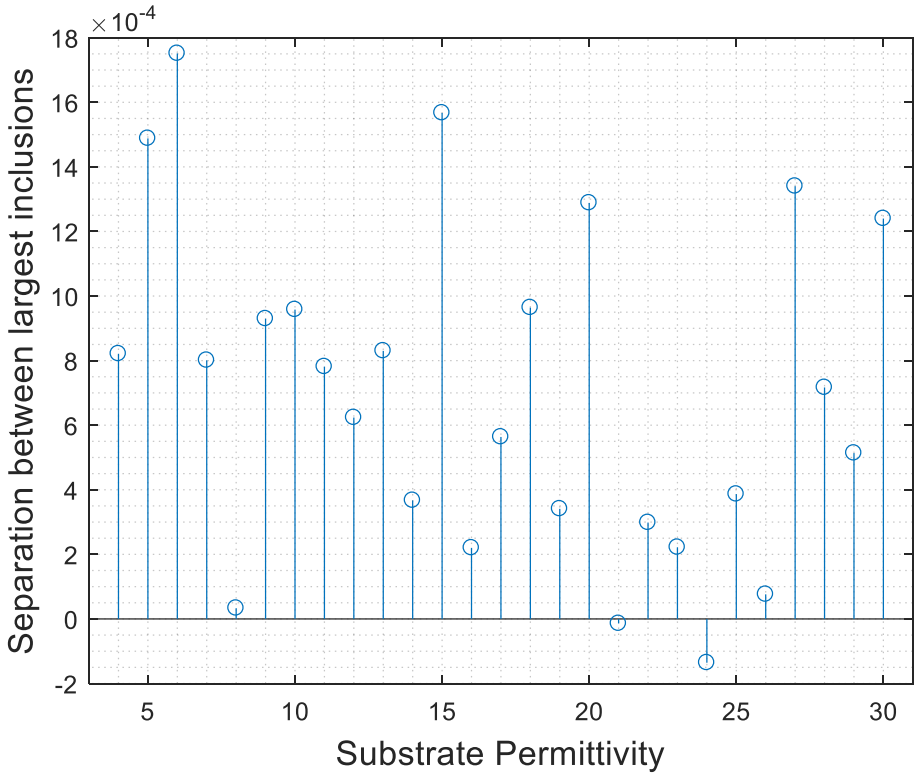

Figure 26: Difference between the lattice constant and double the largest inclusion radii for the positive index case

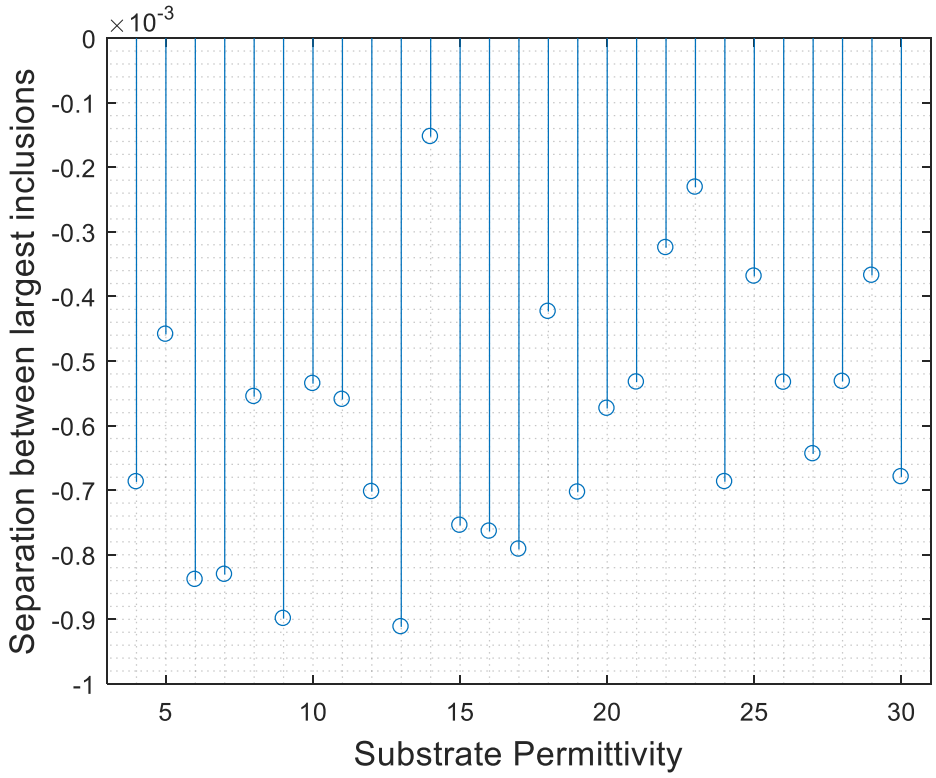

Figure 27: Difference between the lattice constant and double the largest inclusion radii for the negative index case

It is evident that the figures display discordance in the required values of the constituents resulting from the pseudo-random distribution of initialized search points and concurrent volatility of the selected solutions in the *MULTISTART* algorithm. This inconsistency prevents the development of a trend for the desired values over the range of substrate permittivities such that the generalization of properties and comparisons therein are limited to the instance detailed above. The resonant inclusions detailed in figures 5a, 5b, 6a, and 6b delineate cubic lattices in which the dimensions of the magnetic mode coupling particulate exceed their corresponding electric values which appears antithetical to the relation anticipated from the available literature. Comparison of these values to the lattice constants of Figures 7a and 7b, indicates that the leniency in the defined inequality constraint permitted the algorithm to tolerate a fractional contrast in the value of the lattice constant with respect to the sum of the inclusion radii. Under

this condition, for the negative index case and less prominently in the positive index case, the larger spherical inclusions coalesce as a result of their presupposed separation being insufficient to prevent overlap which was not accounted for in the system constraints. As a single particle, the effective material properties described through the Mie resonance conditions on the assumed spherical particulate is invalidated by the combined form of the adjoining magnetic inclusions. This represents one of the fundamental challenges in the application of the lattice based all-dielectric approach as the formulation disregards the effects of coupling magnetic and electric dipoles arising from particles in close proximity [50]. These coupling modes offset and split the frequency at which resonance occurs such that the refractive index achieved can differ substantially from the predicted value. When these modes are considered, the algorithm is less likely to converge to solutions that lead to their formation. It can be further noted that the particles are treated individually even when they are presented as occupying the same spatial region as a result of the black box instated by the effective medium interpretation. The algorithm can therefore misinterpret the configuration of the unit cell and issue deceptive transmittance values that do not correspond with the physical system. Although it is speculated that the particle sizes should be somewhat comparable to the wavelength in the inclusion material, the inverse method is entirely reliant on the effective properties derived from Mie theory to determine the plausibility of the constituent values. Provided a predetermined inclusion permittivity, the boundaries on the remaining unknowns could be defined in congruence with the mediums wavelength; however, the contrast parameter which exists as a ratio of the inclusion to background refractive index, is a significant contributor to the resonance condition and it is therefore not suggested to emplace such restrictions. In order to circumvent many of the

challenges surrounding particle proximity, the inequality conditions can be redefined such that a separation is provided to reduce the development of coupled modes, as follows:

$$2.5(r_e + r_m) \leq s$$

Wherein the associated array notation for the algorithm can be implemented as:

$$[0, 2.5, 2.5, -1]$$

Under these conditions, the algorithm is observed to restrict the available solution space to permit only constituents associated with positive index values. This is believed to occur as the result of the secondary inequality which enforces the lattice to remain within the boundary of the host medium. Consequently, the concurrent amendment to the requirement on the lattice constant imposes a more substantial constraint on the system that can make some values of the inclusion radii infeasible. This is especially true for the negative index case which displayed a propensity to overlap the larger inclusions. Recalling the discussion of the previous section, this finding supports the assumption that larger medium thicknesses are required to accommodate the cubic lattice and accordingly achieve resonance. Increasing the thickness of the material would therefore enable simultaneously negative material parameters, however, reduces its viability as an alternative to the current FSS based rectification method. The evaluation is consequently restricted to constituents that produce positive material parameters, as detailed in the following figures. In order to more adequately handle the variance in solution values between executions of the algorithm, a 90 percent confidence interval is determined for each variable from 40 sample solutions using the t-distribution. This confidence integral estimates the probability of the true mean for an entire population to exist within a given region from a small proportion of the population. For a sample size of 40, the t-distribution and normal distribution become congruent

and their functions can therefore be interchanged at the discretion of the researcher. It should be mentioned that the inequality condition mentioned earlier was not determined by coupled mode theory but exists as an approximation based on the available literature of the separation required to lessen coupling interactions. These interactions are often neglected in studies of Mie resonance based all-dielectric metamaterials; where they can lead to spurious conclusions on the metamaterial's efficacy.

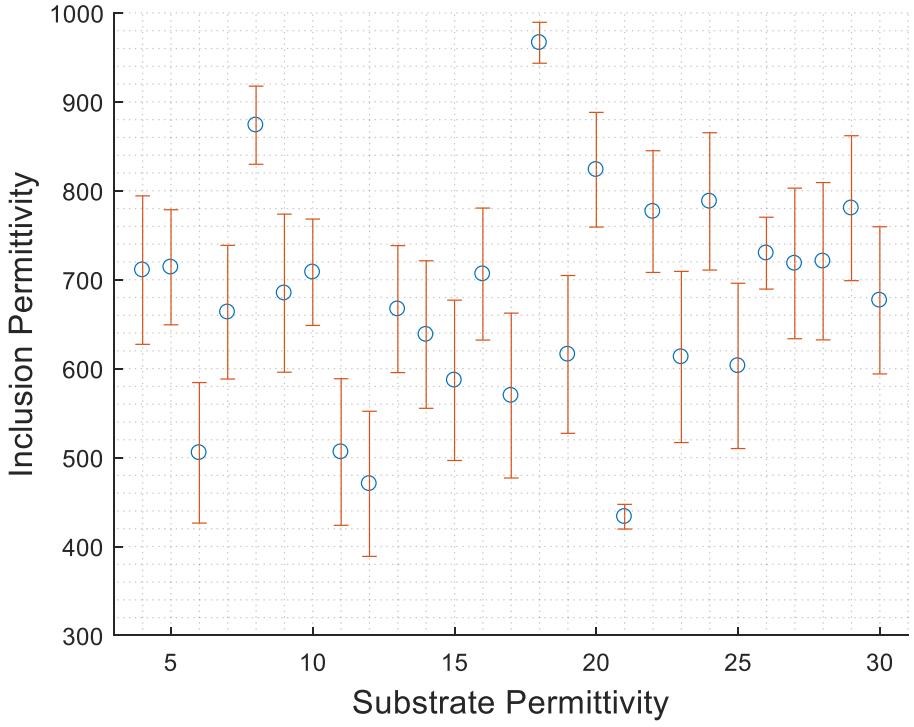

Figure 28: Confidence interval and sample mean of the permittivity for the inclusions after adjusting the inequality condition

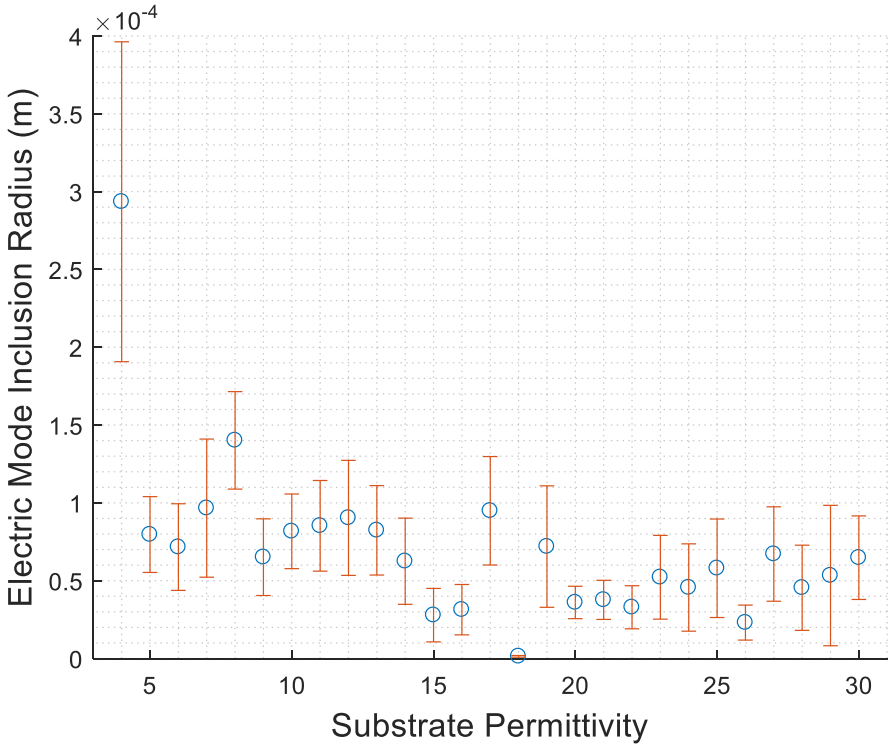

Figure 29: Confidence interval and sample mean for the electric mode coupling inclusion radii after adjusting the inequality condition

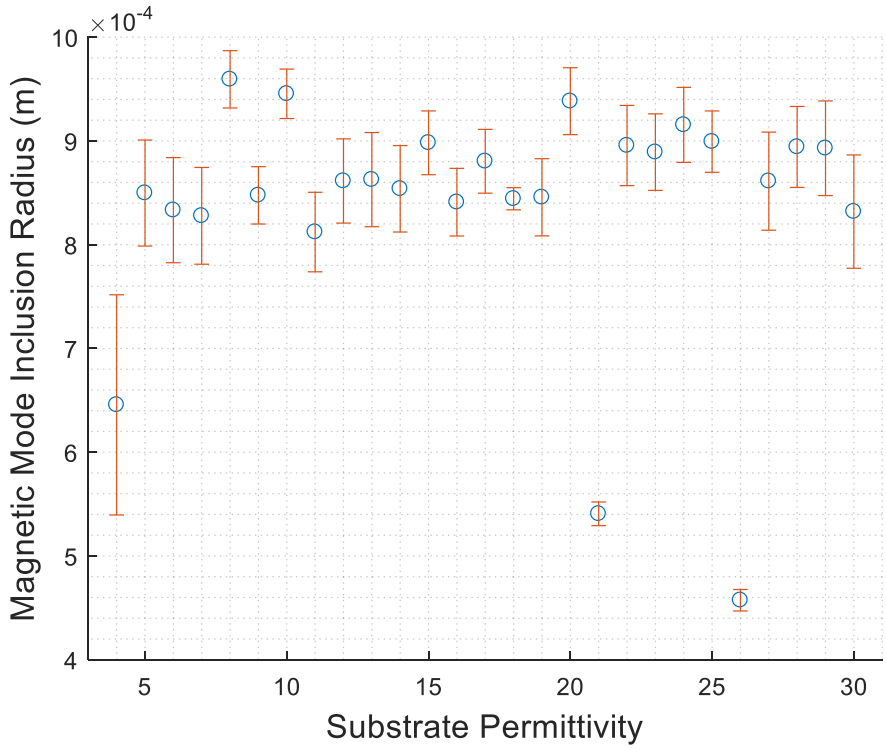

Figure 30: Confidence interval and sample mean for the magnetic mode coupling inclusion radii after adjusting the inequality condition

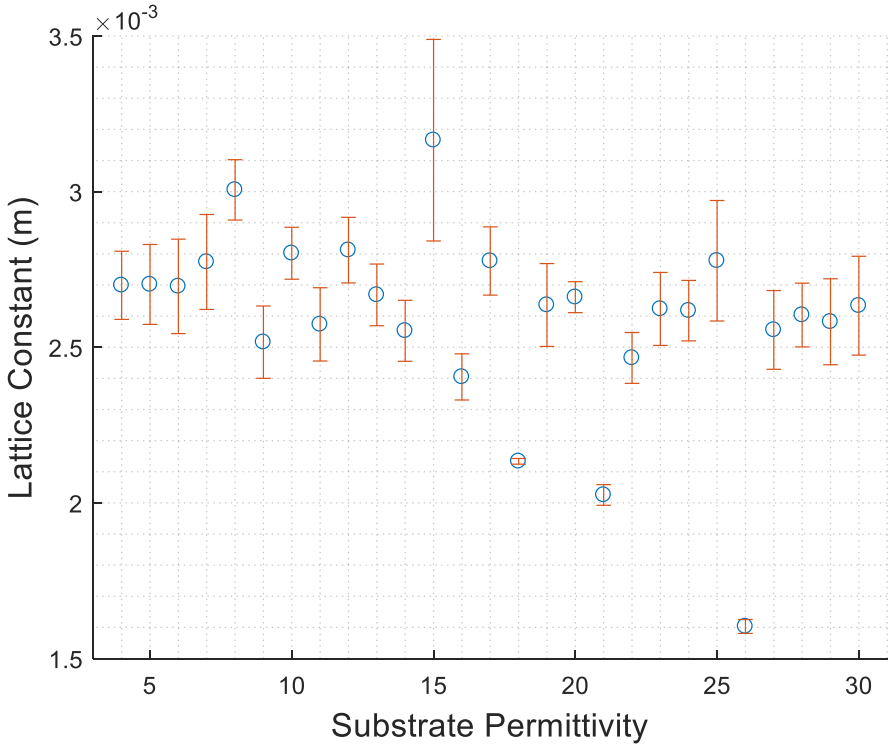

Figure 31: Confidence interval and sample mean for the lattice constant after adjusting the inequality condition

The reciprocity of the contrast and size parameters for the inclusions make the results difficult to interpret quantitatively. From a qualitative perspective, it can be understood that the parameters are able to take on values that exist about those displayed previously for the positive index case by redistributing the responsibility for achieving the necessary refractive index between the inclusion permittivity and dimensions. These properties primarily determine the material parameters as governed by the equations in section 2.5.2 and are likewise congruent with the scattering coefficients that dictate resonance modes. From figure 28, it can be seen that the sample mean inclusion permittivity values predominantly lie within the midrange of the designated solution space for each substrate tested. The width of the confidence intervals for each case is relatively consistent and indicates a large standard deviation from the mean value. This consistency is dissimilar to the electric and magnetic mode inclusion radii values, as given

in figures 29 and 30, where a much wider variability in available solutions is indicated for the lowest permittivity tested. The larger spread presents a decreased reliability in assessing the true mean of the system, which is likely to exist within the bounds of the confidence interval. It is necessary to mention that the spread is not indicative of the systems ability to achieve the desired value over a continuous range but is representative of the systems mean and standard deviation for discrete solutions. In the case of the electric inclusion radii, the sample mean values fall more generally within the lower regions of the solution space and are therefore antithetical to that which can be concluded for the magnetic inclusion radii. The values on the plot which appear to align with the x-axis are, in truth, existing at the lowest available radius given for the solution space and are consequently insignificant compared to the majority of cases. As a final note it should be mentioned that post observation of the largest inclusion radii determined them to be sufficiently separated under the revised inequality condition for the presented sample cases.

Despite the simplicity of the underlying theory, the intricacy of the structure and implied susceptibility to the size parameter significantly restrict the viable fabrication methods. It has been suggested in the available documentation that these restrictions can prevent the physical realization of the structure through current fabrication technology. In similar applications, the configuration of elements in a lattice was determined by imposed forces used to influence the constituents to predesignated positions in a process known as directed self-assembly. For the manufacturing of micron sized spheroidal particles involving polymer, glass, or ceramic, it is common to use a melt cooling process which relies on the surface tension to generate near perfect symmetry[51]. Through this collaborative approach, it is feasible to attain the results detailed above, however, the adaptation of this technique to Mie resonance based metamaterials has not been rigorously detailed. It is therefore beneficial to consider the admissible variation in

the value of the constituents for which the attained transmittance exceeds a set threshold as an alternative to a specified tolerance value. This variation can be likened to generalized deficiencies in the manufacturing process that impose a requirement for accommodation in the magnitude of the designable variables. The defined tolerance boundaries are accordingly made to exceed those of common manufacturing approaches to account for the ambiguity in the applied process. Convergence of the allowable change in the constituent property to the upper and lower extremums of the established tolerance range can be understood as the result of truncation for values that fall outside of this region. The current implementation considers a 20 percent variability in the parameter values about their algorithmically determined optima over 40 iterations whereby the confidence interval can be determined in a similar fashion to that used for each parameter value. The following figures detail the analysis performed on the positive refractive index metamaterial sublayer parameters assuming an allowable drop from the desired transmittance value of 10 percent.

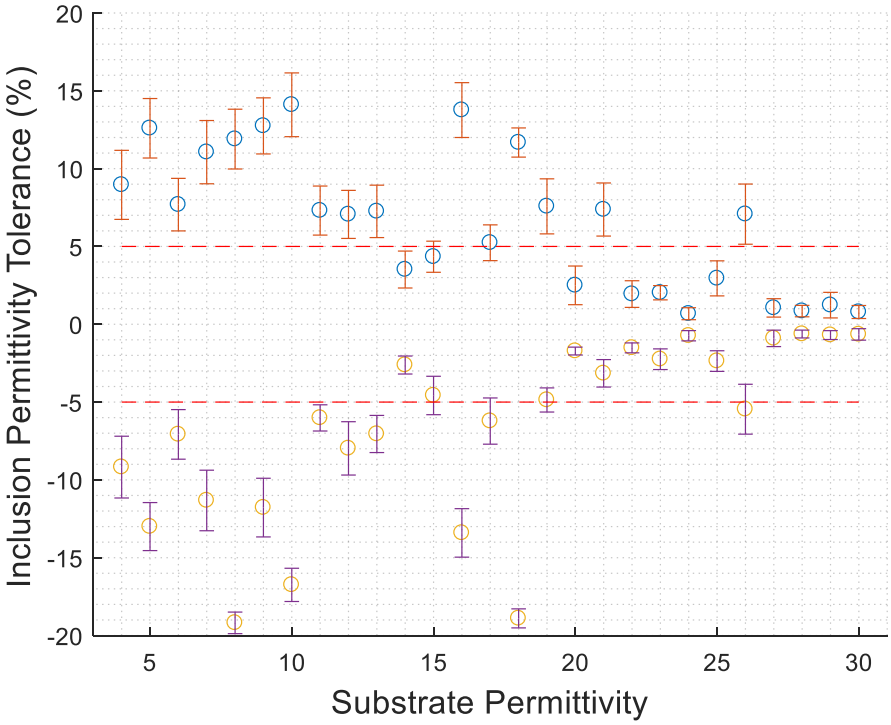

Figure 32: Confidence interval and sample mean describing the allowable deviation in the inclusion permittivity

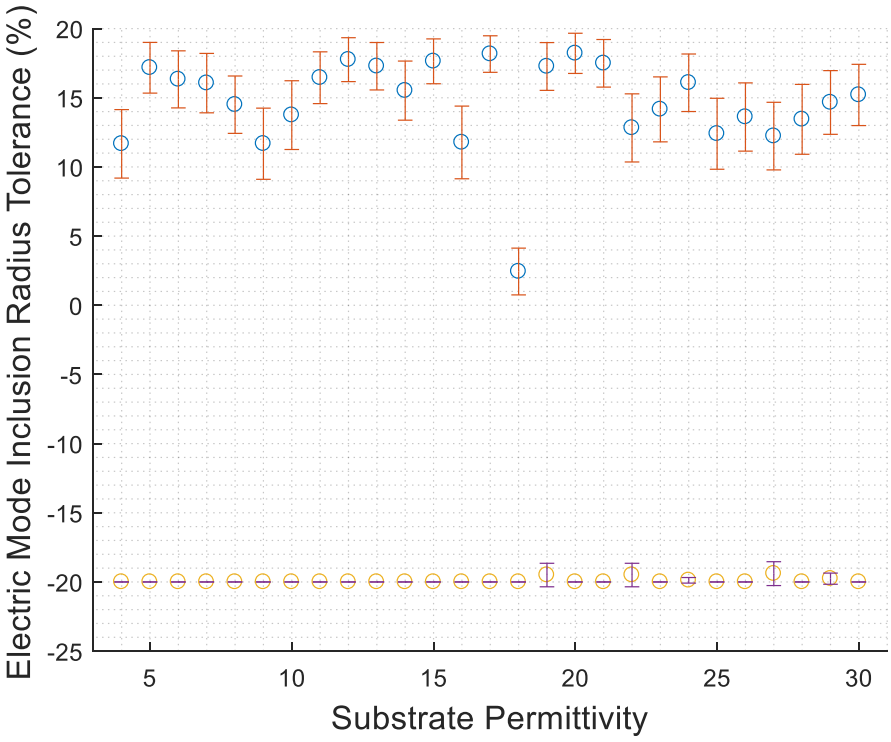

Figure 33: Confidence interval and sample mean describing the allowable deviation in the electric mode radii

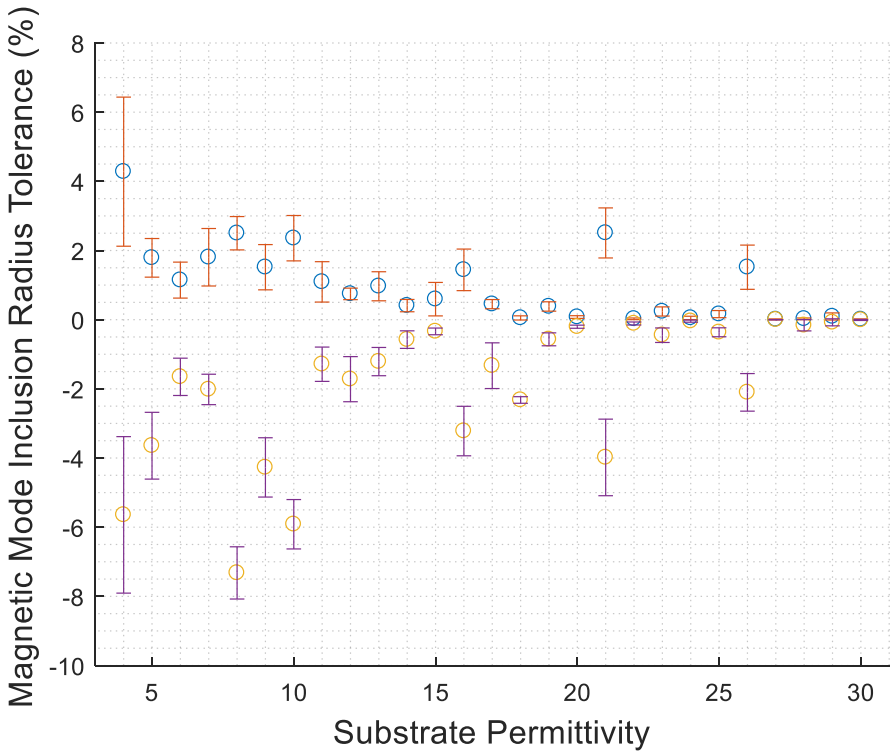

Figure 34: Confidence interval and sample mean describing the allowable deviation in the magnetic mode radii

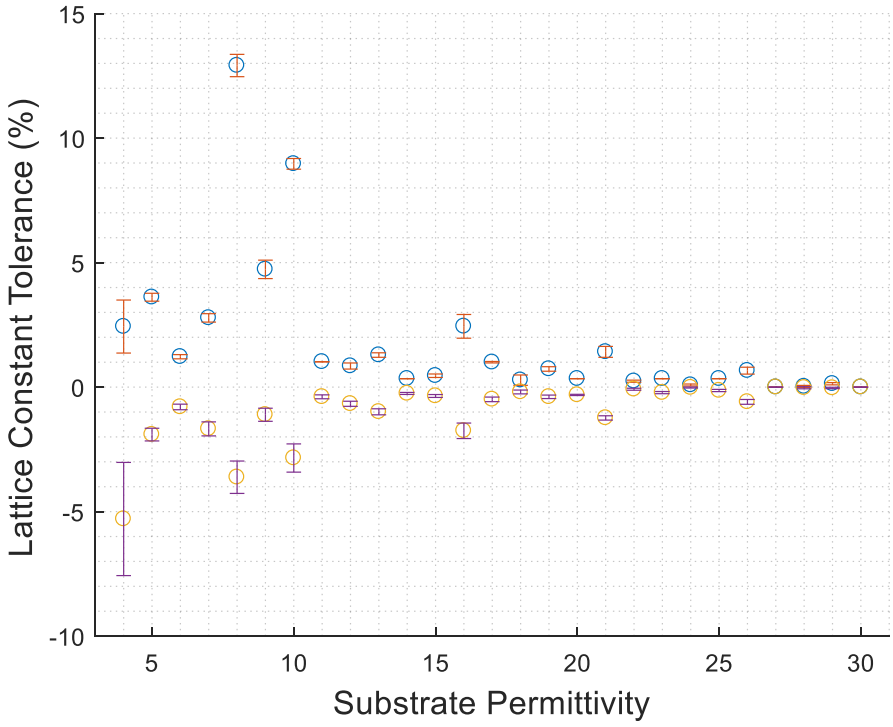

Figure 35: Confidence interval and sample mean describing the allowable deviation in the lattice constant

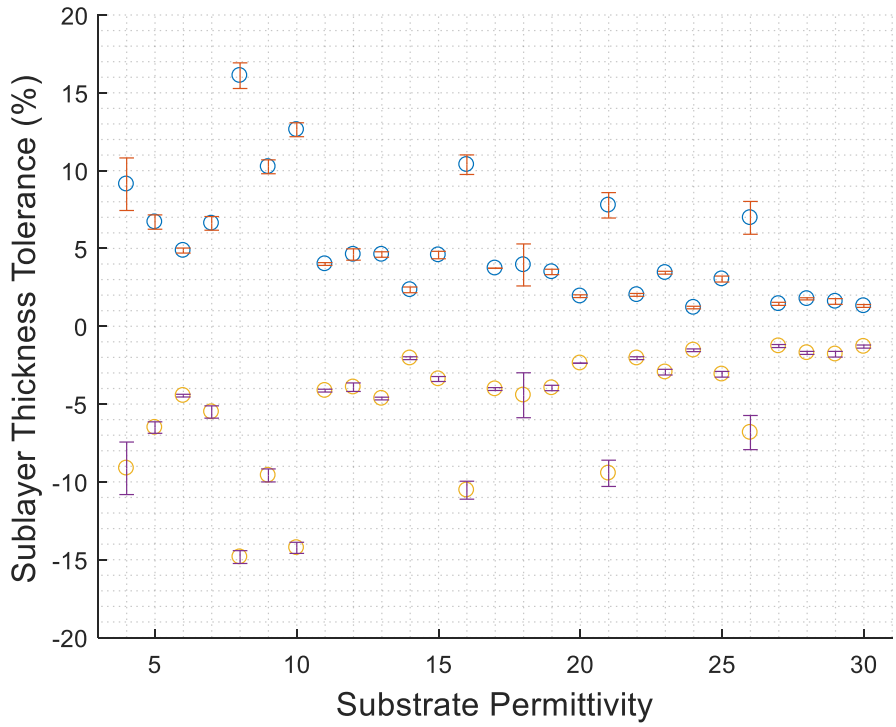

Figure 36: Confidence interval and sample mean describing the allowable deviation in the layer thickness

As a consequence of the inaccuracies introduced by the manufacturing process, the dielectric constant of a composite medium is expressed in a range about the intended value that accounts for deviations in its precise constitution. For applications in which the presupposed value of the permittivity exceeds 100, the tolerance afforded for manufacturing deviation is on the order of 5 to 20 percent [52]. Comparison of this range to the confidence intervals for the permissible variability in the inclusion permittivity detailed in Figure 6a, indicates an inability of the available process to sufficiently meet the criteria required for the all-dielectric metamaterial to be produced for a large proportion of the population; a result which is most predominantly observed in the upper range of substrate permittivity. Furthermore, the cases where the confidence interval bounds extend below the threshold value cannot be presumed to reliably meet the criteria with each iteration. Although the sample mean may exist outside of the infeasible region, the spread

of solutions indicates that the criteria can only be met inconsistently. The figure also exhibits points where the 90 percent confidence intervals are nearly convergent upon the mean value. This invariability suggests that despite deviation in the inclusion permittivity values between iterations, the ability of these systems to tolerate change is similar. Where the solutions exhibit sample means that are greatly in excess of the 5 percent tolerance and the confidence interval about the respective values are likewise surpassing the minimum tolerance value, the solutions are achievable. In contrast with the required tolerance for the inclusion permittivity, it has been indicated in the available literature that current fabrication techniques can achieve an accuracy of roughly 1μm for millimeter sized spherical dielectric inclusions. Furthermore, the melt cooling process for the micrometer range detailed previously is recognized as providing exceptionally high accuracy for certain glasses and ceramics [51]. In this regard, the requirements for the electric inclusion, as depicted in figure 35, can be understood to designate these spheres as physically realizable solutions due to their sample mean values broaching either limit of the windowed space. This relative immutability is not shared by the magnetic inclusions and lattice constant whose allowable mean variation values trend towards zero for substrates with a higher permittivity. In consonance with these regions, the respective confidence intervals exhibit infinintesimal width; whereby it can be assumed that regardless of the sample solution utilized, the requirements on the transmittance cannot be met without perfect accuracy to the designed system. It should be mentioned that the boundary utilized in the algorithm can be redefined to incorporate null values of the magnetic mode coupling inclusions. Under this definition, the system would separately engage the electric field and therefore operate with an effective permittivity in the absence of magnetic dipole formation at the frequency of interest. This would permit the positive refractive index to be achieved by a solitary lattice of inclusions and

consequently ease some of the constraints placed on manufacturing; however, it is believed that this rectification to the structure would result in a similar dependency on fewer variables that ultimately yields the same inefficacy of implementation. As a final note, it is important to recognize that all metamaterials are prone to very small bandwidths as a result of limited resonance regions wherein the material properties align. Outside of the alignment condition, where the material parameters assume opposite signs, the refractive index is purely imaginary and the resultant field is evanescent. In this case, no propagation occurs and the frequencies that are part of this region are precluded from transmission through the structure. Although it is theoretically plausible to use the coupling effects previously dicussed to improve the bandwidth through properly tailoring the separation such that multiple close proximity resonance peaks occur, the fabrication of the structure would remain infeasible and therefore the metamaterial is exempt from further consideration.

3.5 Measurement of Performance Bandwidth

In a regular dielectric medium for which the molecular constituents are known, the dispersion relation ascribes the frequency dependent nature of the permittivity to the atomic oscillatory displacement of the electrons under an applied harmonic field [53]. The vibration attributed to the electron can be approximated in one dimension through the damped harmonic motion equation wherein the natural frequency of the electron oscillation, ω_0, is defined with respect to the analogous spring constant, K [54]. Assuming that the magnetic field of the incident plane wave is only minimally influential to the force relative to the electric field, the motion equation has the form (3.5.1).

$$m[\ddot{x} + \gamma\dot{x} + {\omega_0}^2 x] = -eE(x,t) \tag{3.5.1}$$

$$\omega_0 = \sqrt{\frac{K}{m}}$$

Where e is the charge of the electron, γ is damping from collision and radiation, and E and x are given to display the same time dependence:

$$E = E(x)e^{-j\omega t}$$

$$x = xe^{-j\omega t}$$

The equation describes the propensity of the electron to form a dipole under an applied electric field, E, with the solution comprising a proportion of the dipole moment, p (3.5.2).

$$p = -ex = \frac{e^2 E}{m({\omega_0}^2 - \omega^2 - j\omega\gamma)} \tag{3.5.2}$$

The superposition of the contributions established in the previous equation for each electron contained in the molecules of the dielectric determine the molecular polarizability for the system. Representing the sum of the contributions in accordance with the fraction of electrons in the molecule, f_i, that display equivalent natural frequencies, ω_{0i}, and damping coefficients, γ_i, the molecular polarizability has the form (3.5.3).

$$p_{mol} = \sum_i \frac{f_i e^2 E}{m({\omega_{0i}}^2 - \omega^2 - j\omega\gamma_i)} \tag{3.5.3}$$

The total polarizability, P, is then found as the product of the number of molecules per unit volume, N, and the molecular polarizability.

$$P = Np_{mol}$$

This quantity can be substituted into the electric flux density formula, $= \varepsilon_0 E + P$, from which the relative permittivity is readily determined (3.5.4).

$$\varepsilon_r = \frac{\varepsilon}{\varepsilon_0} = 1 + \frac{Ne^2}{\varepsilon_0 m} \sum_i \frac{f_i}{{\omega_{0i}}^2 - \omega^2 - j\omega\gamma_i} \tag{3.5.4}$$

It can be seen from the equation that a resonance condition arises when the incident wave approaches the natural frequency of the electron oscillations [53]. In the vicinity of this location, the relative permittivity exhibits rapid variation between maxima and minima as a consequence of the dispersion relation. The condition for resonance is not unique but occurs at frequencies on the order of the natural frequency for any electron in the system. In situations where the incident wave is far outside of the resonance region, the natural frequency term dominates the dispersion function and the variation in permittivity is negligible. With knowledge of the desired functionality it is possible to tailor the response to be within or external to this region by proper choice of the materials.

For simplicity, it is assumed that the frequency dependent variation in permittivity across a 2 GHz band about the center frequency of the transmitted signal is infinitesimal such that the deviation in transmittance can be determined by consideration of the frequency change in transmission matrix properties independently. Applying a similar window to the previous section wherein the improvement in transmittance with the dielectric sublayer is allowed to degrade by ten percent within the region of interest, an operational bandwidth for the system can be established which represents the high and low frequency limits of the incident signal where acceptable transmittance levels are maintained. Providing for the refractive index and thickness values for the sublayer as determined in section 4.3, the maximum frequency bandwidth around the 9 GHz center frequency for each substrate is presented below.

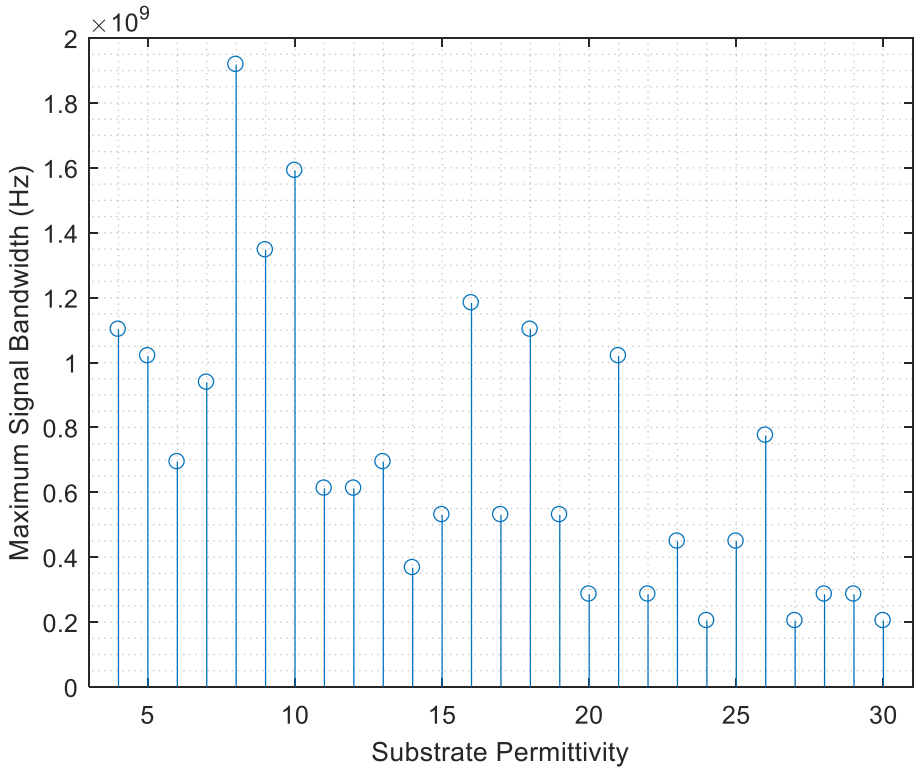

Figure 37: Expected functional bandwidth of the device for permissible transmittance greater than 90 percent

The figure indicates a tendency of the permissible frequency variation to decline in response to increasing substrate permittivity. The minima in the bandwidth about the frequency of transmission of approximately 200 MHz accordingly exists in the upper limit of the tested region at concurrent permittivity values of 24, 27, and 30. Conversely, the maximum bandwidth is slightly offset from the lowest tested substrate value where unaided transmission through the patch is on the order of 90 percent at the center frequency of the incident wave. It should be noted that in the non-dispersive medium, the frequency variation predominately determines the adjustment in the phase term of the transfer matrix equation and therefore governs the alignment of interfering modes within the structure. For higher disparity in the permittivity between interfacing media, the reflection is generally more pronounced and the system is consequently increasingly reliant on subsequent cancellation to improve the transmission. In this respect, the

initial lower bandwidth value for the lowest tested permittivity substrate can be accounted for by the corresponding higher permittivity sublayer used in transmission correction. The decreasing trend therefore generally holds true as a result of the likewise increase in sublayer refractive index with increasing substrate permittivity.

IV. CONCLUSION

4.1 Overview

An investigation into the suitability of a metamaterial sublayer for the resolution of signal attenuation effects arising from an antecedent concentric antenna layer was performed through a simplified combined effective medium-transfer matrix approach under the assumption of low dielectric losses. The Schneider model permitted the approximation of the overlying rectangular patch element as an effective uniform system of a given real valued permittivity. The sublayer and patch antenna could then be viewed as a system of layered semi-infinite media for which the one-dimensional transfer matrix equations applied. The desired transmittance behaviour was established utilizing Schott B270 Ultra-white crown glass as an analogue from which the necessary sublayer refractive index and thickness were determined through successive evaluation of the residual. The results indicated an equivalence between positive and negative indices of the same magnitude in achieving transmittance enhancement. A sequential quadratic programming optimization algorithm was used to determine the necessary constituent parameter values for an all-dielectric metamaterial implementation exhibiting the required refractive indices. For efficiency, the objective function was redefined in terms of the transmittance as a product with an expression denoting the sign of the effective material properties. This coefficient facilitated explicit delineation between positive and negative index values that superseded the fitness and consequently enabled their constituents to be viewed independently. It was noted that the underdetermined system presented by the objective function required the metamaterial to be viewed through confidence intervals about a sample mean at each substrate permittivity value. These intervals were formed on a small number of sample solutions using a t-distribution to handle the occurrence of multiple optima in the solution space while maintaining a short runtime.

An emblematic system was established for a sample solution comprising both positive and negative index values wherein the insufficiency of the inequality condition in maintaining adequate separation between larger inclusions was exemplified. It followed that the convergence of particles in the lattice prevented the description of the scattering properties by the utilized theory and consequently rendered the constituent properties delineated thereby inaccurate to the physical system. Furthermore, the coupling of electric and magnetic dipoles in a matrix of close proximity particles was presented as a concern regarding the position of resonance peaks which could be shifted and separated by the interaction. The inequality condition was therefore revised to reflect the necessity to reduce this interaction by increasing the lattice constant as a multiple of the sum of inclusion radii. It was found that the increased constraints prevented the realization of the negative index values for the metamaterial, however, this condition could be partially alleviated by enabling larger thicknesses of the layer. Subsequent evaluation revealed the tendency of the sample mean inclusion permittivity to exist within the midrange of the provided solution space with confidence intervals indicative of a large variability in the value between iterations. The confidence regions for the electric and magnetic inclusion radii contrarily suggested that these parameters predominantly remained in the respective lower and upper regions of the designated space; with maximum deviation in their values displayed at the lowest substrate permittivity. Similar to the trend for the inclusion permittivity, the region primarily occupied by solutions of the lattice constant existed in the midrange of the solution space provided to the *fmincon* function. In evaluation of the tolerance to variability of each system parameter, the confidence intervals revealed significant impairment in the manufacturability of the system instated by immutability of both the lattice constant and magnetic inclusion radii from their designed values. This issue was compounded by the failure to adequately and consistently

meet the minimum conditions emplaced by fabrication methods for large permittivity dielectric composites across all tested substrates. Consequently, it was suggested that regular dielectric composites offer a more viable alternative to the all-dielectric metamaterials. The functional bandwidth of the regular dielectric case was analyzed in accordance with its ability to exceed both 90 percent transmittance and 90 percent improvement in the transmittance over the isolated antenna in the absence of dispersive effects. It was indicated that the trend for the bandwidth in the former case was piecewise declining in congruence with the sublayer refractive index. This was believed to be the result of changes to the phase term that cancels the more prominent reflection at the boundary.

4.2 Future Works

The above investigation revealed the plausibility of an all-dielectric based transfer correction mechanism for an approximation of the surface. It should be noted that as a result of the model, which assumes the form of a semi-infinite medium, edge effects on the transfer mechanism are not considered but could impact the achievable transmittance. Furthermore, it is believed that the transfer matrix method is insufficient in providing an accurate description of the system as, in its current form, the patch is viewed in isolation and consequently ignores the potential for co-occurring interference. The process utilized was chosen to provide a simple and rapid analysis platform, however, did not fully detail the internal modes of the structure or validity of the approximation. It therefore remains necessary to perform a thorough evaluation of the time-harmonic progression of the field through the medium. A finite-difference time domain simulation with total-field scattered-field set-up would be sufficient to relay much of the information about the scattering mechanism of the system and associated transmittance and

reflectance properties. For standard simulation software, the transmittance and reflectance can also be resolved from field monitors about the structure which provide either the power or field at the input and output region. The simulation would additionally provide an opportunity to view the fields as they traverse the structure and accordingly determine localized problem regions. Frequency variation effects as presented by the signal bandwidth cannot be thoroughly detailed through the standard transfer matrix approach without knowledge of the dielectric function for each material present in the structure. The complexity of the dispersion relation presented in section 3.5 is compounded by the requirement for precise information on the electron binding frequency and damping coefficient in predominantly composite dielectric media. There are simplified functions for a select group of materials, however, they are not common to all dielectrics and typically require information about the system that can be difficult to obtain. This issue can be partially avoided in electromagnetic evaluation software as they generally have extensive repositories of sample data for standard dielectrics. For the planar dielectric case, the fabrication can be executed through standard processes and it may be pertinent to compare simulated features with physical evaluation. The Mie resonance based all-dielectric metamaterial described herein imposes strenuous conditions on manufacturing primarily due to the necessity for spherical inclusions. It is possible to alleviate some of these difficulties by examining dielectric implementations with more reasonable feature shapes such as those exhibiting cylindrical or cuboid inclusions. The structure considered in this report is comprised of two overlapping rectangular patch arrays, however, it is believed that the basic theory can be applied to larger multi-array systems consisting of more complex radiative elements. The effective medium approximation for different element geometries may not exist which would render the

transfer matrix method ineffectual. Observation of the transfer behaviour would therefore require application of the FDTD methods described previously.

REFERENCES

[1] P. Ragulis *et al*., “Shift and elimination of microwave Fabry-Perot resonances in a dielectric covered with a thin metal layer,” J. Appl. Phys., vol. 117, no. 16, 2015

[2] J. B. Pendry and S. A. Ramakrishna, “Focusing of light using negative refraction,” J. Phys. Condens. Matter, vol. 15, no. 37, pp. 6345-6364, 2003

[3] P. Hui *et al*., “Minimization of microwave reflections from EC-coated glass slabs,” IEEE Microw. Compon. Lett., vol. 8, no. 11, 1998

[4] P. Ragulis *et al*., “Reflection and transmission of microwaves by a modern glass window,” presented at Asia Electromagnetics Symposium, Jeju, Republic of Korea, 2015

[5] V. G. Veselago, “The Electrodynamics of Substances with Simultaneously Negative Values of ε and μ,” Phys. Usp., vol. 10, no. 4, 1968

[6] Y. Lai *et al*., “Complementary Media Invisibility Cloak that Cloaks Objects at a Distance Outside the Cloaking Shell,” Phys. Rev. Lett., vol. 102, no. 9, 2009

[7] S. R. Entezar and H. Rahimi, “Transmission properties of a double-periodic quasi-crystal containing single-negative materials,” Opt. Commun., vol. 284, no. 24, pp. 2833-2838, 2011

[8] S. Kameda *et al*., “Effective Medium Theory for Calculating Reflectance from Metal-Dielectric Multilayered Structures,” Jpn. J. Appl. Phys., vol. 51, no. 4, pp. 042202 - 042202-9, 2012

[9] M. Maldovan *et al*., “Validation of the effective-medium approximation for the dielectric permittivity of oriented nanoparticle-filled materials: effective permittivity for dielectric nanoparticles in multilayer photonic composites,” Appl. Phys. B, vol. 76, no. 8, pp. 877-884, 2003

[10] L. Levin, "The Electrical Constants of a Material Loaded with Spherical Particles", Proc. Inst. Elec. Eng. Part III, vol. 94, pp. 65-68, 1947

[11] C.L. Holloway et al., "A Double Negative (DNG) Composite Medium composed of Magnetodielectric Spherical Particles Embedded in a Matrix", IEEE Trans. on AP, vol. 51, no. 10, pp. 2596-2603, 2003

[12] O. G. Vendik and M. S. Gashinova, “Artificial double-negative media composed by two different dielectric sphere lattices,” In 34th European Microwave Conference, pp. 1209-1212, 2004

[13] L. Jylha et al., “Modelling of isotropic backward-wave materials composed of resonant spheres,” J. Appl. Phys., vol. 99, no. 4, pp. 043102 - 043102-7, 2006

[14] I. B. Vendik et al., “3D isotropic metamaterial based on a regular array of resonant dielectric spherical inclusions,” Metamaterials, vol. 3, no. 3, pp. 140-147, 2009

[15] S. E. Harris, “Electromagnetically Induced Transparency,” Physics Today, vol. 50, no. 7, pp. 36-42, 1997

[16] D. Kohlgraf, “Design and Testing of a Frequency Selective Surface (FSS) Based Wide-Band Multiple Antenna System,” Bachelor’s Thesis, ECE, OSU, Columbus, OH, 2005

[17] E. Y.-C. Lee, “Electromagnetically Transparent Feed Networks for Antenna Arrays,” Ph.D. dissertation, ECE, OSU, Columbus, OH, 2008

[18] M. J. Lockyear, “Electromagnetic Surface Wave Mediated Absorption and Transmission of Radiation at Microwave Frequencies,” Ph. D. Dissertation, Physics and Astronomy, University of Exeter, Exeter, UK, 2004

[19] D. Janning, “Surface Waves in Arrays of Finite Extent,” Ph.D. Dissertation, ECE, OSU, Columbus, OH, 2000

[20] S. Arslanagic et al., “A review of the scattering parameter extraction method with clarification of ambiguity issues in relation to metamaterial homogenization,” *IEEE Antennas Propag. Mag.*, vol. 55, no. 2, 2013

[21] T. Sheret *et al*., “Efficient design of a radome for minimised transmission losses,” IET Microw. Antennas Propag., vol. 10, no. 15, pp. 1662-1666, Dec. 2016

[22] D. Orban and G. J. K. Moernaut, “The Basics of Patch Antennas, Updated,” RF Globalnet newsletter, 29 Sept., 2009

[23] M. V. Schneider, “Microstrip lines for microwave integrated circuits,” Bell Syst. Tech. J., vol. 48, no. 5, pp. 1421-1444, 1969

[24] P. P. Bergonio, “Schwarz-Christoffel Transformations,” M.A. thesis, Univ. of Georgia, Athens, GA, United States of America, 2007

[25] W. P. Calixto *et al*., “Electromagnetic Problems Solving by Conformal Mapping: A Mathematical Operator for Optimization,” Mathematical Problems in Engineering, vol. 2010, pp. 1-19, 2010

[26] A. K. Verma and Nasimuddin, “Analysis of circular microstrip patch antenna as an equivalent rectangular microstrip patch antenna on iso/anisotropic thick substrate,” IEE P. Microw. Anten. P., vol. 150, no. 4, pp. 223-229, 2003

[27] H. Werfelli et al., “Design of rectangular microstrip patch antenna,” in 2016 2nd International Conference on Advanced Technologies for Signal and Image Processing, pp. 798-803, 2016

[28] G. Barbastathis, C. Sheppard, and S. B. Oh. 2.71 Optics. “3D Wave Phenomenon; Introduction to Electromagnetics.” Department of Mechanical Engineering, Massachusetts Institute of Technology, Cambridge, MA, 2009

[29] A. La Rosa. “Huygen’s Principle of Wave Propagation.” Pdx.edu. [Online]. Available: https://www.pdx.edu/nanogroup/sites/www.pdx.edu.nanogroup/files/17-4-C1__Huygens_Principle%2C%20wave%20propagationPRINT.pdf [Accessed February 27, 2017]

[30] “Chapter 3: Thin Films.” [Online]. Available: http://fotonica.intec.ugent.be/download/ocs129.pdf [Accessed February 30, 2017]

[31] K. Barkeshli and S. Khorasani, “Maxwell’s Equations,” in Advanced Electromagnetics and Scattering Theory, Switzerland: Springer International Publishing Switzerland, 2015, ch. 1, sec. 1.4, pp. 11-17

[32] L. W. Henderson, “The Scattering of Planar Arrays of Arbitrarily Shaped Slot and/or Wire Elements in a Stratified Dielectric Medium,” Ph. D. dissertation, ECE, OSU, Columbus, OH, 1983

[33] A. Alu *et al*., "Single-Negative, Double-Negative, and Low-index Metamaterials and their Electromagnetic Applications," in IEEE Antennas and Propagation Magazine, vol. 49, no. 1, pp. 23-36, Feb. 2007

[34] J. B. Pendry and I. Youngs, “Extremely Low Frequency Plasmons in Metallic Mesostructures,” Phys. Rev. Lett., vol. 76, no. 25, pp. 4773-4776, 1996

[35] J. B. Pendry et al., “Magnetism from conductors and enhanced nonlinear phenomena,” IEEE Trans. Microw. Theory Techn., vol. 47, no. 11, pp. 2075-2084, 1999

[36] A. Evan. SIOC 251. Class Lecture, Topic: “Detailed description of Mie theory and the Rayleigh approximation.” SIO Graduate Department, University of California, San Diego, CA, 2017

[37] M. Jarrell. Electrodynamics. Class Lecture, Topic: “Boundary Value Problems in Electrostatics II.” Department of Physics and Astronomy, Louisiana State University, Baton Rouge, LA, 2000

[38] C. McLinden. Class Lecture, Topic: “Rayleigh Scattering.” Earth Science Systems, University of California, Irving, CA, 1999

[39] K. Jain and K. Gupta, “Different Substrates Use in Microstrip Patch Antenna-A Survey,” International Journal of Science and Research, vol. 3, no. 5, pp. 1802-1803, 2014

[40] T. Kin-Chung Lo and Yeongming Hwang, "Microstrip antennas of very high permittivity for personal communications," Proceedings of 1997 Asia-Pacific Microwave Conference, 1997, pp. 253-256 vol.1.

[41] E. Casas. ELEX 3525. Class Lecture, Topic: “Duplexing and Multiple-Access Techniques.” Department of Electrical and Computer Engineering, University of British Columbia, Vancouver, BC, 2015

[42] Edmund Optics, Inc., “Optical Glass.” *Edmund Optics, Inc.*, 2017 [Online]. Available: https://www.edmundoptics.com/resources/application-notes/optics/optical-glass/. [Accessed: May 5, 2017]

[43] SCHOTT, “B 270i Ultra White Glass.” *SCHOTT*, 2013 [Online]. Available: http://www.schott.com/d/advanced_optics/ef3ed49f-7445-4d3e-8713-3c955b853498/1.0/schott-b-270-i-ultra-white-glass-june-2013-eng.pdf. [Accessed: May 5, 2017]

[44] MathWorks, “Equation Solving Algorithms,” *MathWorks Documentation*, 2017. [Online]. Available: https://www.mathworks.com/help/optim/ug/equation-solving-algorithms.html. [Accessed July 25, 2017]

[45] J. Nocedal and S. J. Wright, Numerical Optimization, 2nd ed. New York, NY: Springer Science and Business Media, 2006

[46] MathWorks, “fmincon,” *MathWorks Documentation*, 2017. [Online]. Available: https://www.mathworks.com/help/optim/ug/fmincon.html. [Accessed August 15, 2017]

[47] MathWorks, “createOptimProblem,” MathWorks Documentation, 2017. [Online]. Available: https://www.mathworks.com/help/gads/createoptimproblem.html. [Accessed August 15, 2017]

[48] M. Tsuji et al., “Evaluation method of high-permittivity materials in microwave region using coplanar waveguide,” Electron. Comm. JPN. 2, vol. 90, no. 3, pp. 17-25, 2007

[49] MathWorks, “How GlobalSearch and MultiStart Work,” *MathWorks Documentation*, 2017. [Online]. https://www.mathworks.com/help/gads/how-globalsearch-and-multistart-work.html [Accessed August 17, 2017]

[50] M. S. Wheeler, J. Stewart Aitchison and M. Mojahedi, "Magnetic dipoles induced in dielectric spheres: Coupled interactions," 2009 Conference on Lasers and Electro-Optics and 2009 Conference on Quantum electronics and Laser Science Conference, Baltimore, MD, 2009, pp. 1-2

[51] S. Okamoto et al., “Fabrication of single-crystalline microspheres with high sphericity from anisotropic materials,” *Scientific Reports*, vol. 4, no. 5186, June 5, 2014

[52] I. Vendik et al., “Modelling of isotropic double negative media for microwave applications,” Opto-electronics Review, vol. 14, no. 3, pp.179-186, Sept. 2006

[53] J. Wheeler. Physics 6120: Electrodynamics II. Class Lecture, Topic: “Frequency dependence of the permittivity.” Department of Physics, Utah State University, Logan, UT, Feb. 7, 2016

[54] C. Baily. Upper-Division Electrodynamics. Class Lecture, Topics: “Index of Refraction.” Department of Physics, University of Colorado Boulder, Boulder, CO, 2012

APPENDICES

Fabry-Perot Resonance and Shifting Phenomena

In a plane dielectric slab, near perfect transmission can occur when the half-wavelength of the incident radiation is a unit fraction of the slab thickness [1]. This condition is present at the zeros of the first-order z-domain transfer function for the slab which correspond to null reflection values. Incongruously, conductive metal sheets typically behave as reflectors of incident radiation due to the propensity to engage oscillating charge densities on the surface in opposition to that of the applied field. In free-space, this resultant wave is predominantly or entirely directed towards the origin as dependent upon whether the conductivity of the sheet is finite. When placed over a dielectric slab of given permittivity, the sheet forms a cavity through which a resonance shifting effect can be demonstrated. Similar to the pure dielectric case, the resonance yields transmission on the order of unity. This effect is known as Fabry-Perot resonance shifting and is the result of the metal layer introducing a ninety degree translation in the zero locations of the transmission function. Consequently, the new zero locations occur at the maximum in the reflection of the simple dielectric case. This condition holds for both TE and TM wave polarizations as well as oblique incidence angles, however, the necessary conductivity to achieve full transmission through the structure changes as a function of this angle. The relationship between the conductivity, permittivity of the dielectric layer, and incidence angle can be determined from the step in the tangential magnetic field in proportion to the surface current density at the metal interface. From these boundary conditions, the reflection and transmission coefficient are found and the conductivity which minimizes the reflection can be selected. The equation for this conductivity when operating in the TM mode is given below:

$$\sigma_s^{(s)} = \frac{\varepsilon - 1}{\eta_0 \cos\varphi}\left[1 - \frac{\varepsilon \sin^2\varphi}{\varepsilon - \sin^2\varphi}\right]$$

This represents a quadratic equation in the permittivity which can be reconstituted to yield the resonance condition for the dielectric as a function of the surface conductivity. The resonance condition only applies when the phase shares the following relation:

$$k_n d = \frac{(2n+1)\pi}{2}$$

MATLAB Code for Section 3.1

The Patcheff function determines the effective permittivity according to Schneiders' model with substrate permittivity, eps; substrate thickness, h; and patch width, w. The width of the patch was found from equation 2.1.6 for each substrate.

```
function P=Patcheff(eps,h,w)
P=(eps+1)/2 + ((eps-1)/2)*1/sqrt(1+12*h/w);
end
```

The result of the previous function was then substituted into the function, PatchTrans, with the frequency of the incident wave, whereby the transmittance was resolved from the transfer matrix method outlined in section 2.4.

```
function F=PatchTrans(eps_eff,f)
   ng=sqrt(eps_eff);
   n0=1.00029;
   k0=(2*pi*f)/(3*10^8);
   kg=k0*ng;
   dg=1.6e-3;
   rg_1=(n0-ng)/(n0+ng);
   tg_1=(2*n0)/(n0+ng);
   rg_2=(ng-n0)/(n0 + ng);
   tg_2=(2*ng)/(n0+ng);
   phi_g=kg*dg;
   T_g1=(1/tg_1)*[1 rg_1; rg_1 1];
   Tg=[exp(i*phi_g) 0; 0 exp(-i*phi_g)];
   T_g2=(1/tg_2)*[1 rg_2; rg_2 1];
   T=T_g1*Tg*T_g2;
   F=abs(1/T(1,1))^2;
end
```

The code for section 3.2 is very similar to this code with the effective patch refractive index replaced by that of the glass. The thickness is then optimized by taking discrete steps across a given solution space and thereby determining the value which leads to the highest transmittance. This value is used in the proceeding sections for evaluation.

MATLAB Code for Section 3.3

The optimSpec function determines the thickness, th, and refractive index, n, that lead to a minimization of the residual between acquired transmittance and desired through analysis of the residual at discrete points throughout a subspace of parameter values. The parameters are set to have values within a predefined range that is congruent with reasonable expectations on their limits. The returned values are those that lead to a global minimization in the observation region. The actual transmittance, Ts, is also provided.

```
function [Ts,n,th]=optimSpec(eps_eff,f)
    h=1.6e-3;
    neff=sqrt(eps_eff);
    n0=1.00029;
    omega=2*pi*f;
    k0=omega/(3e8);
    nmed=linspace(-5,-5,50);
    d=linspace(0.001,0.015,50);
    k1=k0*nmed;
    k2=k0*neff;
    r01=(n0-nmed)./(n0+nmed);
    t01=(2*n0)./(n0+nmed);
    r12=(nmed-neff)./(neff+nmed);
    t12=(2*nmed)./(neff+nmed);
    r23=(neff-n0)/(n0+neff);
    t23=(2*neff)/(n0+neff);
    Tp=zeros(length(nmed),length(d));
    for j=1:length(nmed)
        for m=1:length(d)
            phi_1=k1(j)*d(m);
            phi_2=k2*h;
            T_01=(1/t01(j))*[1 r01(j); r01(j) 1];
            T_1=[exp(i*phi_1) 0; 0 exp(-i*phi_1)];
            T_12=(1/t12(j))*[1 r12(j); r12(j) 1];
            T_2=[exp(i*phi_2) 0; 0 exp(-i*phi_2)];
            T_23=(1/t23)*[1 r23; r23 1];
            T=T_01*T_1*T_12*T_2*T_23;
            Tp(j,m)=abs(1/T(1,1))^2;
        end
    end
   [Ts,v,q]=globMin(Tp);
    n=nmed(v);
    th=d(q);
```

```
end
```

where globMin finds the value(s) of the refractive indices that minimize the difference with the desired transmittance and has the form:

```
function [V,x,y]=globMin(T)

des=0.9925;

P=round(T,4);

V=P(abs(P-des)==min(min(abs(P-des))));

V=V(1,1);

[x,y]=find(P==V,2);

End
```

MATLAB Code for Section 3.4

The function detConfInt determines the 90 percent confidence interval from 40 samples at each substrate permittivity value utilizing the t-distribution. The confidence interval relies on the mean, x, and standard deviation, s, of each of the designable variables. The variable *sect* is the proportion of the thickness and transmittance values corresponding to a specified permittivity as determined within the previous step. This function is capable of providing confidences for both the metamaterial inclusion parameters and their according tolerance values.

```
function [mu,muto,x,x2]=detConfInt(sect,eps)

%confidence interval using the t-distribution (for low sample number)

%90 percent confidence

th=sect(5);

Ts=sect(2);

f=9e9;

fr=14e9;

h=1.6e-3;

w=((3e8)/(2*fr))*sqrt(2/(eps+1));

eps_eff=Patcheff(eps,h,w);

helpr=zeros(6,40);

for c=1:40

   [ei,re,rm,s,nact]=miesave(th,eps_eff,f,Ts);

   Tact=actTrans(nact,th,eps_eff,f);
```

```
    med_l=[ei,re,rm,s,nact,Tact]';
    helpr(:,c)=med_l;
end
x=mean(helpr,2);% 1 per (6 total)
s=std(helpr,0,2);% 1 per (6 total)
t_crit=1.699;%90% CI
mu=[x-t_crit.*(s./sqrt(40)),x+t_crit.*(s./sqrt(40))]; %2 per (12 total)
%%%%%%%%%%%%%%%%%%%%%%%%%%%%%%%%%%%%%%%%%%%%%%%%%%%%%%%%%%
%%%%%%%%%%%%%%%%%%%%%%%%%
repr=zeros(10,40);
for p=1:length(helpr)
    tol=newsless(helpr(:,p),f,fr,h,eps,th);
    repr(:,p)=tol;
end
x2=mean(repr,2);
s2=std(repr,0,2);
muto=[x2-t_crit.*(s2./sqrt(40)),x2+t_crit.*(s2./sqrt(40))];
end
```

The miesave function utilizes the effective medium adaptation of Mie theory, as discussed in section 2.5.2, to resolve the necessary dimensions and permittivity value for the all-dielectric metamaterial. Each equation is set-up as an anonymous function in the unknown variables to conform to the function handle type requirement for insertion into the optimization solver. The lower and upper bounds are set such that the variable remains within a user defined appropriate region. The purpose of the variable, sigbit, as well as the left and right hand sides of the inequality constraints Aineq and Bineq, are detailed in section 3.4. The optimized parameter set is returned by the function after completion of the SQP optimization step. The two values of Pri denote whether the desired constituents lead to a negative or positive refractive index based on the value of sigbit.

```
function [ei,re,rm,s,nact]=miesave(thick,eps_eff,f,Ts)
eb=1;
fe=@(x) (4/3)*pi*(x(2)/x(4))^3;
fm=@(x) (4/3)*pi*(x(3)/x(4))^3;
k0=2*pi*f/(3e8);
k=@(x) k0*sqrt((1e7)*x(1));
te=@(x) k(x)*x(2);
```

```
tm=@(x) k(x)*x(3);

Fe=@(x) (2*sin(te(x))-te(x)*cos(te(x)))/((te(x)^2-1)*sin(te(x))-te(x)*cos(te(x)));

Fm=@(x) (2*sin(tm(x))-tm(x)*cos(tm(x)))/((tm(x)^2-1)*sin(tm(x))-tm(x)*cos(tm(x)));

v=@(x) (fe(x)/eb)*((2*eb+(1e7)*x(1)*Fe(x))/(eb-(1e7)*x(1)*Fe(x)))+(fm(x)/eb)*((2*eb-
(1e7)*x(1)*Fm(x))/(eb-(1e7)*x(1)*Fm(x)));

eps=@(x) eb*(2*v(x)+1)/(1-v(x));

mu=@(x) (2*fm(x)*((2+Fm(x))/(1-Fm(x)))+1)/(1-fm(x)*((2+Fm(x))/(1-Fm(x))));

sigbit=@(x) (1i)^((eps(x)<0 && mu(x)<0)*((eps(x)<0) + (mu(x)<0)));

valt=@(x) sigbit(x)*sqrt(eps(x)*mu(x))*isreal(sqrt(eps(x)*mu(x))); %*(sigbit(x)<0);

%Pri=@(x) actTrans(valt(x),thick,eps_eff,f)-0.5*(sigbit(x)>=0);

Pri=@(x) actTrans(valt(x),thick,eps_eff,f)-0.5*(sigbit(x)<0);

fun=@(x) abs(Pri(x)-Ts);

opts=optimoptions(@fmincon,'Algorithm','sqp');

problem=createOptimProblem('fmincon','objective',fun,'x0',[7e-5 50e-6 100e-6 4000e-
6],'Aineq',[0 2.5 2.5 -1;0 1 1 1],'bineq',[0;thick],'lb',[2e-5 1e-6 1e-6 4e-5],'ub',[1e-4 1000e-6
1000e-6 5000e-6],'options',opts);

ms=MultiStart;

ms.StartPointsToRun='bounds';

x=run(ms,problem,50);

ei=(1e7)*x(1);

re=x(2);

rm=x(3);

nact=valt(x);

s=x(4);

end
```

The tolerance testing is then performed on the values by varying them by ten percent about the solutions determined from the previous function. The tolmie function resolves the acceptable range by finding the consecutive values that meet the transmittance condition around the desired value. The maximum and minimum of these values are then recorded in the tol output. The variable helpr is a proportion of the previous variable pro.This code is presented below for convenience:

```
function tol=tolmie(helpr,f,fr,h,eps,th)

s=helpr(4);
```

```
erg=eps;
ore=helpr(2);
delre=linspace(-0.2*ore,0.2*ore,60);
orm=helpr(3);
delrm=linspace(-0.2*orm,0.2*orm,60);
re=delre+ore;
rm=delrm+orm;
ret=sort([re,ore]);
rmt=sort([rm,orm]);
ekj=helpr(1)/(1e7);
w=((3e8)/(2*fr))*sqrt(2/(erg+1));
eps_eff=Patcheff(erg,h,w);
for c=1:length(re)
   if(2.5*(re(c)+orm)<s && re(c)+orm+s<th)
      tsa(c)=miecheck([ekj,re(c),orm,s],th,eps);
   else
      tsa(c)=0;
   end
end
di=find(ret==ore);
idx=(tsa>0.9*helpr(6));
nedr=[idx(1:di-1),1,idx(di:end)];
if(~all(nedr))
   I1=strfind(nedr,[0 1])+1;
   if(isempty(I1)) I1=1; end
   I2=strfind(nedr,[1 0]);
   if(isempty(I2)) I2=length(ret); end
   I1=I1(I1<=di);
   if(isempty(I1)) I1=1; end
   I2=I2(I2>=di);
   if(isempty(I2)) I2=length(ret); end
```

```
    I1=I1(abs(I1-di)==min(abs(I1-di)));
    I2=I2(abs(I2-di)==min(abs(I2-di)));
else
    I1=1;
    I2=length(ret);
end
tol_re_min=((ret(I1)-ore)/ore)*100;
tol_re_max=((ret(I2)-ore)/ore)*100;
for c=1:length(rm)
    if(2.5*(ore+rm(c))<s && ore+rm(c)+s<th)
        psa(c)=miecheck([ekj,ore,rm(c),s],th,eps);
    else
        psa(c)=0;
    end
end
di=find(rmt==orm);
idx=(psa>0.9*helpr(6));
nedr=[idx(1:di-1),1,idx(di:end)];
if(~all(nedr))
    I1=strfind(nedr,[0 1])+1;
    if(isempty(I1)) I1=1; end
    I2=strfind(nedr,[1 0]);
    if(isempty(I2)) I2=length(rmt); end
    I1=I1(I1<=di);
    if(isempty(I1)) I1=1; end
    I2=I2(I2>=di);
    if(isempty(I2)) I2=length(rmt); end
    I1=I1(abs(I1-di)==min(abs(I1-di)));
    I2=I2(abs(I2-di)==min(abs(I2-di)));
else
    I1=1;
```

```
    I2=length(rmt);
end
tol_rm_min=((rmt(I1)-orm)/orm)*100;
tol_rm_max=((rmt(I2)-orm)/orm)*100;
delts=linspace(-0.2*s,0.2*s,60);
ns=delts+s;
nst=sort([ns,s]);
for c=1:length(ns)
    if(2.5*(ore+orm)<ns(c) && (ore+orm+ns(c))<th)
        gsa(c)=miecheck([ekj,ore,orm,ns(c)],th,eps);

    else
        gsa(c)=0;
    end
end
di=find(nst==s);
idx=(gsa>0.9*helpr(6));
nedr=[idx(1:di-1),1,idx(di:end)];
if(~all(nedr))
    I1=strfind(nedr,[0 1])+1;
    if(isempty(I1)) I1=1; end
    I2=strfind(nedr,[1 0]);
    if(isempty(I2)) I2=length(nst); end
    I1=I1(I1<=di);
    if(isempty(I1)) I1=1; end
    I2=I2(I2>=di);
    if(isempty(I2)) I2=length(nst); end
    I1=I1(abs(I1-di)==min(abs(I1-di)));
    I2=I2(abs(I2-di)==min(abs(I2-di)));
else
    I1=1;
```

```
    I2=length(nst);
end
tol_s_min=((nst(I1)-s)/s)*100;
tol_s_max=((nst(I2)-s)/s)*100;
delth=linspace(-0.2*th,0.2*th,60);
nth=delth+th;
ntht=sort([th,nth]);
for c=1:length(nth)
    if(orm+ore+s<th)
    ksa(c)=miecheck([ekj,ore,orm,s],nth(c),eps);
    else
    ksa(c)=0;
    end
end
di=find(ntht==th);
idx=(ksa>0.9*helpr(6));
nedr=[idx(1:di-1),1,idx(di:end)];
if(~all(nedr))
I1=strfind(nedr,[0 1])+1;
if(isempty(I1)) I1=1; end
I2=strfind(nedr,[1 0]);
if(isempty(I2)) I2=length(ntht); end
I1=I1(I1<=di);
if(isempty(I1)) I1=1; end
I2=I2(I2>=di);
if(isempty(I2)) I2=length(ntht); end
I1=I1(abs(I1-di)==min(abs(I1-di)));
I2=I2(abs(I2-di)==min(abs(I2-di)));
else
    I1=1;
    I2=length(ntht);
```

```
end
tol_th_min=((ntht(I1)-th)/th)*100;
tol_th_max=((ntht(I2)-th)/th)*100;
delekj=linspace(-0.2*ekj,0.2*ekj,60);
esp=ekj+delekj;
est=sort([esp,ekj]);
for c=1:length(esp)
   vpa(c)=miecheck([esp(c),ore,orm,s],th,eps);
end
di=find(est==ekj);
idx=(vpa>0.9*helpr(6));
nedr=[idx(1:di-1),1,idx(di:end)];
if(~all(nedr))
I1=strfind(nedr,[0 1])+1;
if(isempty(I1)) I1=1; end
I2=strfind(nedr,[1 0]);
if(isempty(I2)) I2=length(est); end
I1=I1(I1<=di);
if(isempty(I1)) I1=1; end
I2=I2(I2>=di);
if(isempty(I2)) I2=length(est); end
I1=I1(abs(I1-di)==min(abs(I1-di)));
I2=I2(abs(I2-di)==min(abs(I2-di)));
else
   I1=1;
   I2=length(est);
end
tol_ei_min=((est(I1)-ekj)/ekj)*100;
tol_ei_max=((est(I2)-ekj)/ekj)*100;
tol=[tol_re_min;tol_re_max;tol_rm_min;tol_rm_max;tol_s_min;tol_s_max;tol_th_min;tol_th_max;tol_ei
_min;tol_ei_max];
end
```

MATLAB Code for Section 3.5

This code determines the bandwidth for the system in a similar fashion to those used for the tolerance with the exception that the frequency is the varied property. This test is presented below:

```
BW=zeros(1,length(ei));
for p=1:length(ei)
h=1.6e-3;
eps=ei(p);
fr=14e9;
f=linspace(8e9,10e9,50);
fo=9e9;
fet=sort([f,fo]);
w=((3e8)/(2*fr))*sqrt(2/(eps+1));
eps_eff=Patcheff(eps,h,w);
nact=pro(10,p);
th=pro(5,p);
nes=zeros(1,length(f));
Tsec=zeros(1,length(f));
Tpat=zeros(1,length(f));%%%%%%%%%%%%%%%%%%%%%%%%%%%%%%%%%%%%
for k=1:length(f)
Tact=actTrans(nact, th, eps_eff, f(k));
Tsec(k)=Tact;
Tpat(k)=PatchTrans(eps_eff,f(k));%%%%%%%%%%%%%%%%%%%%%%%%%%%
end
di=find(fet==fo);
idx=((((Tsec-Tpat)./Tpat).*100)>0.9*(pro(3,p)));
%idx=Tsec>0.9;
```

```
nedr=[idx(1:di-1),1,idx(di:end)];
if(~all(nedr))
I1=strfind(nedr,[0 1])+1;
if(isempty(I1)) I1=1; end
I2=strfind(nedr,[1 0]);
if(isempty(I2)) I2=length(fet); end
I1=I1(I1<=di);
I2=I2(I2>=di);
I1=I1(abs(I1-di)==min(abs(I1-di)));
I2=I2(abs(I2-di)==min(abs(I2-di)));
else
   I1=1;
   I2=length(fet);
end
BW(p)=2*min(abs(fet(I1)-9e9),abs(fet(I2)-9e9));
end
```

CIRRICULUM VITAE

Name: Matthew Bester

Post-secondary Education and Degrees:

The University of Western Ontario
London, Ontario, Canada
2010-2014 B. Eng

Related Work Experience:

Teaching Assistant
The University of Western Ontario
2015-2017

Research Associate
The University of Western Ontario
2017-2018